SIMULATION OF SHIP MOTION AND DECK WETTING DUE TO STEEP RANDOM SEAS

A Thesis

by

ADAM ADIL

Submitted to the Office of Graduate Studies of
Texas A&M University
in partial fulfillment of the requirements for the degree of

MASTER OF SCIENCE

December 2004

Major Subject: Ocean Engineering

SIMULATION OF SHIP MOTION AND DECK-WETTING DUE TO STEEP RANDOM SEAS

A Thesis

by

ADAM ADIL

Submitted to Texas A&M University
in partial fulfillment of the requirements
for the degree of

MASTER OF SCIENCE

Approved as to style and content by:

C.H. Kim (Chair of Committee)	M.H. Kim (Member)
A. Stoessel (Member)	Paul N. Roschke (Head of Department)

December 2004

Major Subject: Ocean Engineering

ABSTRACT

Simulation of Ship Motion and Deck Wetting due

to Steep Random Seas. (December 2004)

Adam Adil, B.Tech.,

Cochin University of Science and Technology,

Kerala, India

Chair of Advisory Committee: Dr. C. H. Kim

The extreme motion and load of ships have been assessed using a linear frequency domain method or a linear energy spectral method and RAOs, which may be too approximate to be used for estimation of ship motion in severest seas. The new technology uses simulation in the time domain to deal with the non-linear responses to the random seas. However, the current simulation technique has been successful only up to the sea state of 7 ("high seas"), defined by the significant wave height of 9 meters. The above cannot provide the extreme wave loads and motions for seas higher than the sea state 7. The ultimate goal of this work would be to develop a new technique that can simulate responses to the seas of states 8 and 9.

The objective of the present study is to simulate the vertical relative motion and wave topping of a moored ship in the time domain by varying the significant wave heights. The analysis was able to predict with a fair accuracy the relative motion characteristics of a freely floating body in the head and beam sea conditions. The resonance aspects and its significance in the overall response are also analyzed.

DEDICATION

To God and my family for guiding me throughout my life

ACKNOWLEDGMENTS

This research was conducted at Texas A&M University and was supported by the Department of Civil Engineering, Texas A&M University through the Texas Engineering Experiment Station (TEEX).

I would like to thank my chair, Dr. C.H. Kim, for his guidance and contribution to my understanding of this research and the subject of ship motions as a whole. I would also like to thank my advisory committee members: Dr. M.H. Kim and Dr. Achim Stoessel, for their trust and guidance throughout this research project.

I also wish to thank my fellow classmates and friends for their active help and contribution, Mr. Nungsoo Kim, Mr. Harish S. Pillai, and Mr. Vinu P. Kuriakose.

Special thanks to my family for their constant support and motivation without which I would have never come this far.

TABLE OF CONTENTS

Page

ABSTRACT iii

DEDICATION iv

ACKNOWLEDGMENTS v

TABLE OF CONTENTS vi

LIST OF FIGURES viii

LIST OF TABLES xiii

1 INTRODUCTION 1

1.1 Motivation 1
1.2 Application 2
1.3 Approach 3
1.3.1 Linear and non-linear models 3

2 THE UNIOM MODEL 4

2.1 Literature review 4
2.2 The strip theory method 5
2.3 Modeling approach 7
2.4 Procedure 8
2.5 The ship motion program 11
2.6 Computational methodology 11
2.6.1 ITTC spectrum 12
2.6.2 JONSWAP spectrum 13

3 ANALYSIS METHODOLOGY 15

3.1 Impulse analysis 15
3.2 Response analysis 17
3.3 Spectral response analysis 17
3.4 Zero crossing analysis 18
3.5 Most probable peak analysis 19

4 ANALYSIS RESULTS 20

4.1 Head sea condition 20
4.1.1 Case #1: Hs = 3.0 m 20
4.1.2 Case #2: Hs =6.0 m 27

Page

4.1.3 Case #3: Hs = 9.0 m 35
4.1.4 Case #4: Hs = 11.0 m 43
4.2 Beam sea condition 50
4.2.1 Case #1: Hs = 3.0 m 50
4.2.2 Case #2: Hs =6.0 m 62
4.2.3 Case #3: Hs =9.0 m 73
4.2.4 Case #4: Hs =11.0 m 83
4.3 Deck wetness analysis 94

5 CONCLUSION 98

REFERENCES 100

APPENDIX A 102

APPENDIX B 105

APPENDIX C 107

APPENDIX D 112

VITA 117

LIST OF FIGURES

Page

Figure 2-1: Universal non-linear input output model....4

Figure 2-2: V section (Lewis 1929) 7

Figure 2-3: The coordinate system....9

Figure 4-1: Head sea-Hs 3.0m-input wave data, heave, pitch and relative response....20

Figure 4-2: Head sea-Hs 3.0m-probability of exceedence for input wave....22

Figure 4-3: Head sea-Hs 3.0m-heave RAO....23

Figure 4-4: Head sea-Hs 3.0m-pitch RAO....24

Figure 4-5: Head sea-Hs 3.0m-heave probability of exceedence....25

Figure 4-6: Head sea-Hs 3.0m-pitch probability of exceedence....25

Figure 4-7: Head sea-Hs 3.0m-relative motion RAO 26

Figure 4-8: Head sea-Hs 3.0m-relative motion probability of exceedence....27

Figure 4-9: Head sea-Hs 6.0m-input wave data, heave, pitch and relative response....28

Figure 4-10: Head sea-Hs 6.0m-probability of exceedence for input wave....30

Figure 4-11: Head sea-Hs 6.0m-heave RAO 30

Figure 4-12: Head sea-Hs 6.0m-pitch RAO....31

Figure 4-13: Head sea-Hs 6.0m-probability of exceedence for heave motion....32

Figure 4-14: Head sea-Hs 6.0m-probability of exceedence for pitch motion....32

Figure 4-15: Head sea-Hs 6.0m-relative motion RAO 33

Figure 4-16: Head sea-Hs 6.0m-probability of exceedence for relative motion....34

Figure 4-17: Head sea-Hs 6.0m-input wave data, heave, pitch and relative response....35

Figure 4-18: Head sea-Hs 9.0m-probability of exceedence for input wave....37

Page

Figure 4-19: Head sea-Hs 9.0m-heave RAO 38

Figure 4-20: Head sea-Hs 9.0m-pitch RAO 39

Figure 4-21: Head sea-Hs 9.0m- probability of exceedence for heave motion.....40

Figure 4-22: Head sea-Hs 9.0m- probability of exceedence for pitch motion 41

Figure 4-23: Head sea-Hs 9.0m- relative motion RAO.....41

Figure 4-24: Head sea-Hs 9.0m- probability of exceedence for relative motion 42

Figure 4-25: Head sea-Hs 6.0m-input wave data, heave, pitch and relative response.....43

Figure 4-26: Head sea-Hs 11.0m-probability of exceedence for input wave.....45

Figure 4-27: Head sea-Hs 11.0m-heave RAO 45

Figure 4-28: Head sea-Hs 11.0m-pitch RAO 46

Figure 4-29: Head sea-Hs 11.0m-probability of exceedence for heave motion.....47

Figure 4-30: Head sea-Hs 11.0m-probability of exceedence for pitch motion 47

Figure 4-31: Head sea-Hs 11.0m-relative motion RAO 48

Figure 4-32: Head sea-Hs 11.0m-probability of exceedence for relative motion 49

Figure 4-33: Beam sea-Hs 3.0m-input wave data, heave, and pitch response 50

Figure 4-34: Beam sea-Hs 3.0m-heave RAO.....51

Figure 4-35: Beam sea-Hs 3.0m-pitch RAO 52

Figure 4-36: Beam sea-Hs 3.0m-probability of exceedence for heave motion.....53

Figure 4-37: Beam sea-Hs 3.0m-probability of exceedence for pitch motion 53

Figure 4-38: Beam sea-Hs 3.0m-relative motion RAO [leeward side].....54

Figure 4-39: Beam sea-Hs 3.0m-roll natural frequency.....55

Figure 4-40: Beam sea-Hs 3.0m-roll RAO 56

Page

Figure 4-41: Beam sea-Hs 3.0m- relative motion with and without roll resonance [leeward side] 56

Figure 4-42: Beam sea-Hs 3.0m- relative motion probability of exceedence 58

Figure 4-43: Beam sea-Hs 3.0m- relative motion RAO [weather side] 59

Figure 4-44: Beam sea-Hs 3.0m- relative motion with and without roll resonance [weather side] 60

Figure 4-45: Beam sea-Hs 3.0m- probability of exceedence for relative motion 61

Figure 4-46: Beam sea-Hs 6.0m-input wave data, heave, and pitch response 62

Figure 4-47: Beam sea-Hs 6.0m-heave RAO 63

Figure 4-48: Beam sea-Hs 6.0m-pitch RAO 64

Figure 4-49: Beam sea-Hs 6.0m- probability of exceedence for heave motion 65

Figure 4-50: Beam sea-Hs 6.0m- probability of exceedence for pitch motion 66

Figure 4-51: Relative motion RAO [leeward side] 67

Figure 4-52: Beam sea-Hs 3.0m- relative motion with and without roll resonance 68

Figure 4-53: Beam sea-Hs 6.0m- probability of exceedence for relative motion 69

Figure 4-54: Relative motion RAO [weather side] 70

Figure 4-55: Beam sea-Hs 6.0m- relative motion with and without roll resonance 70

Figure 4-56: Beam sea-Hs 6.0m- probability of exceedence for relative motion 72

Figure 4-57: Beam sea-Hs 9.0m-input wave data, heave, pitch response 73

Figure 4-58: Beam sea-Hs 9.0m-heave RAO 74

Figure 4-59: Beam sea-Hs 6.0m-pitch RAO 75

Figure 4-60: Beam sea-Hs 9.0m- probability of exceedence for heave motion 75

Page

Figure 4-61: Beam sea-Hs 9.0m- probability of exceedence for pitch motion 76

Figure 4-62: Relative motion RAO [leeward side] 77

Figure 4-63: Beam sea-Hs 9.0m-relative motion with and without roll resonance [leeward side] 77

Figure 4-64: Beam sea-Hs 9.0m- probability of exceedence for relative motion [leeward side] 79

Figure 4-65: Relative motion RAO [weather side] 80

Figure 4-66: Beam sea-Hs 9.0m- relative motion with and without roll resonance 80

Figure 4-67: Beam sea-Hs 9.0m- probability of exceedence for relative motion 82

Figure 4-68: Beam sea-Hs 11.0m-input wave data, heave, pitch response 83

Figure 4-69: Beam sea-Hs 11.0m-heave RAO 84

Figure 4-70: Beam sea-Hs 11.0m-pitch RAO 85

Figure 4-71: Beam sea-Hs 11.0m-probability of exceedence for heave motion 86

Figure 4-72: Beam sea-Hs 11.0m- probability of exceedence for pitch motion. 86

Figure 4-73: Beam sea-Hs 11.0m -relative motion RAO [leeward side] 87

Figure 4-74: Beam sea-Hs 11.0m –roll resonance frequency 88

Figure 4-75: Beam sea-Hs 11.0m –roll RAO 88

Figure 4-76: Beam sea-Hs 11.0m- relative motion with and without roll resonance 89

Figure 4-77: Beam sea-Hs 11.0m- probability of exceedence for relative motion 90

Figure 4-78: Beam sea-Hs 11.0m- relative motion RAO [weather side] 91

Figure 4-79: Beam sea-Hs 11.0m- relative motion with and without roll resonance [weather side] 92

Page

Figure 4-80: Beam sea-Hs 11.0m- probability of exceedence for relative motion 93

Figure 4-81: Beam sea-most probable peak response 95

Figure 4-82: Beam sea-most probable peak response [weather side] 96

Figure 4-83: Beam sea-most probable peak response [leeward side]. 97

LIST OF TABLES

Page

Table 2-1: KRISO data for input wave spectrum (2000) 12

Table 3-1: Sea states and codes 15

1 INTRODUCTION

1.1 Motivation

The green water problem occurs when the relative free surface motion exceeds the freeboard of a floating vessel and the deck of the vessel is wetted. Apart from causing inconvenience to the crew and damage to the equipment fitted on board, the shipping of green water also causes considerable changes in the dynamics of the ship motions. As the water gets shipped onto the deck, the excessive forces on the fore end of the deck causes an imbalance on the deck loading and heave and pitching motions get altered drastically. This causes considerable impact on the mooring of the structures in cases like FPSO and can pose a major threat to the overall structural integrity of the other ship members.

To avoid these problems and to design for such steep random sea states that cause structural failures, a benchmark for the design is essential. This would help the designer to decide upon the freeboard and the possible forecastle deck elevation. The current research is a step in the direction of simulation of relative motion of the hull in high random seas, which would help to predict the safe regime for the design to avert such possible failures as well as causes of failure.

The extreme motion and load of ships have been assessed using linear frequency domain method or linear energy spectral method and RAOs, which may be too approximate to be used for estimation of ship motion in severest seas.

The thesis follows the style and format of *Journal of Ship Research.*

The new technology uses simulation in the time domain to deal with the non-linear responses to the random seas. However, the current simulation technique has been successful only up to the sea state of 7 ("high seas"), defined by the significant wave height of 9 meters. The above cannot provide the extreme wave loads and motions for seas higher than the sea state 7. The ultimate goal of this work would be to develop a new technique that can simulate responses to the seas of states 8 and 9.

1.2 Application

We apply a **U**niversal **N**on-linear **I**nput **O**utput **M**odel (**UNIOM**) that employs the non-linear wave measured in the wave tank as input and it is assumed that the ship motion system is linear, thus expecting the non-linear responses. It uses the real wave data, in- stead of the Gaussian random waves digitized from the given extreme sea spectrum, and the RAOs, which are determined from the linear ship motion theory.

The real random wave data from the experiments is used with the analytical RAOs obtained for the vessel to obtain the time domain response for the various sea states. Thus the application of linear strip theory method on the non-linear wave input yields a response that is non-linear. The accuracy of the estimates is justified by the comparisons of the theoretical strip theory calculation results with that of the real random wave response.

The objective of the present study is to simulate the vertical relative motion and wave topping of a moored ship (which can be simulated as FPSO) in the time domain by varying the significant wave heights. The results are statistically compared with the conventional linear estimations. Due to the lack of model test data, it is difficult to draw

a conclusion that the proposed method will be superior to the conventional method. However we could see that differences in the estimations increases with the sea state.

1.3 Approach

1.3.1 Linear and non-linear models

For any input Gaussian wave into a linear system would yield a linear output. Since the input wave is a linear random wave the response from the linear system RAOs would be again linear. The linear model can be analyzed in frequency domain by the spectral energy methods.

$$S_{yy}(\omega) = \left|G(\omega)\right|^2 S_{xx}(\omega) \qquad (1)$$

is the energy density relation between a random linear input and the output from a linear system. Here the frequency response function $G(\omega)$ is referred to as the Linear Response Amplitude Operator (RAO) that has been used for the estimation of the linear response of offshore structures. The above approach is often referred to as the linear energy spectral method.

The non-linear/non-Gaussian input of wave into a non-linear system would produce a non-linear result. The non-linear models can only be analyzed in the time domain. A fully experimental or field data is used for this type of model.

$$\mathrm{Rel}(t) = \sum_{j=1} |Aj||RAO|e^{i(\omega_j t - \phi_j - \varepsilon_j)} \qquad (2)$$

Here the response is obtained in time domain for the RAO of response, which in this case is obtained from the non-linear method. The input wave amplitude for the range of frequencies is multiplied with the RAOs and appropriate phase angles of both are applied to obtain the result.

2 THE UNIOM MODEL

The Universal non-linear input output model assumes that any non-linear input/impulse to a system, which is linear, would yield a non-linear output/response. This is illustrated in Figure 2-1.

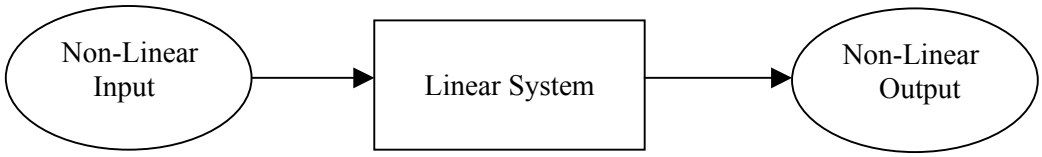

Figure 2-1: Universal non-linear input output model

For the present study the wave data from KRISO, which is non-linear, is used for the analysis. The wave data obtained here follows both ITTC as well as JONSWAP spectrum.

The analysis carried out estimates and statistically compared the linear to that of the non-linear model. The non-linearity as discussed earlier is achieved through the UNIOM approach.

2.1 Literature review

The analytical technique developed to estimate the response motions and loads carried out previously (Kim et al 1980) has provided the main driving force towards this work. They applied the strip-wise computation technique, which is well correlated with the experimental results. The analysis was carried out on the significant hydrodynamic problems such as: wave excited and motion induced forces and moments, wave loads on cross sections and hydrodynamics pressure and relative motion. The relative motion

study and the programs used for the same have helped greatly towards the research. The work on the applications of strip theory (Korvin-Kroukovsky 1955) paved the fundamental approach towards this theory and its applications to ship motion problems. It was successfully applied the strip theory for the prediction of heaving and pitching motions of ship running in longitudinal regular waves.

The evaluation of the wave exciting forces and moments can be performed by using i) The relative motion concept (Korvin-Kroukovsky 1955) ii) the Haskind-Newman relationship (Newman 1962) or by iii) the diffraction forces directly. The computational use of strip theories and its easy use which were discussed (Journee 1992) helped in the understanding of computational formulations of the same. The theories for hydrodynamic coupling (Salvesen et al 1970) reveal the results of coupled motions such as

(a) Heave-induced pitching moment = - pitch induced heaving force.

Sway-induced yawing moment = - yaw induced swaying force.

Yaw induced rolling moment = - roll induced yawing moment.

(b) Sway induced rolling moment = roll induced swaying force.

2.2 The strip theory method

Since its inception in 1950 linear strip theory (Salvesen et al 1970) has been widely used by academia as well as by the industry and has yielded the best possible results from the design standpoint. In this, ship is assumed to be a two-dimensional beam, and the physical three-dimensional flow near the hull is limited in planes of transverse sections during ship motions. The amplitudes of incident waves and ship motions are small with reference to ship dimensions. The hydrodynamic forces acting on

each section are integrated over the ship length, and then the ship responses are determined.

Although the three-dimensional theories are used and practiced these days, the verification as well as validation of the results is not yet fully achieved. This makes the accuracy and adequacy of such theories questionable. At the same time the two-dimensional theories have been used extensively and the authenticity of the results have been proved repeatedly.

The main hydrodynamic problems that are analyzed using the strip theory are the wave excited and motion induced forces and moments, wave loads on the cross sections as well as hydrodynamic pressure and relative motion.

The calculations in strip theory are carried out in the frequency domain and are as follows:

- The ship hull is divided longitudinally into a number of transverse sections and the hydrodynamic coefficients such as added mass, damping coefficients, wave excitation forces and responses are estimated for each of the sections.
- These individual sectional characteristics are then integrated along the length and the global coefficients for the coupled motions are estimated. The vertical and horizontal plane motions are considered for analysis separately where by heave-pitch motions and sway-roll-yaw motions get segregated in analysis.
- These equations of motions are then solved to estimate the relevant forces and the corresponding response spectra.

2.3 Modeling approach

There are two common methods for modeling the strips for the analysis.

Conformal mapping: In this method the ship sections are mapped to unit circles using a conformal mapping. The simplest of these is the Lewis mapping (Lewis 1929) which uses three parameters to define the mapping. The coefficients of the mapping parameters are calculated from the section beam, draught and cross sectional area. The mapping can be made more accurate by increasing the number of mapping parameters. An example for such a kind of mapping is shown in Figure 2-2.

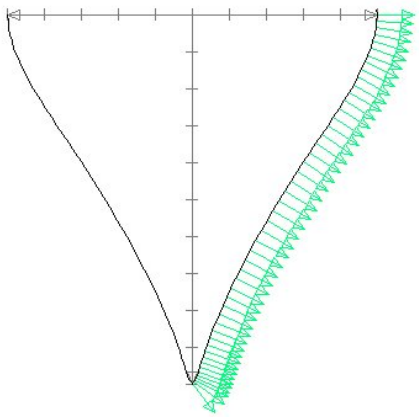

Figure 2-2: V section (Lewis 1929)

Singularities on section contour: This method uses pulsating source singularities on the surface of the section. The strengths of the singularities are chosen to satisfy the boundary conditions on the free surface (zero pressure) and body (no normal flow). This method is often called the Frank close fit method.

2.4 Procedure

Here we are attempting to use the strip theory method and extend it to severe sea states in the range of code 6 (Tupper 1996) and above, which involve significant wave heights of 6-9 meters and above.

The equations of motions for six degrees of freedom for a sailing ship, influenced by external loads, are based upon Newton's second law of dynamics. Because of the symmetry of a ship, two uncoupled sets of three coupled equations of motion can be distinguished. In a right-handed co-ordinate system, with the origin in the ship's centre of gravity, these equations read as follows:

$$\sum_{j=1}^{6} \left\{ \left(M_{kj} + A_{kj} \right) \ddot{x}_j + B_{kj} \dot{x}_j + C_{kj} x_j \right\} = X_k \qquad \text{for } k = 1, 2, 3, 4, 5, 6 \tag{3}$$

Where:

k = 1, 3, and 5: Coupled surge, heave and pitch motions

k = 2, 4, and 6: Coupled sway, roll and yaw motions

$\ddot{x}_j$ Acceleration of harmonic oscillation in direction j

The method we employ here is that of a linear impulse-response function method. In this non-linear wave system which is the input is processed using a linear system and the resultant RAOs and A|Φ| are multiplied to obtain the non-linear motion.

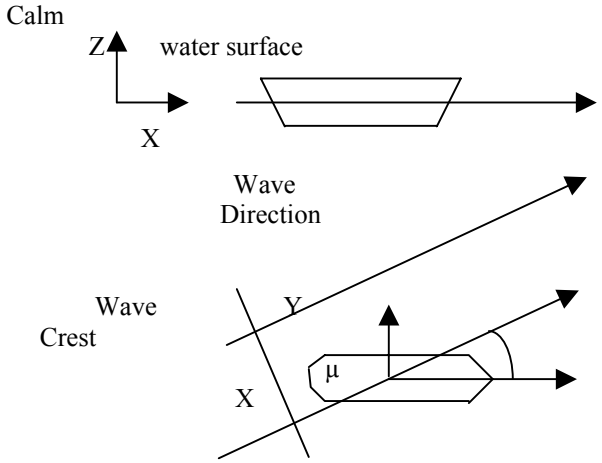

Figure 2-3: The coordinate system

Consider the coordinate system shown in Figure 2-3 above. In this figure the ship motion is considered to undergo six degrees of freedom oscillations about its mean position. The senses of the direction are assumed to be the standard along the three coordinate axes and ξ,η,ζ represent surge, sway and heave respectively whereas ϕ,ψ,χ represent the roll, pitch and yaw motions.

The oblique wave is given by

$$h = ae^{i(\upsilon_0 y\cos\mu + \upsilon_0 y\sin\mu - \omega t)} \qquad (4)$$

With $\omega = \omega_0 - \upsilon_0 U\cos\mu$ (5)

The ship motion in response to this wave is calculated by solving the linear coupled heave-pitch and sway-yaw-roll equations.

$$\begin{pmatrix} \left\{(B_{\zeta\zeta} - \omega^2 M_{\zeta\zeta}) - i\omega N_{\zeta\zeta}\right\} & \left\{(B_{\psi\zeta} - \omega^2 M_{\psi\zeta}) - i\omega N_{\psi\zeta}\right\} \\ \left\{(B_{\zeta\psi} - \omega^2 M_{\zeta\psi}) - i\omega N_{\zeta\psi}\right\} & \left\{(B_{\varphi\varphi} - \omega^2 M_{\psi\psi}) - i\omega N_{\psi\psi}\right\} \end{pmatrix} \begin{pmatrix} \zeta / a \\ \varphi / a \end{pmatrix} = \begin{pmatrix} F_\zeta / a \\ F_\psi / a \end{pmatrix} \qquad (6)$$

$$\begin{pmatrix} (-\omega^2 M_{\eta\eta} - i\omega N_{\eta\eta})(-\omega^2 M_{\chi\eta} - i\omega N_{\chi\eta})(-\omega^2 M_{\phi\eta} - i\omega N_{\phi\eta}) \\ (-\omega^2 M_{\eta\chi} - i\omega N_{\eta\chi})(-\omega^2 M_{\chi\chi} - i\omega N_{\chi\chi})(-\omega^2 M_{\phi\chi} - i\omega N_{\phi\chi}) \\ (-\omega^2 M_{\eta\phi} - i\omega N_{\eta\phi})(-\omega^2 M_{\chi\phi} - i\omega N_{\chi\phi})(-\omega^2 M_{\phi\phi} - i\omega N_{\phi\phi}) \end{pmatrix} \begin{pmatrix} \eta / a \\ \chi / a \\ \phi / a \end{pmatrix} = \begin{pmatrix} F_\eta / a \\ F_\chi / a \\ F_\phi / a \end{pmatrix} \quad (7)$$

Where the time factor $e^{-i\omega t}$ is omitted in both cases.

In the first matrix B, M and N represent the restoring, inertial and damping forces per unit displacement, acceleration, and velocity respectively. The inertial term M in the diagonal elements represent virtual mass. The off diagonal elements indicate cross coupling terms in which the first subscript represents the mode of motion, whereas the second the mode of induced force. The second column matrix in the equation represents the RAOs while the third column indicates the wave exciting forces.

The relative motions between the motion of the at-rest waterline and the adjacent surface of the wave both on weather and leeward sides is obtained by solving the equations (3) and (4) and using it with the hydrodynamic pressure distribution along the mean waterline.

The dynamic swell-up (Kim et al 1980) or the wave elevation due to the hydrodynamic pressure along the at-rest waterline is given by

$$\frac{P_{DS}}{\rho g a} = \frac{(P_I + P_D + P_R)}{\rho g a} \quad (8)$$

The vertical motion $Z_\pm$ of the at-rest waterline itself is given by

$$Z_\pm(x) = \zeta - x\psi + \frac{iU}{\omega}\psi \pm \frac{B(x)}{2}\phi \quad (9)$$

Where $\pm$ indicates the right and left sides of the ship section along the waterline, respectively, whereas $\frac{B(x)}{2}$ indicates the half section beam in the water plane. Hence,

the relative motion between the at-rest waterline and the adjacent surface of the wave (dynamic swell-up) is given by

$$\frac{r_{\pm}}{a} = \frac{P_{DS\pm}}{\rho g a} - \frac{z_{\pm}}{a} \qquad (10)$$

2.5 The ship motion program

Dr. C.H. Kim developed the ship motion program SHMB5, which implements the linear strip theory. The same has been modified and upgraded to the latest version and is used to compute the relative motions in head as well as beam sea conditions using other relevant sub routines.

The program uses the strip theory as the basis for the estimation of sectional forces and bending moments. For modeling the hull the Frank close fit (employing the singularities on the contour) technique is employed.

The main program has a module known as SHMB5 that computes the basic ship motions in regular oblique waves. The program PRDMR5 calculates the relative motions using the data generated of the main module of SHMB5.

The much tested and analyzed typical SL-7 containership data is considered for the present study. For the analysis purpose, especially for the zero speed condition this model can be considered to bear close similarities in terms of the relative motion characteristics of a moored FPSO.

2.6 Computational methodology

The data obtained from the wave generation in KRISO (Korea Research Institute of Ships and Ocean Engineering) had datasets for wave heights 3.0, 4.0, 6.0, 7.0, 9.0 and 11.0 respectively. The wave heights of 3.0 and 4.0m respectively follow the ITTC

spectrum whereas others follow JONSWAP spectrum. The peaked ness parameters and zero-crossing periods for the same where given and are listed in Table 2-1.

Table 2-1 KRISO data for input wave spectrum (2000)

Data No.	Sea State	Proto		Model		γ	Remarks
		Hs (m)	Tz/Tp	Hs (m)	Tz/Tp		
#042	**A1**	4.0	8.0/11.26	0.073	1.079/1.519	**1.0**	**ITTC**
#010	**A2**	6.0	9.5/12.09	0.109	1.281/1.630	**1.5**	**JONSWAP**
#014	**B1**	7.0	9.5/12.09	0.127	1.281/1.630	**2.0**	**JONSWAP**
#020	**B2**	9.0	10.0/12.73	0.164	1.348/1.717	**2.5**	**JONSWAP**
#028	**B3**	11.0	10.5/13.37	0.200	1.416/1.803	**2.5**	**JONSWAP**
#043	**C1**	3.0	8.0/11.26	0.055	1.079/1.519	**1.0**	**ITTC**

Tz : zero-upcrossing period
Tp : peak period

2.6.1 ITTC spectrum

The 15th International Towing Tank Conference recommended the use of a form of the Bretschneider spectrum for average conditions and not fully developed seas, given the wave height and modal period as

$$S(\omega) = \frac{A}{\omega^5} \exp \frac{-B}{\omega^4} \qquad (11)$$

Where A and B are constants and which can be calculated once the significant wave heights $\zeta_{\frac{1}{3}}$ and characteristic period T_1 is known using the relation:

$$A = \frac{173\zeta_{\frac{1}{3}}^{2}}{T_1^4} \qquad B = \frac{691}{T_1^4} \qquad (12)$$

2.6.2 JONSWAP spectrum

The Joint North Sea Wave Project (JONSWAP) was carried out in 1968 along a line extending over 100 miles (160 km) into the north sea from the Sylt Island, Germany. From an analysis of the reportedly about 2000 wave records, (Hasselmann 1975) derived JONSWAP spectrum being representative of wind-generated seas with a fetch limitation.

For simplicity as well as consistency with the sea-keeping performance assessment, it is desirable to have a modified version of JONSWAP spectrum that depends on only the significant wave height and modal period for a given γ , but as is the case with the usual fetch-dependent JONSWAP spectrum. The modified (Lee and Bales, 1980) JONSWAP spectrum for the average value of γ = 3.3. When γ is variable, it is expressed:

$$S(\omega) = \frac{5}{16} H_s^2 \omega_m^4 \omega^{-5} \exp\{-1.25(\frac{\omega_m}{\omega})^4\}(1 - 0.287\ln\gamma)\gamma^{\exp\left[-\frac{(\omega-\omega_m)^2}{2\sigma^2\omega_m^2}\right]} \qquad (13)$$

Where $\omega_m = \left(\frac{3}{5}\right)^{1/4} \frac{2\pi}{T_p}$

The above is a modified JONSWAP that is identical to Bretschneider spectrum multiplied by the enhancement term with the factor $(1 - 0.287\ln\gamma)$. This is widely used as a standard form when no specific information is available for α . The above formula is a three paramter spectrum of *Hs* , T_m and γ , or two-parameter spectrum with a given overshoot parameter γ .

The components of the input wave spectrum namely amplitude, frequency and phase angle are obtained by applying Fourier transformation. The frequency range for which spectral amplitudes are prominent is selected. For the given ship model [SL-7 containership] in zero speed/moored condition the motion RAOs in the heave, pitch and relative motion are estimated using the ship motion program. The RAO is of complex nature and can be separated into real and imaginary parts. The phase angle for the RAO is also obtained.Once we have obtained the above, the response time series is obtained by the relation.

$$\begin{aligned} &\mathrm{Re}\left\{\sum_{j=1}|Aj||RAO|e^{i(\omega_j t-\phi_j-\varepsilon_j)}\right\} \\ &=\sum_{j=1}|Aj||RAO|\cos(\omega_j t-\phi_j-\varepsilon_j) \qquad (14) \\ &\mathrm{Rel}(t)=\sum_{j=1}|Aj||RAO|e^{i(\omega_j t-\phi_j-\varepsilon_j)} \end{aligned}$$

An attempt is made here to statistically compare the response from the theoretical linear wave theory and the non-linear response obtained through the UNIOM approach. Since we know the spectrum of the input wave we can obtain the corresponding spectral densities, which would give the response spectrum through the relation:

$$S_{yy}(\omega)=|G(\omega)|^2 S_{xx}(\omega) \qquad (15)$$

From this the statistical parameters such as the variance, standard deviations etc are calculated and used in suitable equations to obtain Rayleigh probability of exceedance. The statistical study of the above response time series would help in predicting the accuracy of two dimensional wave theories when applied to non-linear wave and its corresponding response phenomena.

3 ANALYSIS METHODOLOGY

3.1 Impulse analysis

The analysis of the response was carried out mainly for the head sea and beam sea conditions. The various sea states are commonly indicated by the significant wave heights, which define the sea severity. The common classification of the sea states is given in Table 3-1.

Table 3-1: Sea states and codes

Code	Description of sea	Hs (m)
0	Calm (glassy)	0
1	Calm (rippled)	0.00—0.10
2	Smooth (wavelets)	0.10—0.50
3	Slight	0.50—1.25
4	Moderate	1.25—2.50
5	Rough	2.50—4.00
6	Very rough	4.00—6.00
7	High	6.00—9.00
8	Very high	9.00—14.00
9	Phenomenal	Over 14.00

The input for the analysis is the time series of the wave data for different significant sea states. The wave data obtained is converted into the frequency domain using the fourier transform. The computation of fourier coefficients for any time domain data $\eta(t)$ for a total time interval of T would be as:

$$\eta(t) = A_0 + \sum_{n=1}^{\infty} \left(A_n \cos \omega_n t + B_n \sin \omega_n t \right) \qquad (16)$$

Where

$\omega_1 = 2\pi/T, \quad f = 1/T = \Delta t$ The fundamental frequency

$\omega_n = n\,\omega_1, \; f_n = n\, f_1$ n^{th} harmonic frequency

$\omega_n = 2\pi f_n$

For the zero mean case, the time series can be considered as

$$\eta(t) = \mathrm{Re}\sum_{n=1}^{\infty}(A_n - iB_n)e^{i\omega_n t} \qquad (17)$$

The fourier transformation can be carried out using the Fast Fourier Transform (FFT) routine in MATLAB where the first term in the result would yield A_0 and the rest of the terms would yield the real and imaginary parts of the eqn (17). The results of MATLAB do not consider the time interval Δt and hence the actual result gives N pairs of amplitude and phase angle with the omission of Δt. Hence the value returned by the routine needs to be divided with N which is the total number of records. Since the first N/2 are the required solutions from the FFT and rest of the records are symmetric and redundant, they alone are considered. Thus the transformation of the time series data yields the various frequencies of the time series as well as the corresponding amplitude and phase angles.

The linear transfer function or Response Amplitude Operators (RAOs) as they are commonly called are estimated from the ship motions program SHMB5. The linear transfer function or frequency response function can be defined as the ratio of the output response amplitude to that of the input amplitude and is given as

$$G(\omega) = \frac{A_{out}(\omega)}{A_{in}(\omega)} \qquad (18)$$

Or in other words the ratio of the output fourier transform to that of the input can be called as a linear frequency response function or RAO. The RAOs, which are considered for the analysis, are obtained for station #1 of the SL-7 container and is used for the analysis of response.

3.2 Response analysis

Once we have the input wave information completely in the frequency domain we can use the Linear Transfer Function to obtain the response (heave, pitch and relative motion). The RAOs are multiplied with the amplitudes obtained in the frequency domain transformation and are applied with the various frequencies and phase angles to obtain the time history of response over the entire range. The response time series is obtained from the relation

$$\mathrm{Rel}(t) = \sum_{j=1} |Aj||RAO| e^{i(\omega_j t - \phi_j - \varepsilon_j)} \tag{19}$$

The various response time series for the various degrees of freedom are obtained by using the relevant RAOs. Here we are analyzing the heave, pitch and relative motion using the corresponding RAOs from the ship motion program.

3.3 Spectral response analysis

Since each of the significant wave heights follows a particular spectrum, the spectral response analysis is carried out using the corresponding equations discussed in section 2. The spectra thus obtained are multiplied with the RAOs obtained from the ship motion program using the relation in equation (15) to obtain the theoretical response for the sea state described. The variance m_0 for the spectrum is the area under the curve for the spectrum obtained. The variance is ideally calculated for any data as

$$\sigma_x^2 = E[(x-\mu_x)^2] = \frac{1}{T}\int_0^T (x-\mu_x)^2 dt = \frac{1}{N-1}\sum_{j=1}^{N}(x_j-\mu_x)^2 \qquad (20)$$

Where σ_x^2 is the variance m_0 and μ_x is the mean value. Generally, the spectral moment of one-sided spectra:

$$m_0 = \int_0^\infty S(\omega)d\omega \qquad (21)$$

Where m_n is nth moment of the area under the one-sided spectrum S(ω) and where n normally varies from 0 to 4.

$$\sigma_x = \sqrt{m_0},\ \sigma_{\dot{x}} = \sqrt{m_2},\ \sigma_{\ddot{x}} = \sqrt{m_4} \qquad (22)$$

Once the variance is obtained from the spectral response we can calculate the rayleigh probability of exceedence, which exceeds any reference peak 'a' as

$$\Pr\{peaks \geq a\} = \exp\left(-\frac{a^2}{2m_0}\right) \qquad 0 \leq a \leq \infty \qquad (23)$$

The rayleigh probability of exceedence for the positive peak is compared with the experiments results of the peak response values obtained.

3.4 Zero crossing analysis

The output response data from the time domain approach, which is highly non-linear, is subject to zero crossing analysis to obtain the corresponding crest heights and trough depths. Once they are obtained the probability of exceedence values for the experimental response values are calculated. The FORTRAN routine for the estimation of zero crossing values is used which gives the crest heights as well as periods.

The MATLAB routine, which is attached in the appendix, calculates the exceedence of a particular peak value and estimates its corresponding probability. The

values of the experimental probability of exceedence and the analytical one is plotted for analyzing the probability prediction of the theory compared to that of experiment. This procedure is carried out for all the wave data sets and for both head sea as well as beam seas.

3.5 Most probable peak analysis

From the total observations, we can determine the most probable value among the total N observations. The probability of a value exceeding the maximum value among N observations is 1/N we can determine the maximum probability using the relation

$$\frac{1}{N} = \exp\left[\frac{-a_N^2}{2m_0}\right] \qquad (24)$$

From this we can determine the most probable maximum value from all the observations

$$\hat{a}_N = \sqrt{2 \ln N}\sqrt{m_0} \qquad (25)$$

Where m_0 is the variance of the response motion given by

$$m_0 = \int_0^\infty S(\omega) d\omega \qquad (26)$$

And where $$N = 3600 / Tz \qquad (27)$$

$$Tz = 2\pi\sqrt{\frac{m_0}{m_2}} \qquad (28)$$

The most probable peak is thus obtained for both theoretical and experimental response data and is compared for the various significant wave heights. Here we have used data for a one-hour simulation (3600 sec) with time series representative of the actual sea state.

4 ANALYSIS RESULTS

The data is analyzed under two main sections of head sea and beam sea conditions. The head sea [180º heading] and beam sea [90º heading] are analyzed for all the data sets of input wave data. Here we have restricted the discussion to 1) linear and 2) non-linear cases. The sea states such as Hs =3.0 meters and 6.0 meters would be closely approximated to linear wave conditions. The analysis of such data sets for response motion using the UNIOM approach yields fairly reasonable results between the theory and experiment.

4.1 Head sea condition

The head sea conditions are analyzed for the ship heading in the 180 degree direction to the assumed coordinate axis. The location where the data is analyzed is the station#1, which is the forward end on the SL-7 container model.

4.1.1 Case #1: Hs = 3.0 m

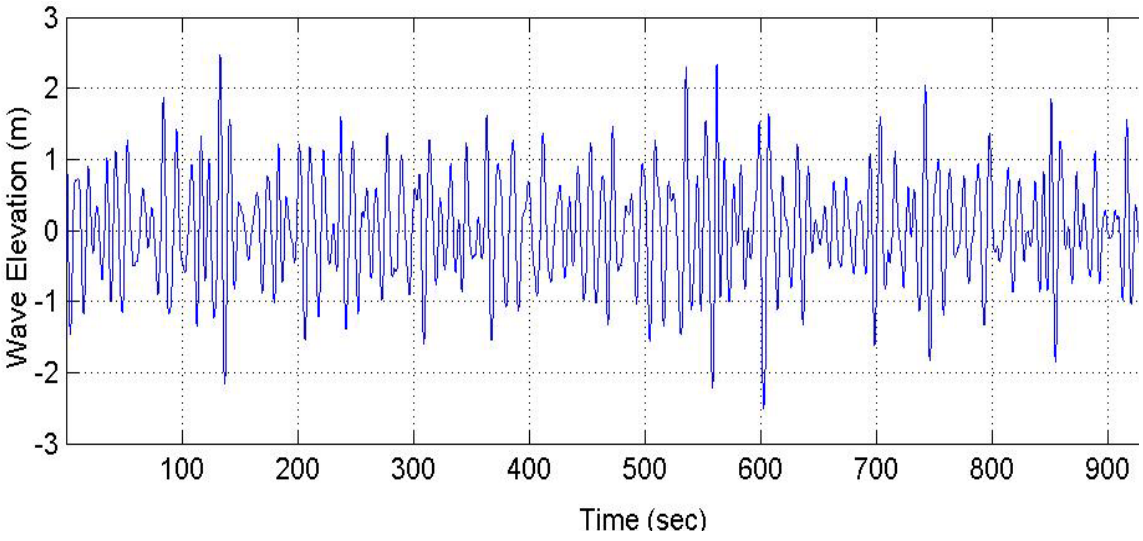

Figure 4-1: Head sea-Hs 3.0m-input wave data, heave, pitch and relative response

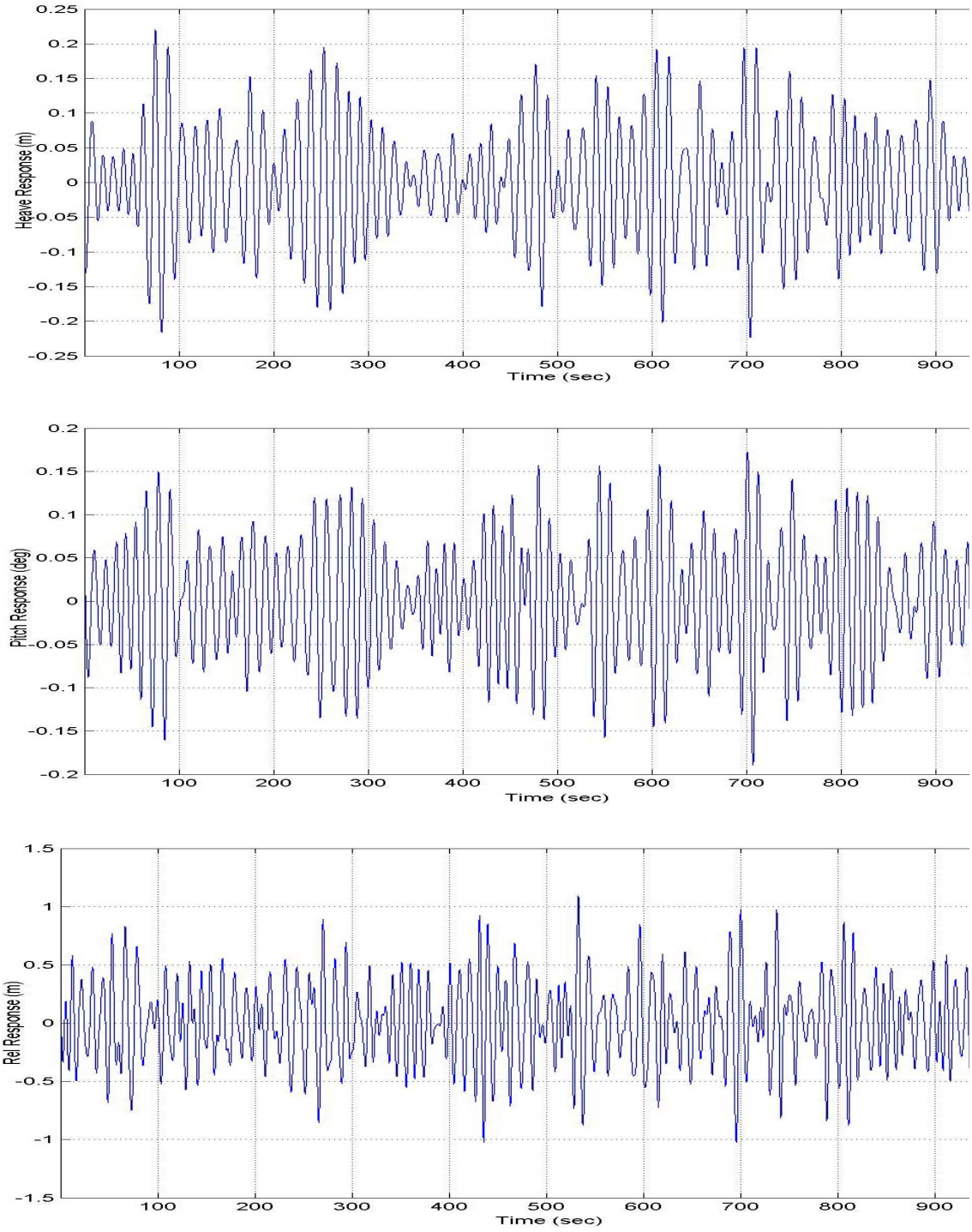

Figure 4-1: Continued

It can be observed in Figure 4-1 that the maximum wave elevation is observed to be around 2.5 meters. The heave response is considerably very low and is close to 0.22 meters. The relative motion response is seen to be much higher and is approximately equal to 1.1 meters.

The probability of exceedence comparison is shown in Figure 4-2 for the input experimental wave. It shows that the theory bears a close contour with the measured results showing the accuracy of the model wave generated.

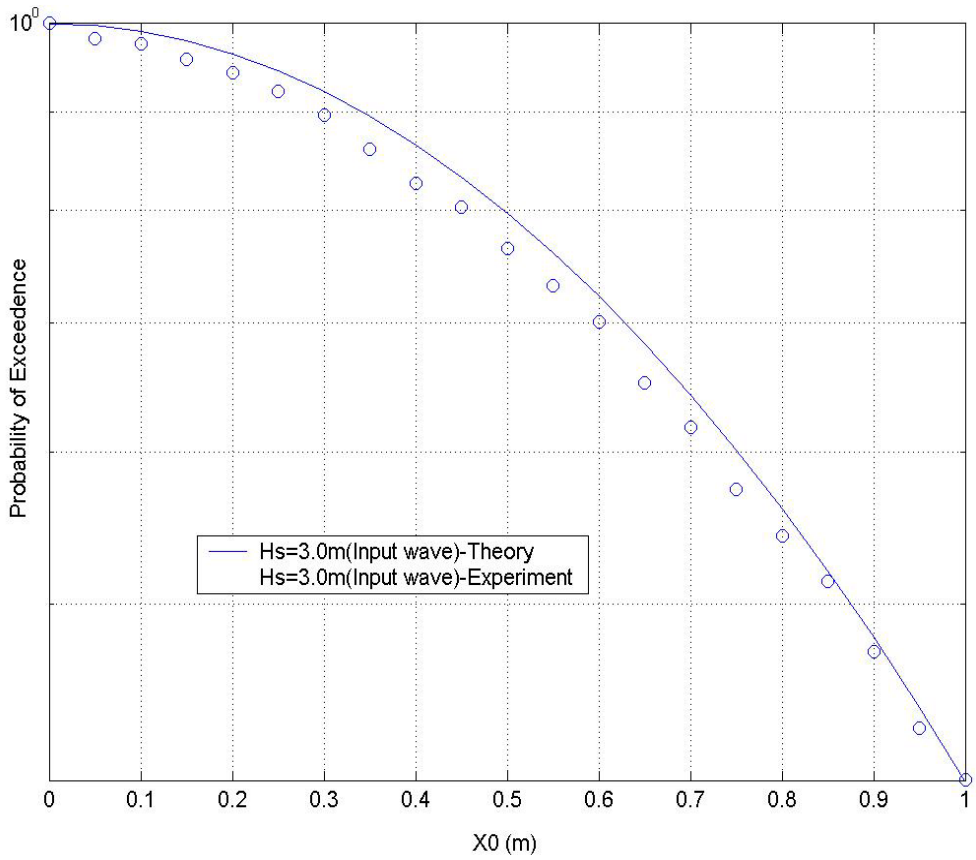

Figure 4-2: Head sea-Hs 3.0m-probability of exceedence for input wave

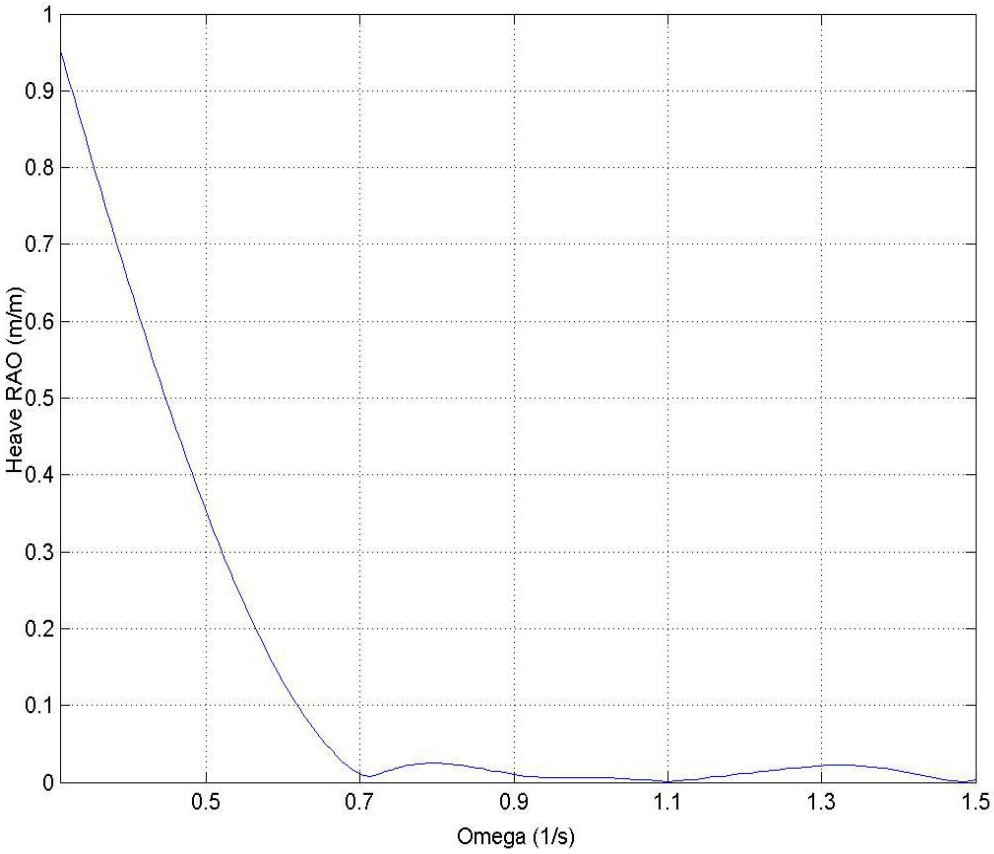

Figure 4-3: Head sea-Hs 3.0m-heave RAO

The heave RAOs for the corresponding omega values is plotted as shown in Figure 4-3. For frequency range from 0.7-1.5 the heave RAO falls drastically showing that the heave response is predominantly due to the low frequency motions.

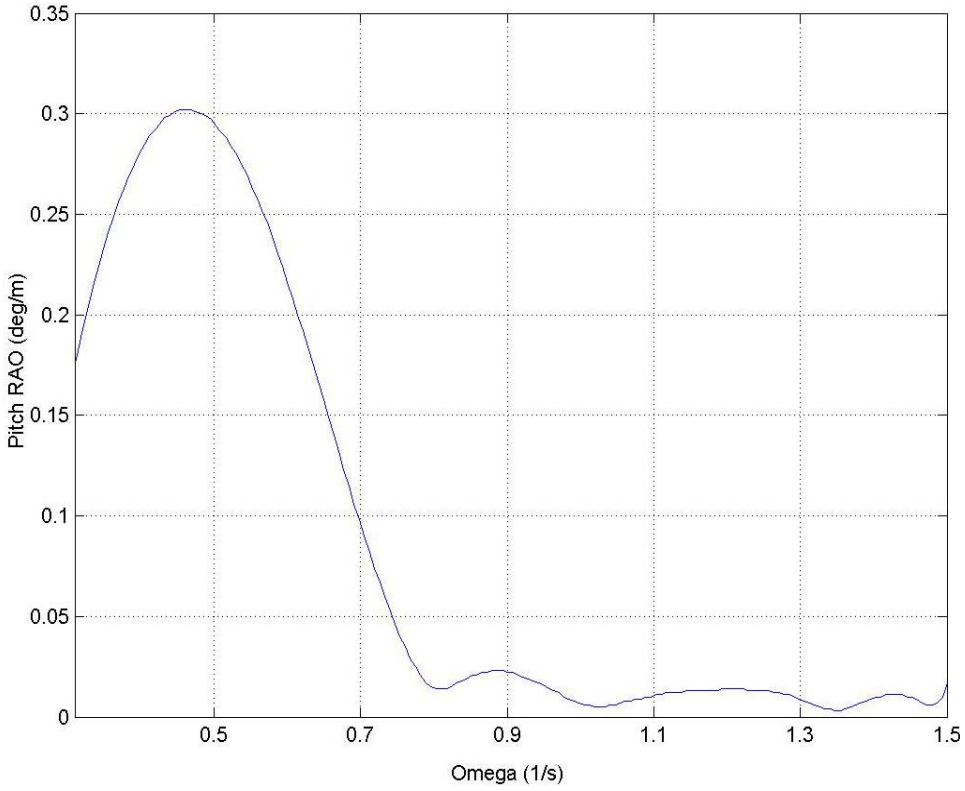

Figure 4-4: Head sea-Hs 3.0m-pitch RAO

The pitch RAO shown in Figure 4-4 also shows the similar trend where the predominant pitch motion is due to the low frequency or long wave response. The pitch RAO shows a peak value at around a frequency of 0.4 rad/sec and falls drastically for increasing frequencies.

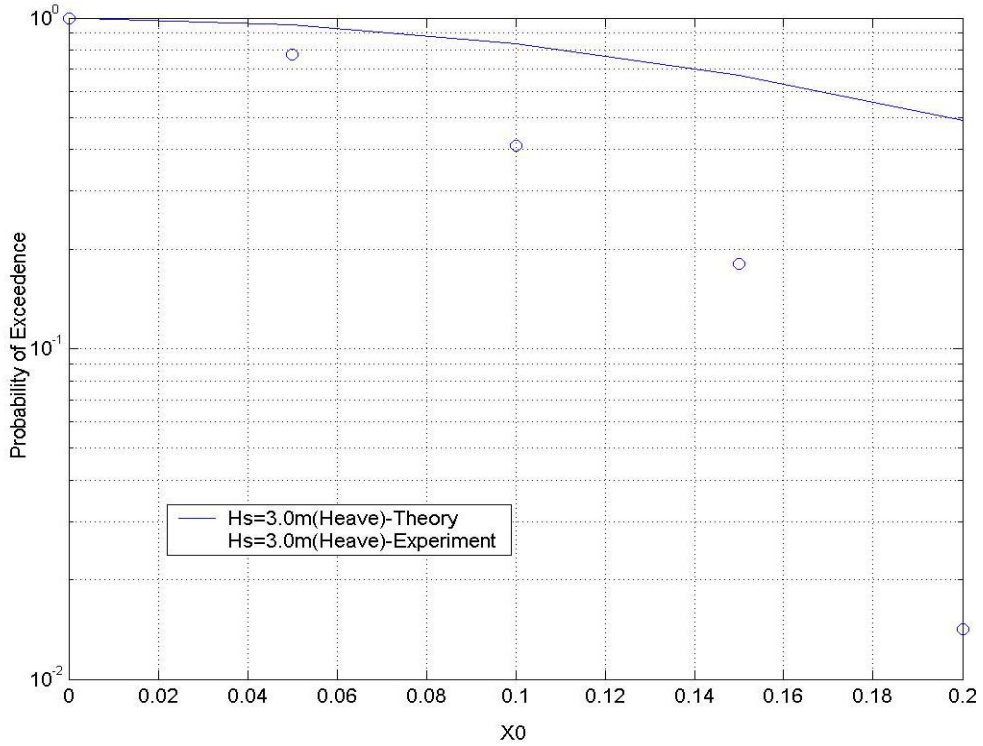

Figure 4-5: Head sea-Hs 3.0m-heave probability of exceedence

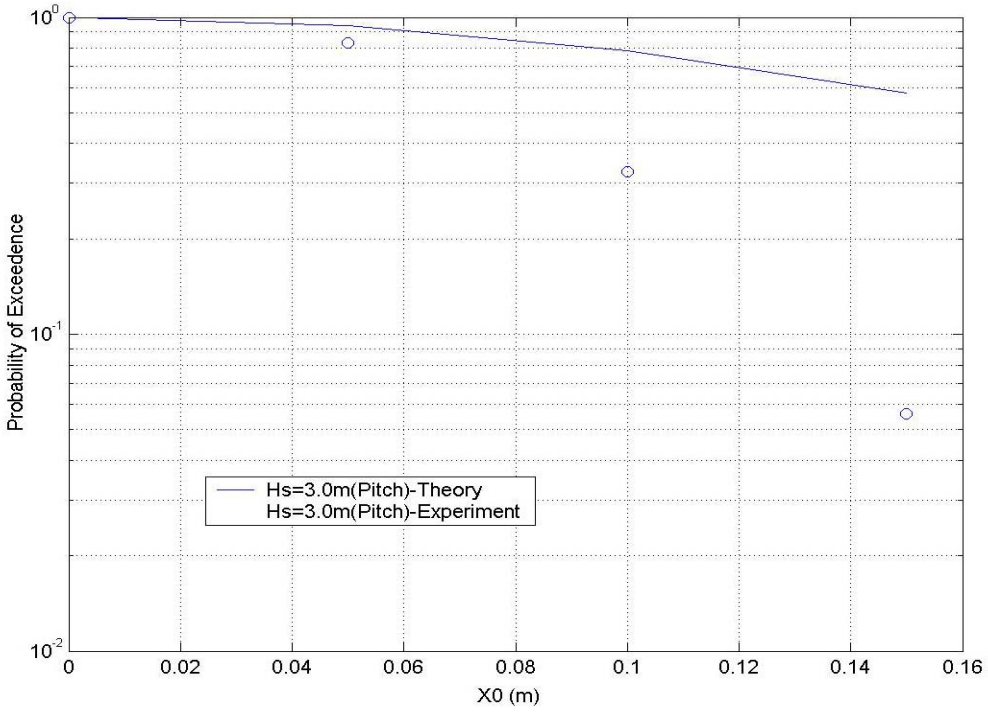

Figure 4-6: Head sea-Hs 3.0m-pitch probability of exceedence

The probability of exceedence values for heave and pitch which are shown in Figure 4-5 and Figure 4-6 describe the trend which are indicative of how much the theory over estimates over the actual or experimental results. The probability of exceedence values for the heave motions is ranging from X0 values of 0 to 0.20, which is the maximum value of the heave response. The probability is plotted over the log scale and can be seen to represent the actual trends of probability for the theory compared to that of the field response data.

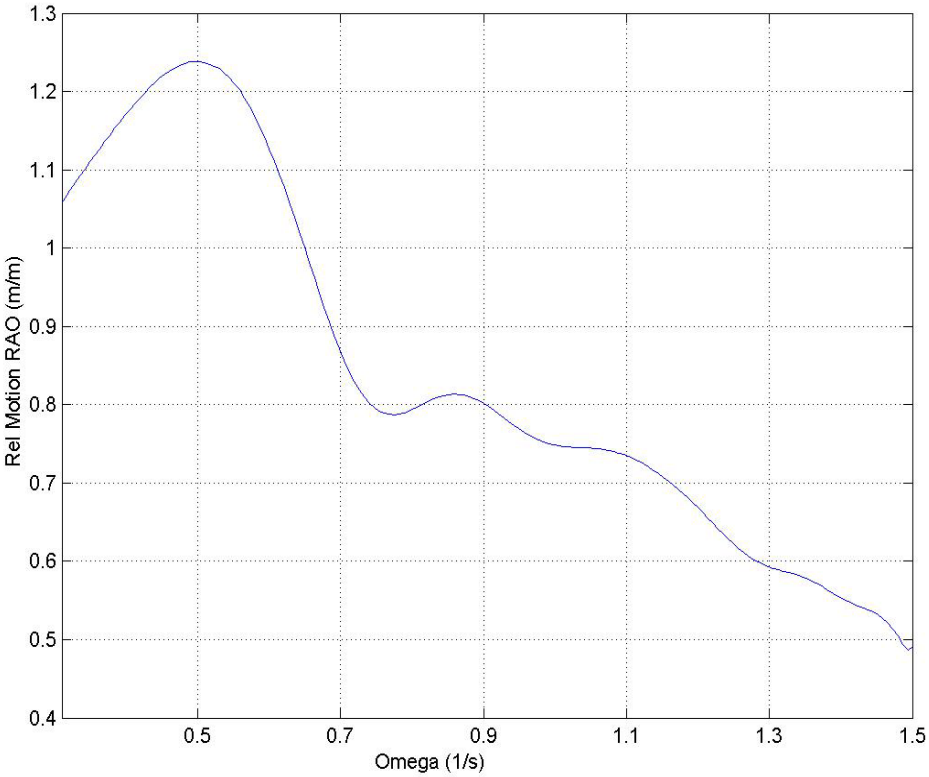

Figure 4-7: Head sea-Hs 3.0m-relative motion RAO

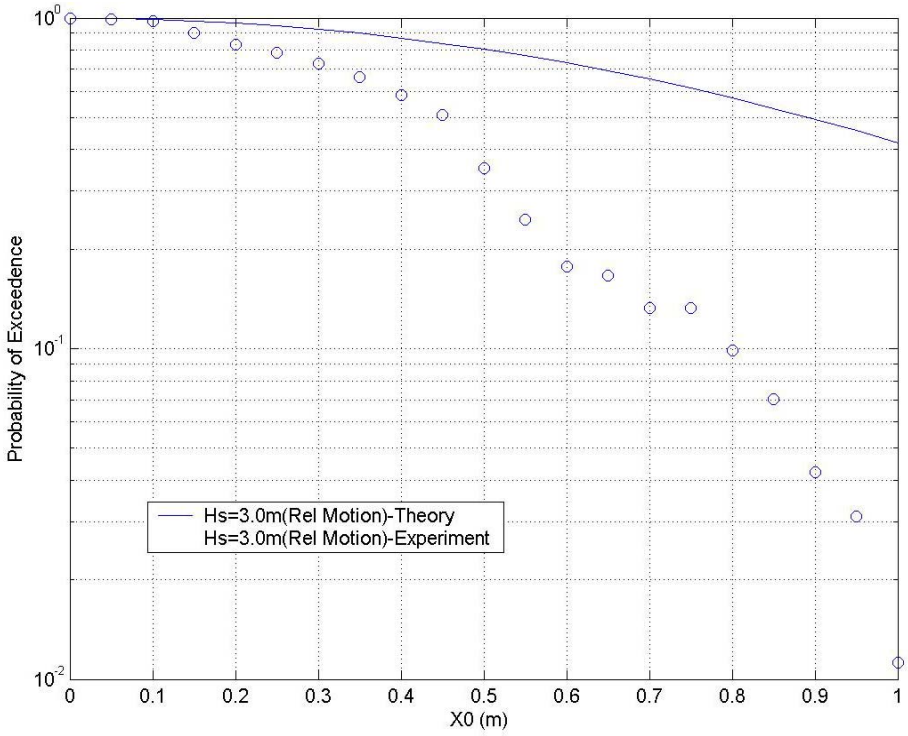

Figure 4-8: Head sea-Hs 3.0m-relative motion probability of exceedence

The relative motion RAO shown in Figure 4-7 also follows more or less a similar trend with peak value of response occurring at a frequency of 0.5 rad/sec and then falling off abruptly over increasing frequencies. The trend in Figure 4-8 indicate that the low frequency motions are more predominant and have an important impact on the relative motion response as well.

4.1.2 Case #2: Hs =6.0 m

This significant wave height, which falls in the category of sea state 6, can be approximated with a fair accuracy as a linear wave system. The wave data here follows the JONSWAP spectrum unlike the Hs = 3.0 m case where it was following the ITTC spectrum. The response is expected to increase with significant sea states and can be observed in Figure 4-9.

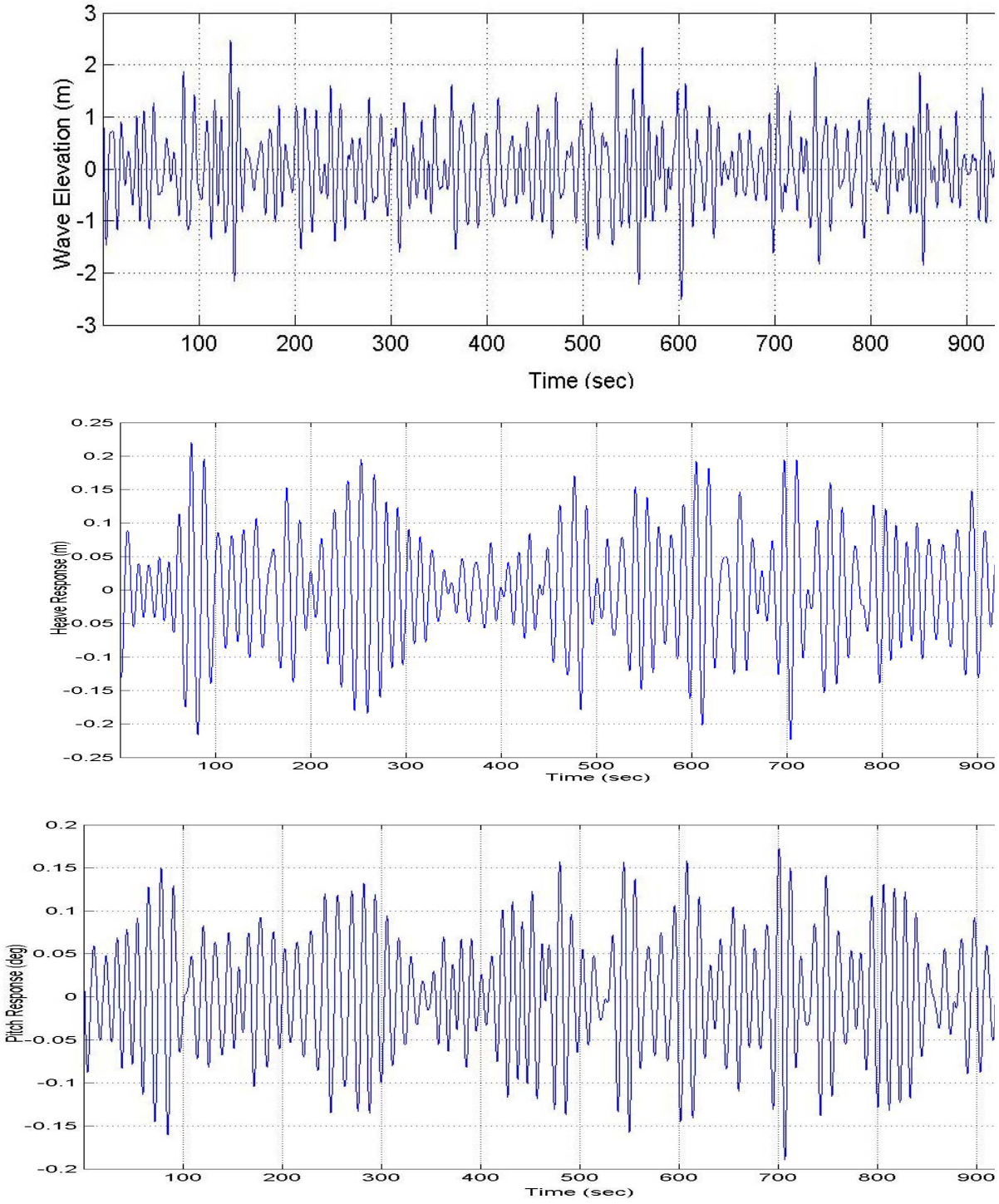

Figure 4-9: Head sea-Hs 6.0m-input wave data, heave, pitch and relative response

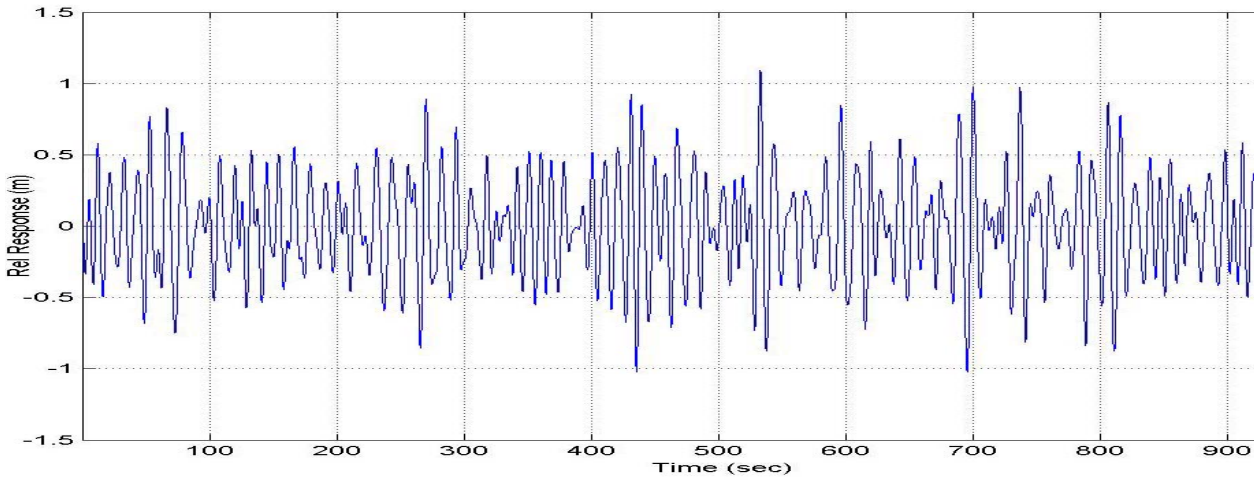

Figure 4-9: Continued

From the data set for the input wave shown in Figure 4-10 it can be seen that the maximum wave elevation would be around 2.6 meters and corresponding heave response is only around 0.25 meters. The pitch response also is seen to be somewhere close to 0.15 deg. The relative response values for this sea state is around 1.1 meters and is also mainly due to the low frequency response.

The probability of exceedence comparison is shown in Figure 4-11 for the input experimental wave. It shows that the theory bears a close contour but deviates slightly for higher values of X0 showing the non-linear effects of the input wave data.

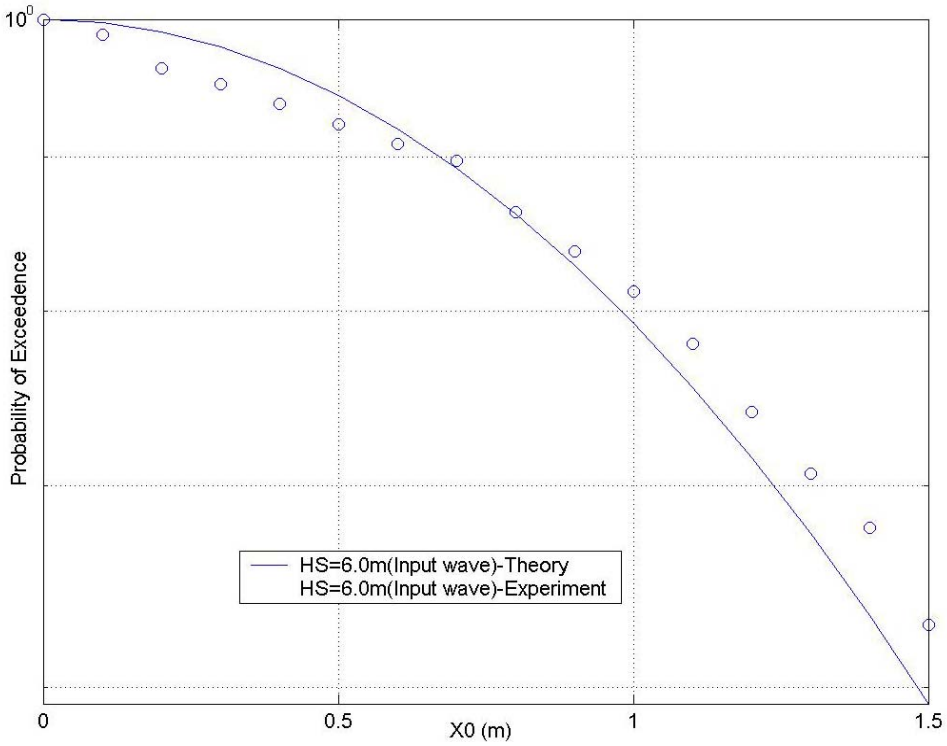

Figure 4-10: Head sea-Hs 6.0m-probability of exceedence for input wave

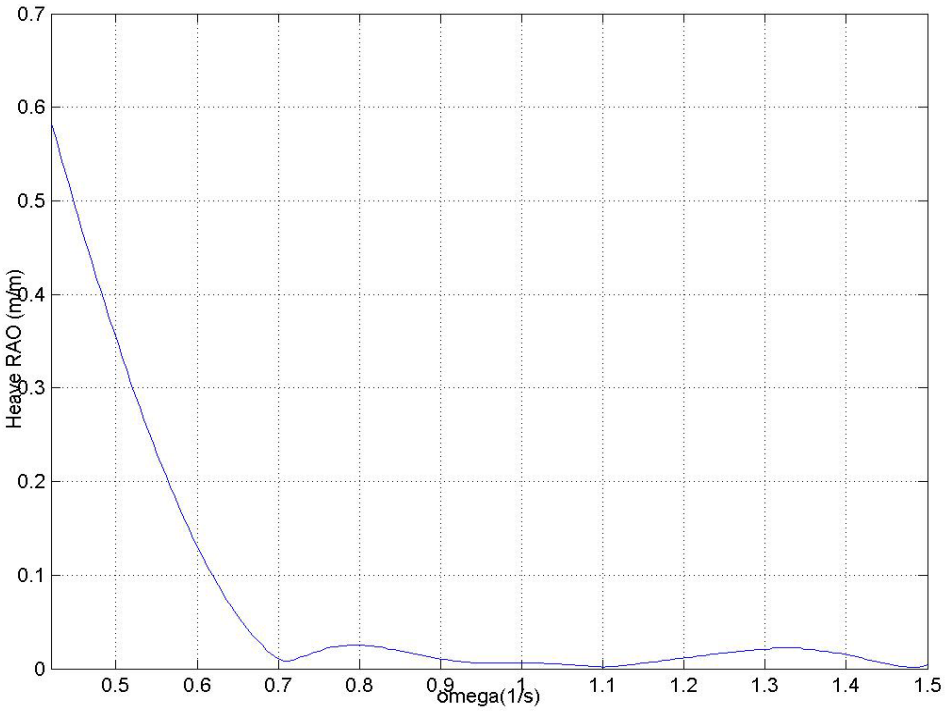

Figure 4-11: Head sea-Hs 6.0m-heave RAO

The heave RAOs for the corresponding omega values is plotted in Figure 4-12. For frequency range from 0.7-1.5 the heave RAO falls drastically showing that the heave response is predominantly due to the low frequency motions.

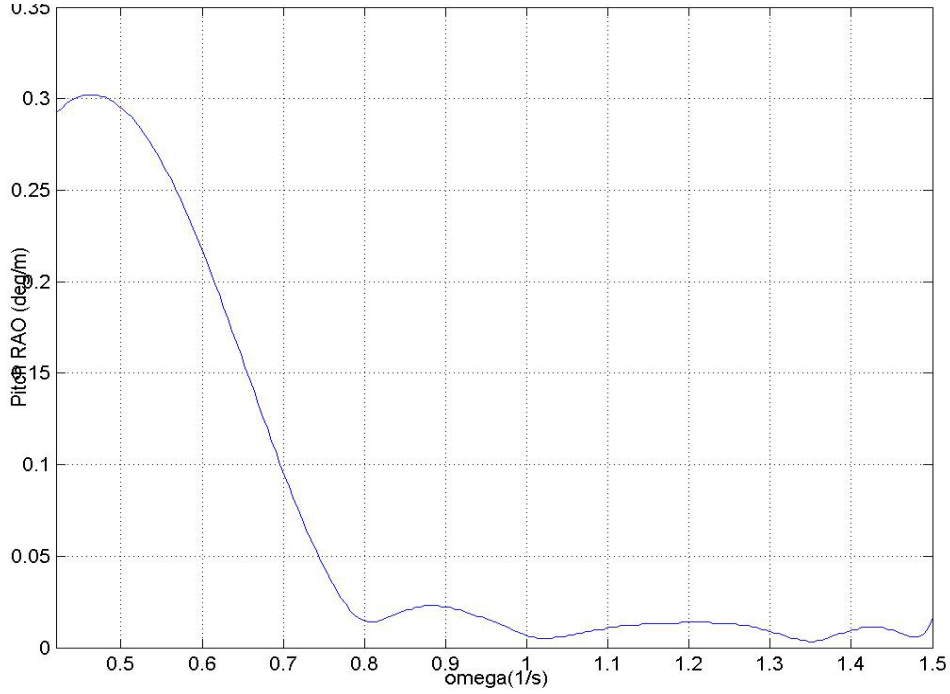

Figure 4-12: Head sea-Hs 6.0m-pitch RAO

The pitch RAO also shown in Figure 4-13 shows the similar trend but the RAO falls real low at a frequency of 0.8 rad/sec. Here again the predominant pitch motion is due to the low frequency or long wave response. The pitch RAO shows a peak value at around a frequency of 0.4 rad/sec and falls drastically for increasing frequencies.

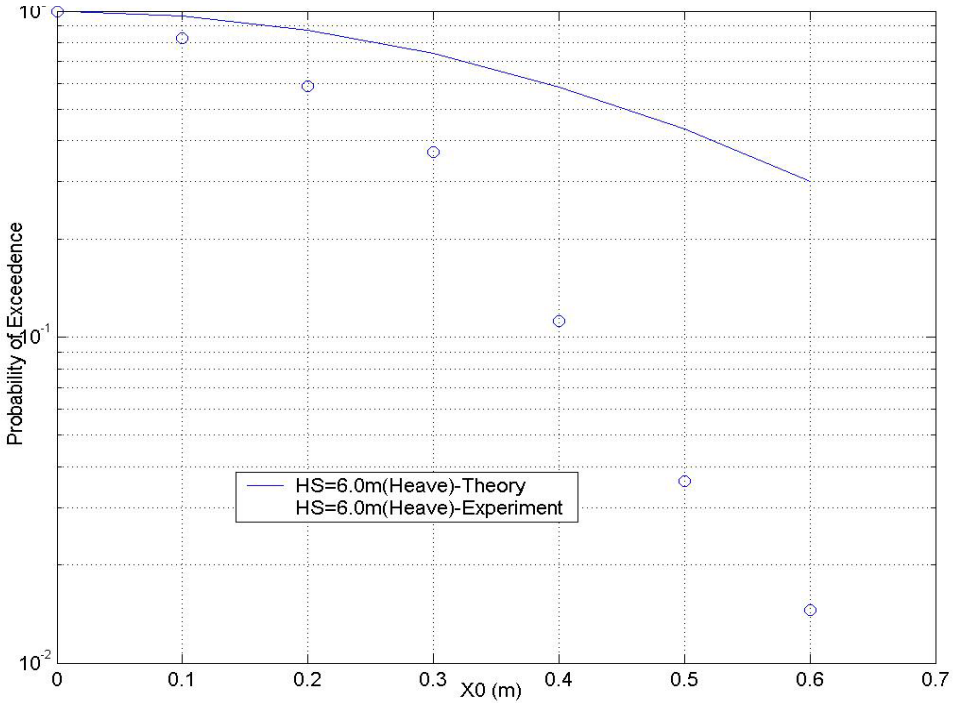

Figure 4-13: Head sea-Hs 6.0m-probability of exceedence for heave motion

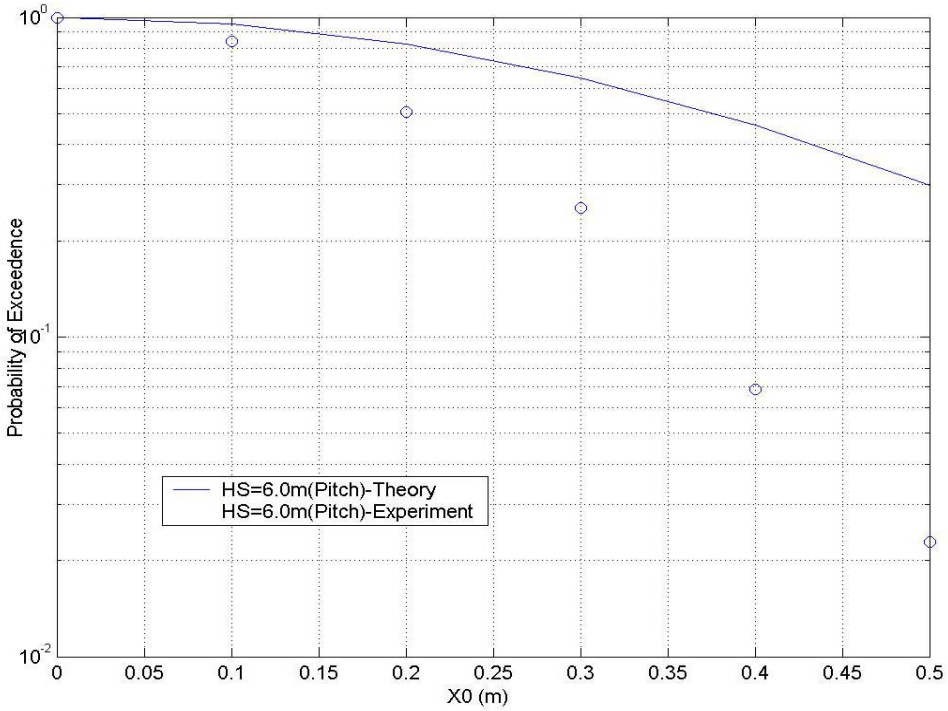

Figure 4-14: Head sea-Hs 6.0m-probability of exceedence for pitch motion

The probability of exceedence values for heave and pitch as shown in Figure 4-14 and Figure 4-15 describe the trends which are indicative of how much the theory over estimates over the actual or experimental results. The probability of exceedence values for the heave motions is ranging from X0 values of 0 to 0.60, which is the maximum value of the heave response. The probability is plotted over the log scale and can be seen to represent the actual trends of probability for the theory compared to that of the field response data.

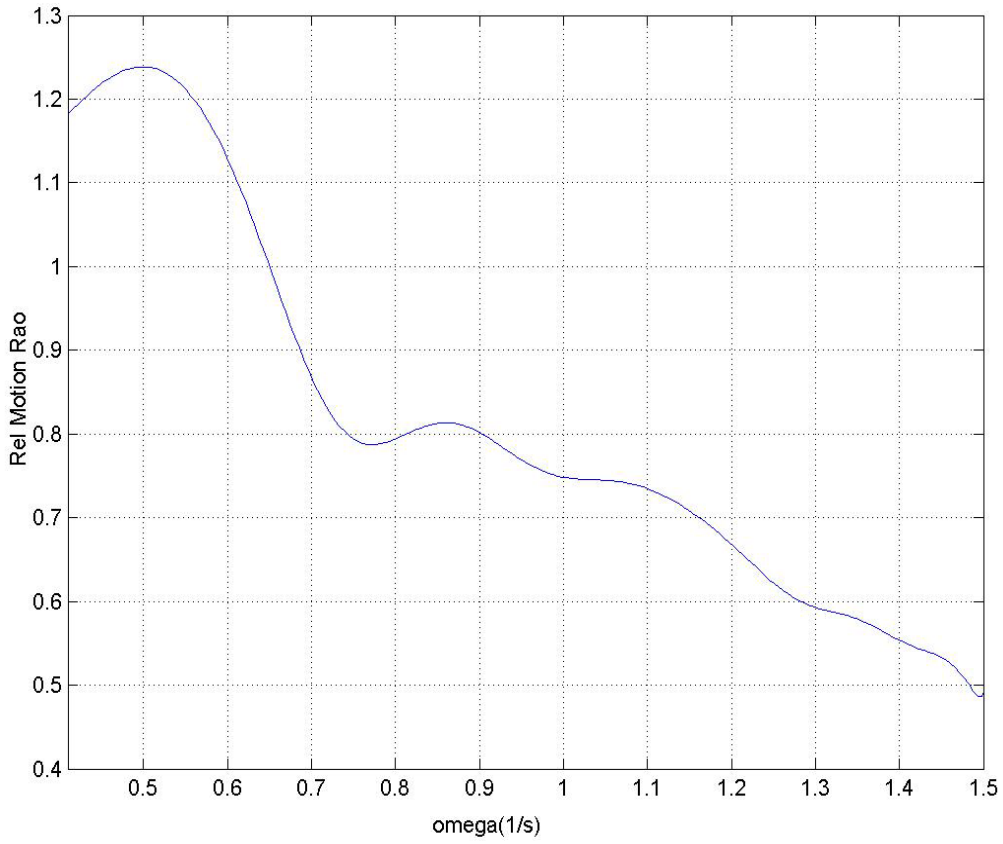

Figure 4-15: Head sea-Hs 6.0m-relative motion RAO

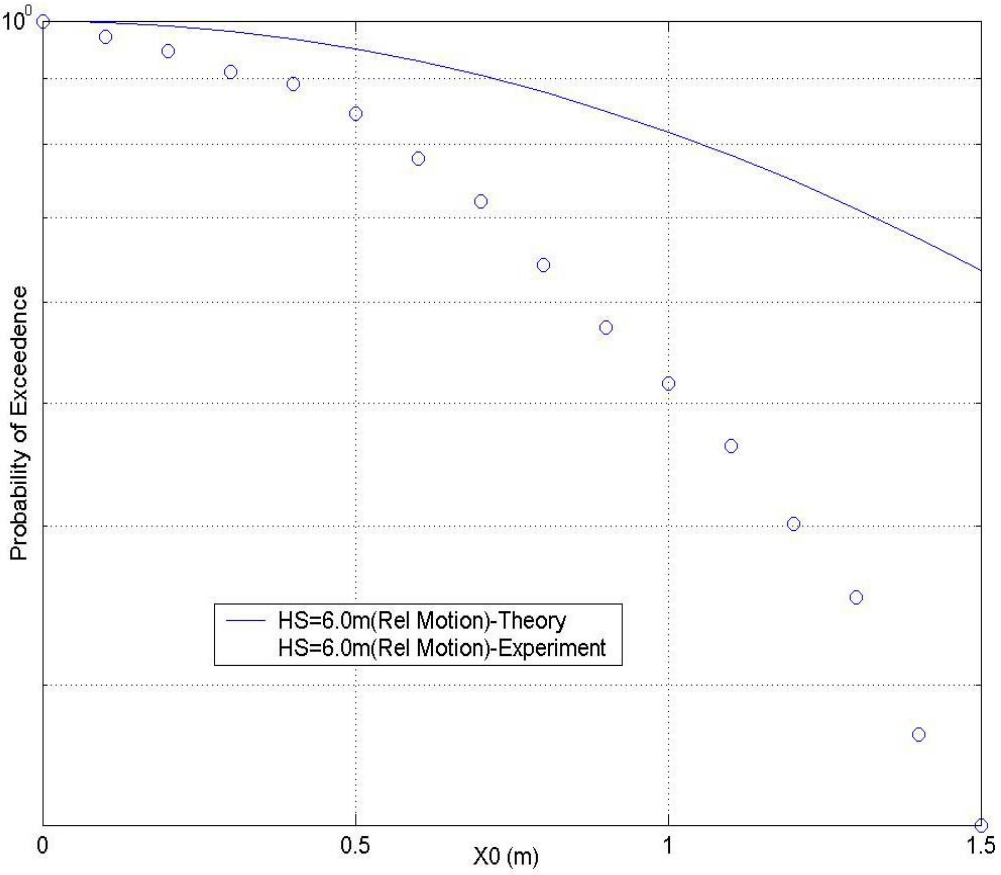

Figure 4-16: Head sea-Hs 6.0m-probability of exceedence for relative motion

The relative motion RAO shown in Figure 4-16 also follows more or less a similar trend with peak value of response occurring at a frequency of 0.5 rad/sec and then falling off abruptly over increasing frequencies. The trend indicates that the low frequency motions are more predominant and have an important impact on the relative motion response as well.

The probability of exceedence for the relative motion in Figure 4-17 show that the theoretical estimates are definitely much above the actual results.

4.1.3 Case #3: Hs = 9.0 m

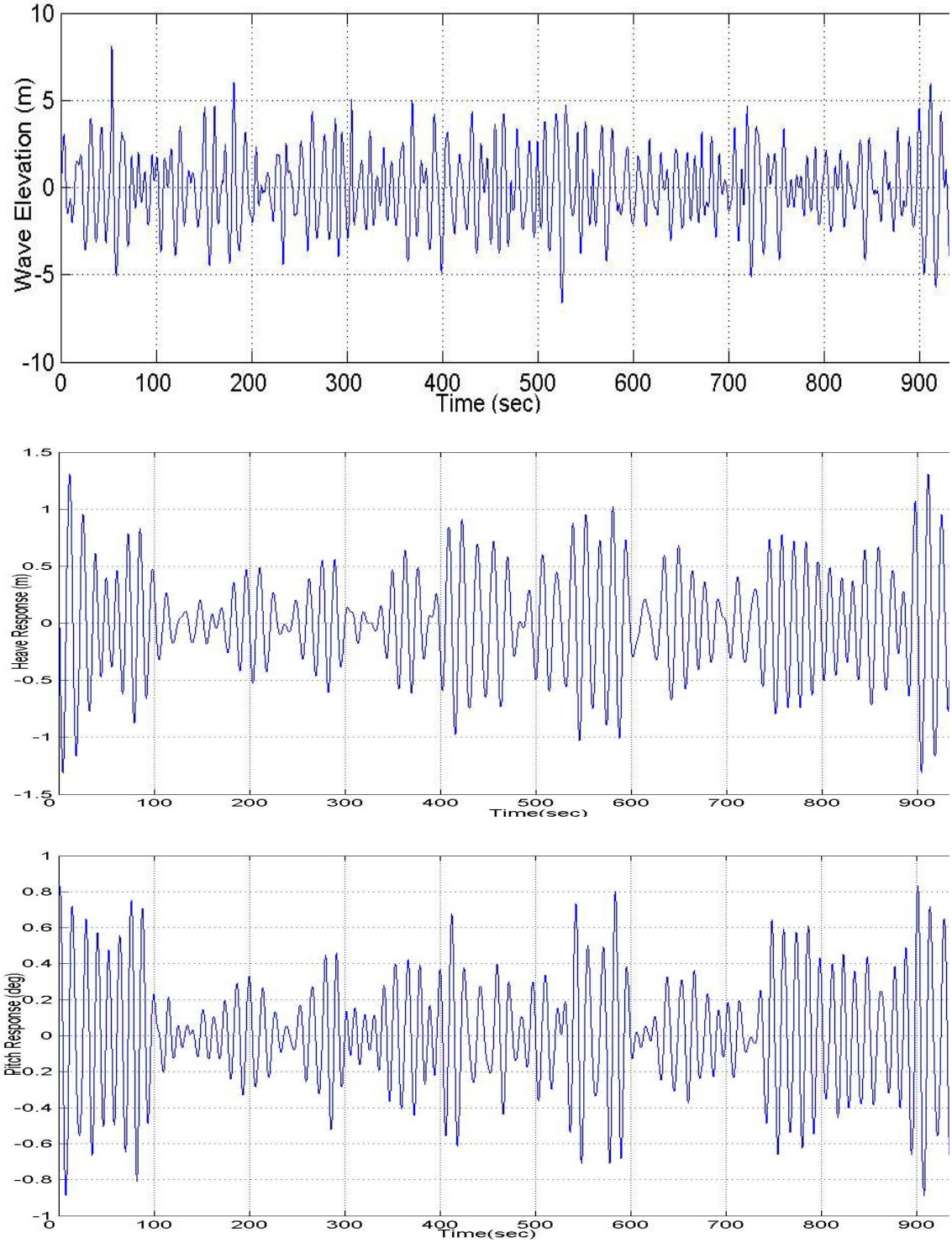

Figure 4-17: Head sea-Hs 6.0m-input wave data, heave, pitch and relative response

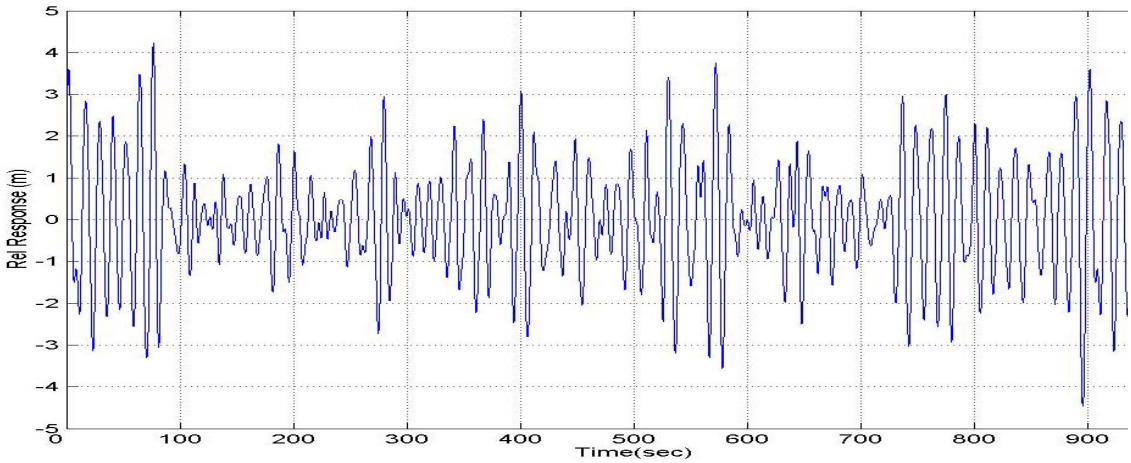

Figure 4-17: Continued

The severe sea states such as sea states 7 shown in Figure 4-18 indicate that the waves are fully non-linear and correspondingly are no longer follow the conventional linear estimates. From the data set for the input wave it can be seen that the maximum wave elevation would be around 7.6 meters and corresponding heave response is around 1.35 meters. The pitch response also is seen to be somewhere close to 0.82 deg. The relative response value for this sea state is observed to be around 4.5 meters.

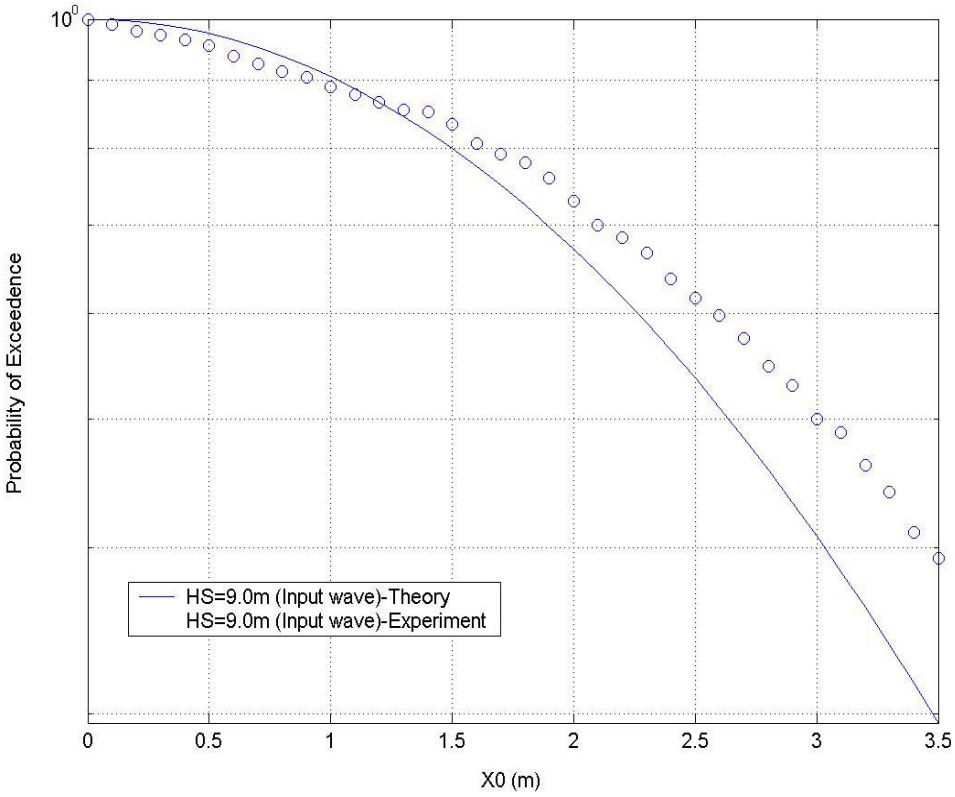

Figure 4-18: Head sea-Hs 9.0m-probability of exceedence for input wave

The probability of exceedence comparison in Figure 4-19 for the input experimental wave with that of theory bears a close contour for X0 values up to 1.25 meters but deviates slightly for higher values of X0 showing the non-linear effects of the input wave data. For lower sea states the input wave for both theory and experiment agrees fairly accurately which is a result of the linear behavior of the input wave. The higher sea states result in the non-linear nature of the input wave that results in the non-linearity and consequent deviation from the theoretical estimates.

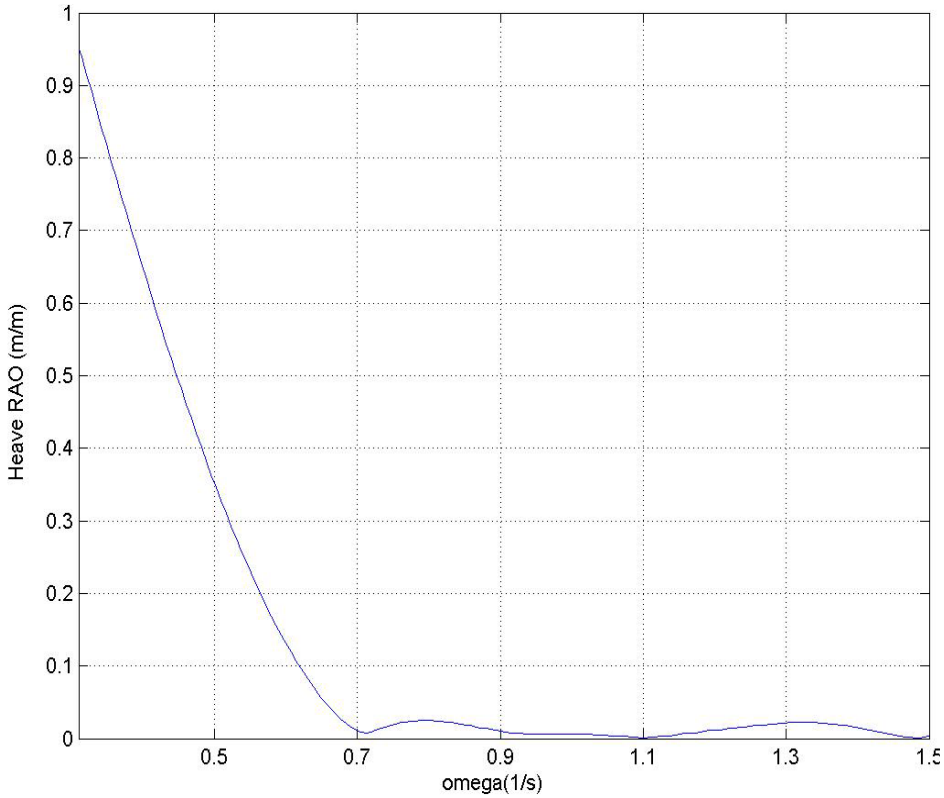

Figure 4-19: Head sea-Hs 9.0m-heave RAO

The heave RAOs for the corresponding omega values is plotted in Figure 4-20. For frequency range from 0.7-1.5 the heave RAO falls drastically showing that the heave response is predominantly due to the low frequency motions. The high frequency motions are almost close to zero and consequently the contribution towards the heave motion is almost negligible from the high frequency components.

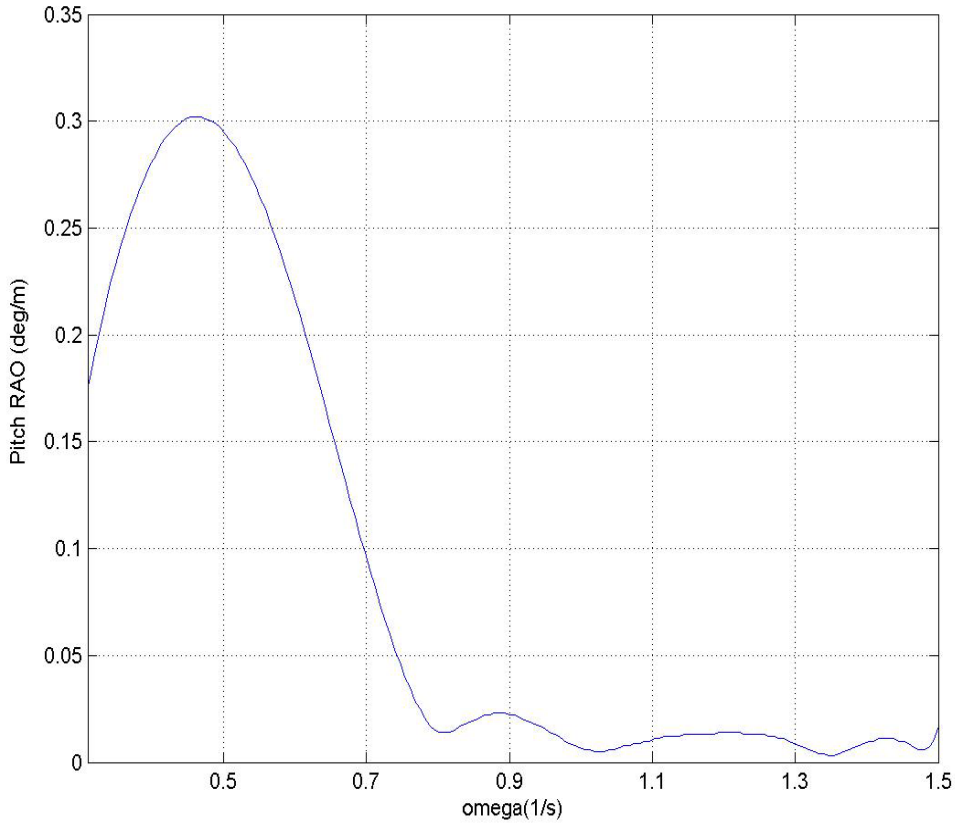

Figure 4-20: Head sea-Hs 9.0m-pitch RAO

The pitch RAO also shown in Figure 4-21 also has a similar trend but the RAO falls real low at a frequency of 0.8 rad/sec. Here again the predominant pitch motion is due to the low frequency or long wave response. The pitch RAO shows a peak value at around a frequency of 0.45 rad/sec and drops drastically for increasing frequencies. The high frequency contribution towards the pitch is small but more than the heave response values. Hence the pitch RAO contributes through the high frequency components which influence the actual pitch response.

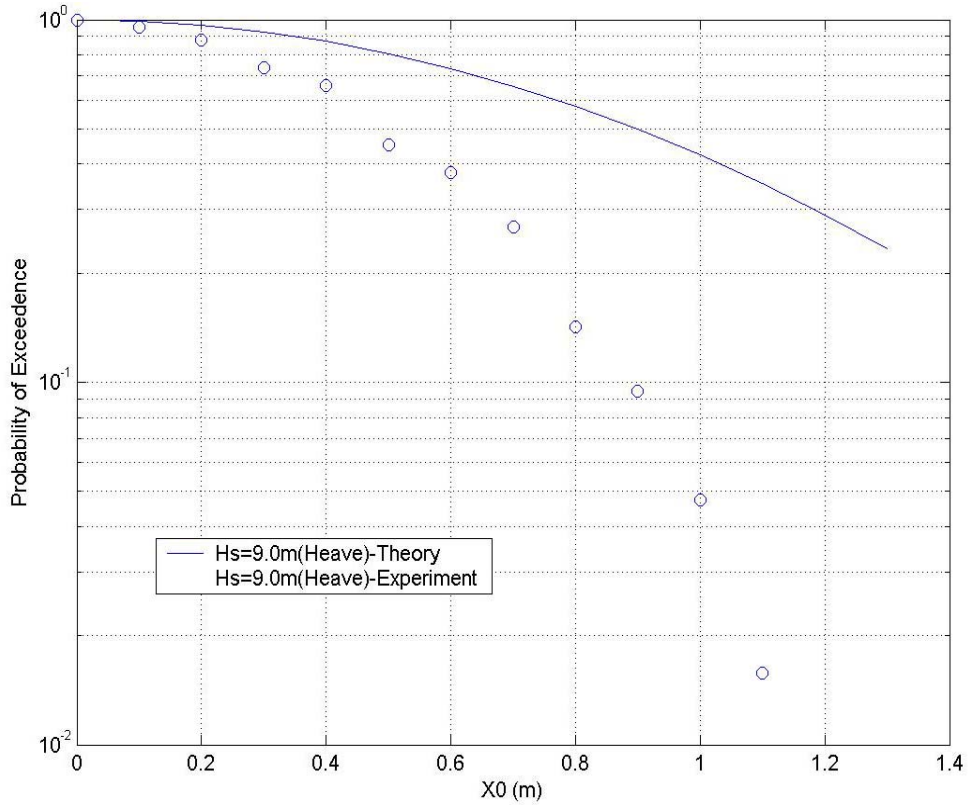

Figure 4-21: Head sea-Hs 9.0m- probability of exceedence for heave motion

The probability of exceedence values for heave and pitch as shown in Figure 4-22 and Figure 4-23 describe the trends which are indicative of how much the theory over estimates over the actual or experimental results. The probability values for the heave motions are ranging from X0 values of 0 to 1.20, which is the maximum value of the heave response. The probability is plotted over the log scale and can be seen that trends of probability for the theoretical results see to be exceedingly large compared to actual experimental results.

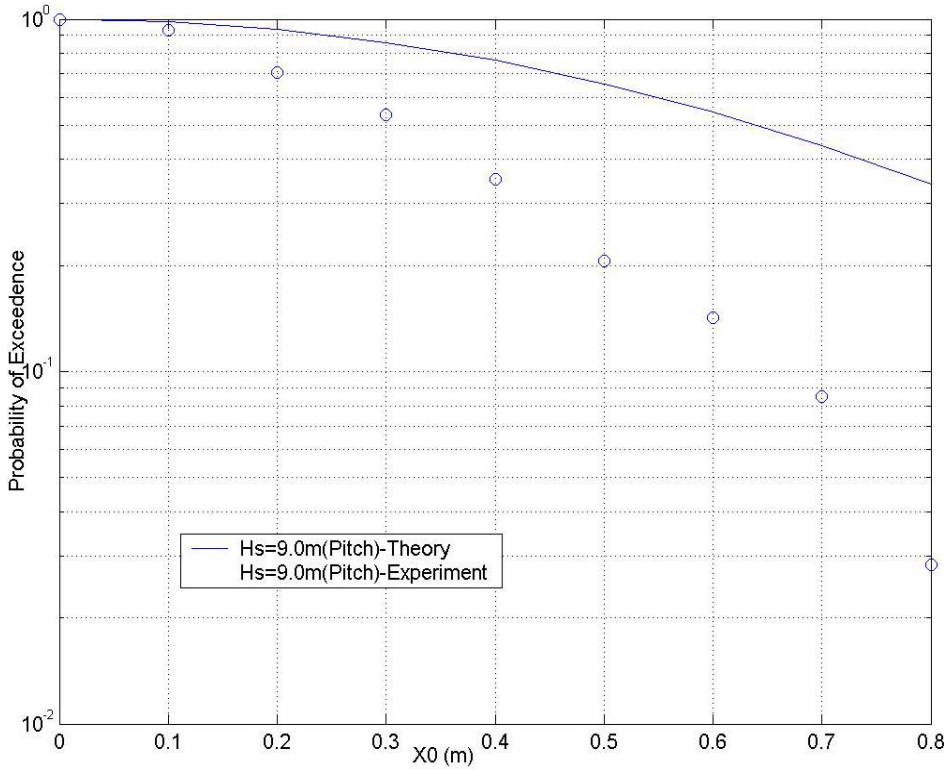

Figure 4-22: Head sea-Hs 9.0m- probability of exceedence for pitch motion

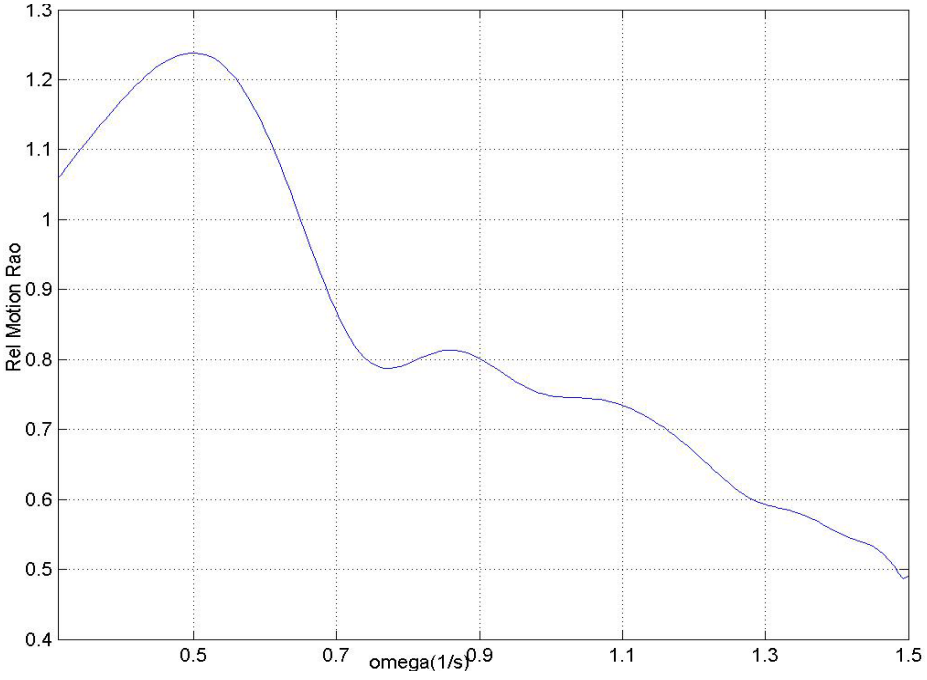

Figure 4-23: Head sea-Hs 9.0m- relative motion RAO

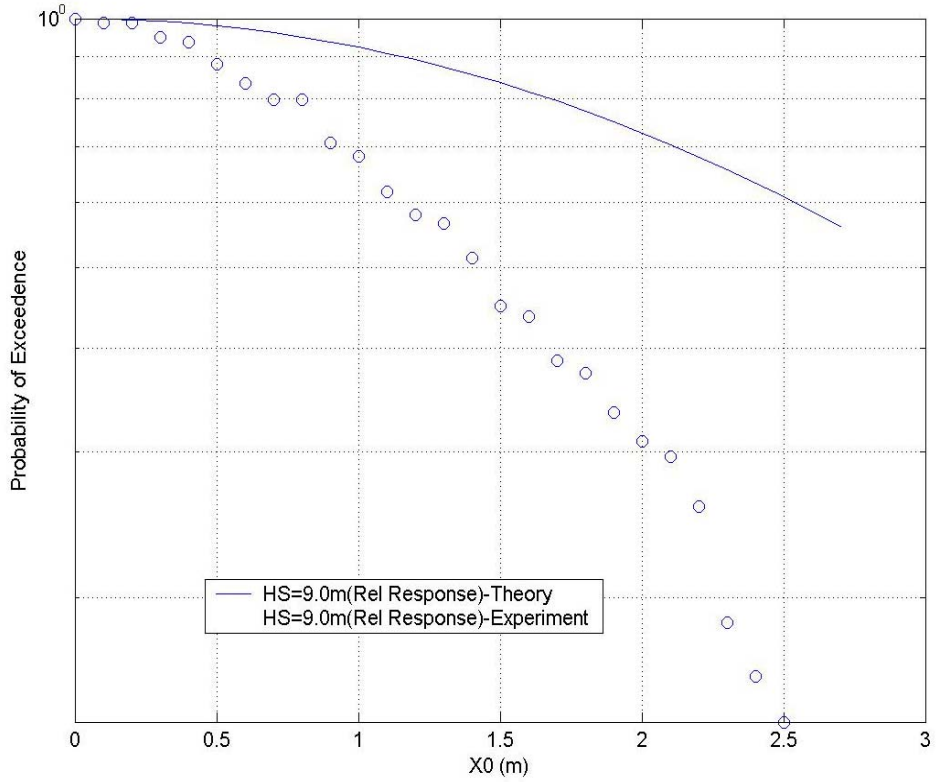

Figure 4-24: Head sea-Hs 9.0m- probability of exceedence for relative motion

The relative motion RAO also follows more or less a similar trend with peak value of response occurring at a frequency of 0.5 rad/sec and then falling off abruptly over increasing frequencies. The trend indicated in Figure 4-24 that the low frequency motions are more predominant and have an important impact on the relative motion response as well.

Also, the probability of exceedence for the relative motion in Figure 4-25 shows that the theoretical estimates are definitely much above the actual results. As the sea state increases the deviation of the theory from that of the actual field data is increasing.

4.1.4 Case #4: Hs = 11.0 m

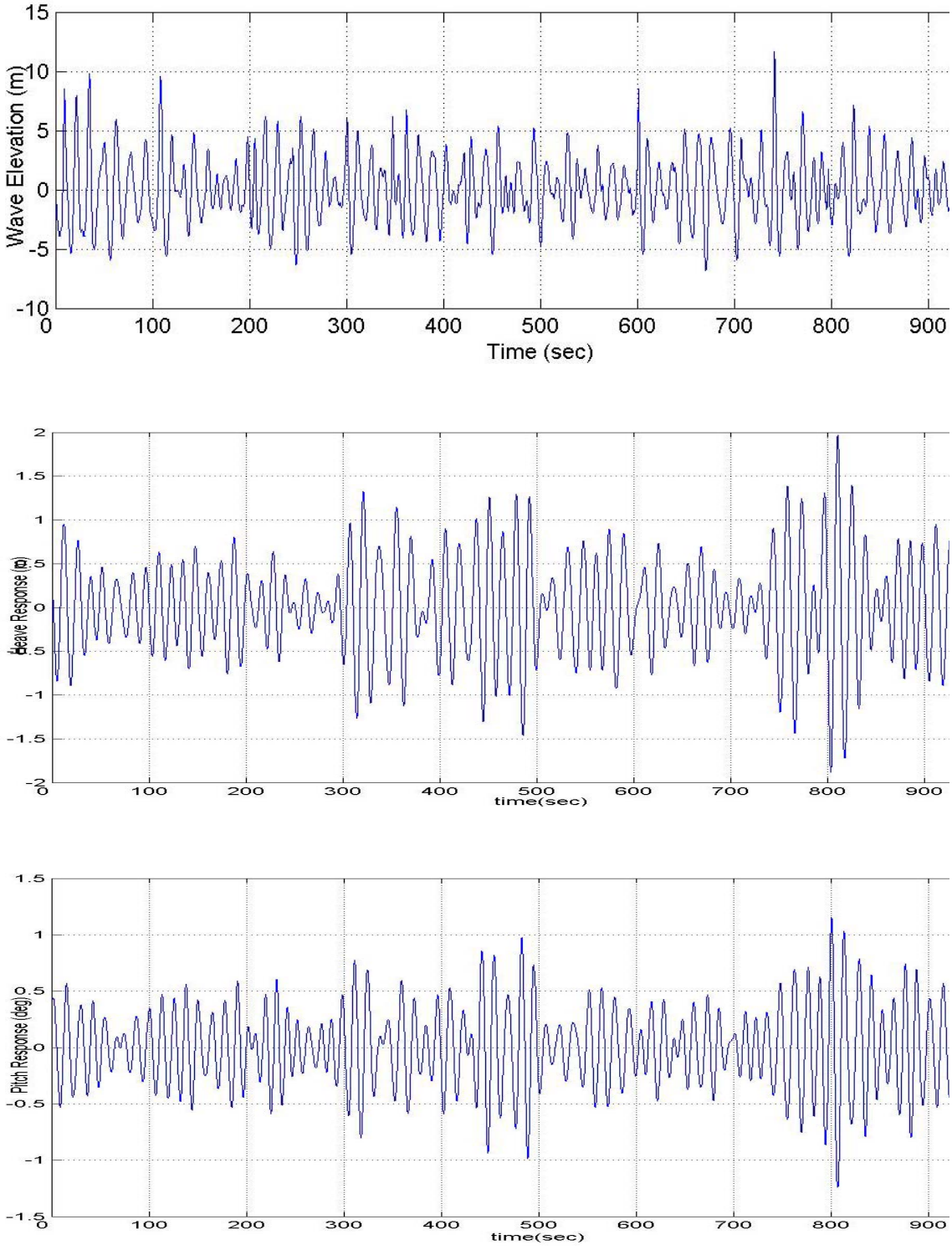

Figure 4-25: Head sea-Hs 6.0m-input wave data, heave, pitch and relative response

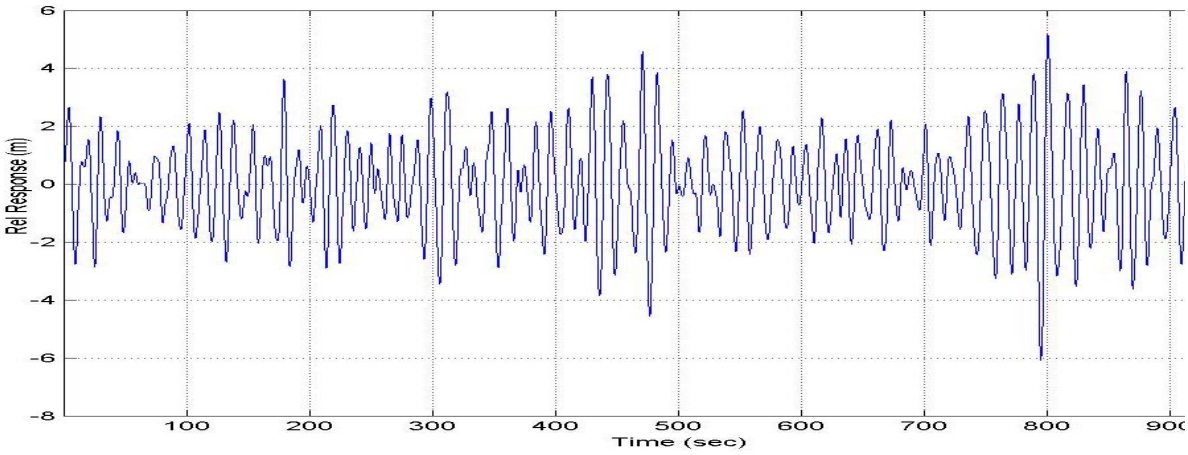

Figure 4-25: Continued

The severe sea states such as sea states 8 describes high and very high seas where the waves are fully non-linear and correspondingly are no longer follow the conventional linear estimates. From the data set for the input wave it can be seen in Figure 4-26 that the maximum wave elevation would be around 10.0 meters and corresponding heave response is around 2.00 meters.

The pitch response also is seen to be somewhere close to 1.25 deg. The relative response value for this sea state is observed to be around 5.5 meters. The relative response values are higher when compared to sea state 7. The probability of exceedence of the input wave for both theory and experiment are plotted in Figure 4-27.

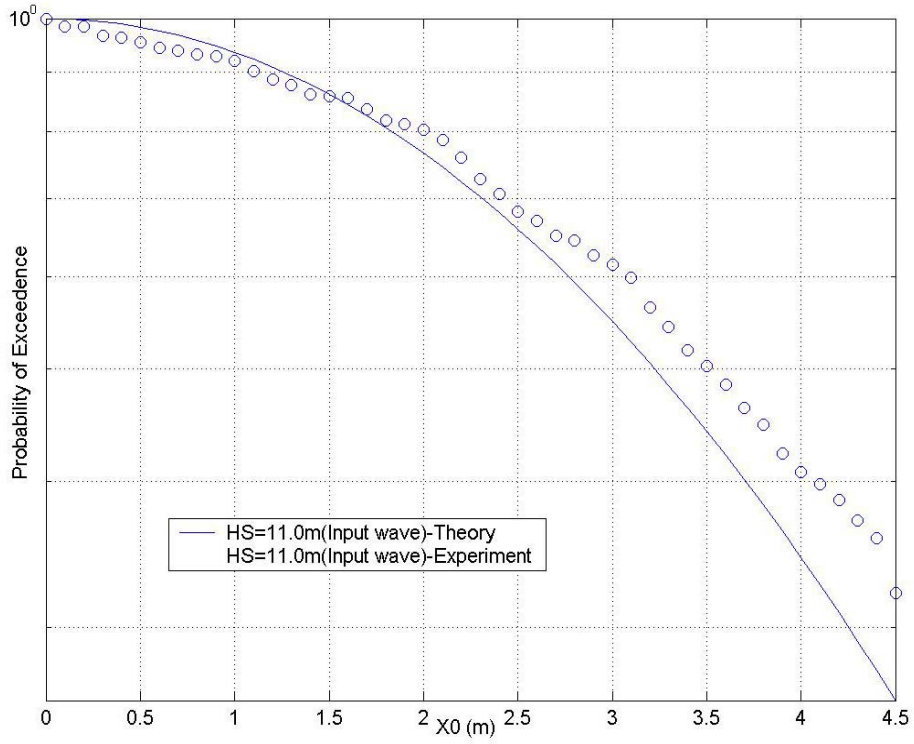

Figure 4-26: Head sea-Hs 11.0m-probability of exceedence for input wave

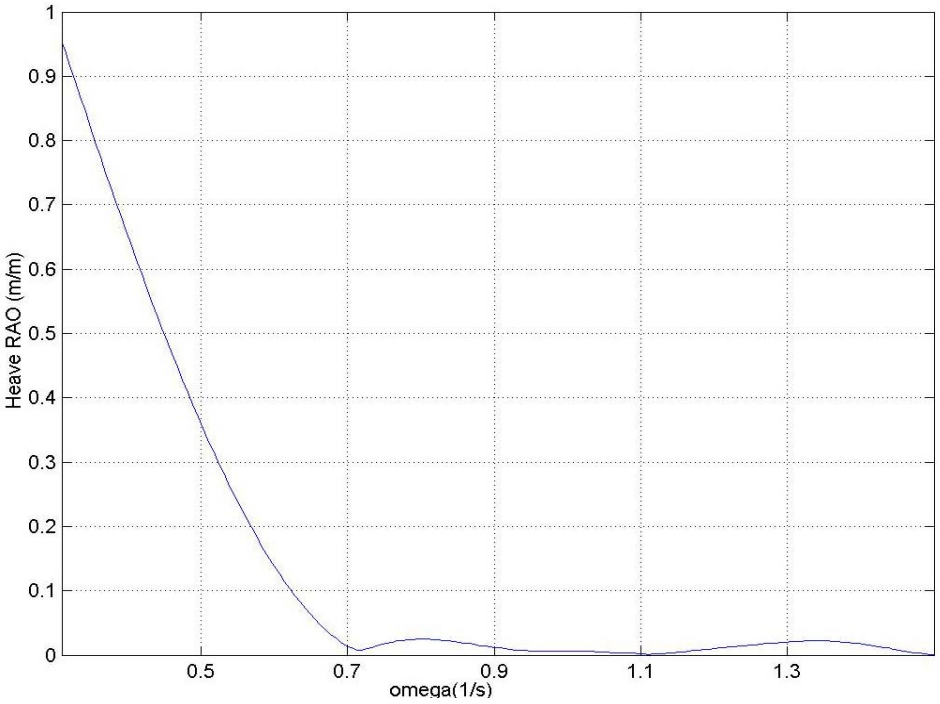

Figure 4-27: Head sea-Hs 11.0m-heave RAO

The heave RAOs for the corresponding omega values is plotted in Figure 4-28. For frequency range from 0.7-1.5 the heave RAO falls drastically showing that the heave response is again predominantly due to the low frequency motions.

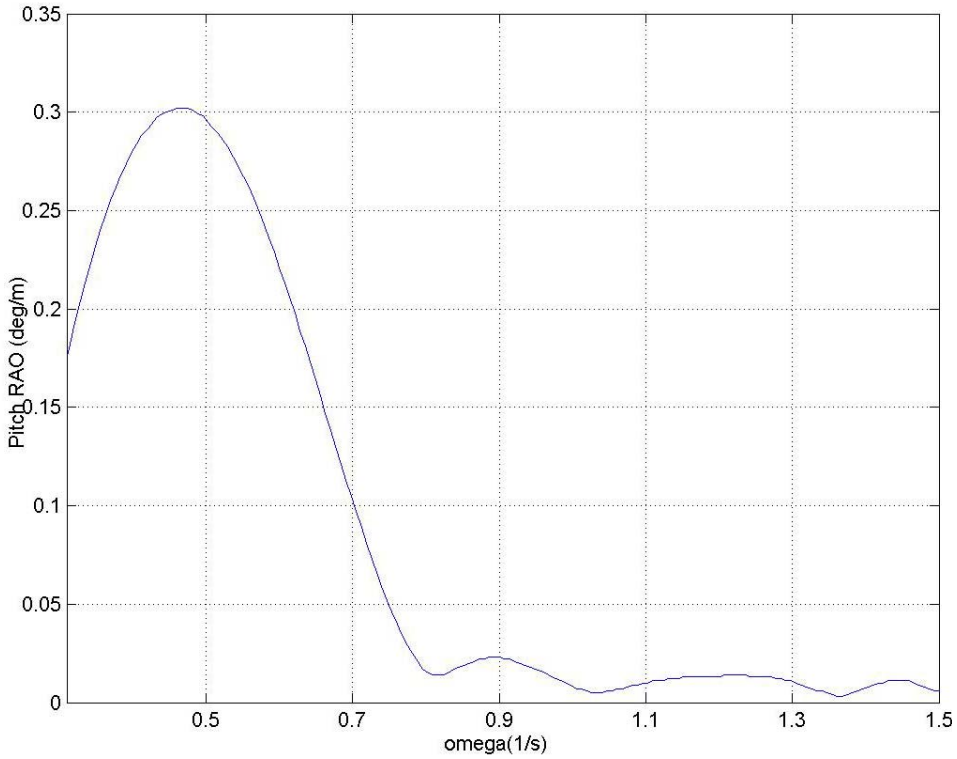

Figure 4-28: Head sea-Hs 11.0m-pitch RAO

The pitch RAO in Figure 4-29 also shows the similar trend but the RAO falls to a really low value at a frequency of 0.8 rad/sec. Here again the predominant pitch motion is due to the low frequency or long wave response. The pitch RAO shows a peak value at a frequency of 0.45 rad/sec and drops drastically for increasing frequencies.

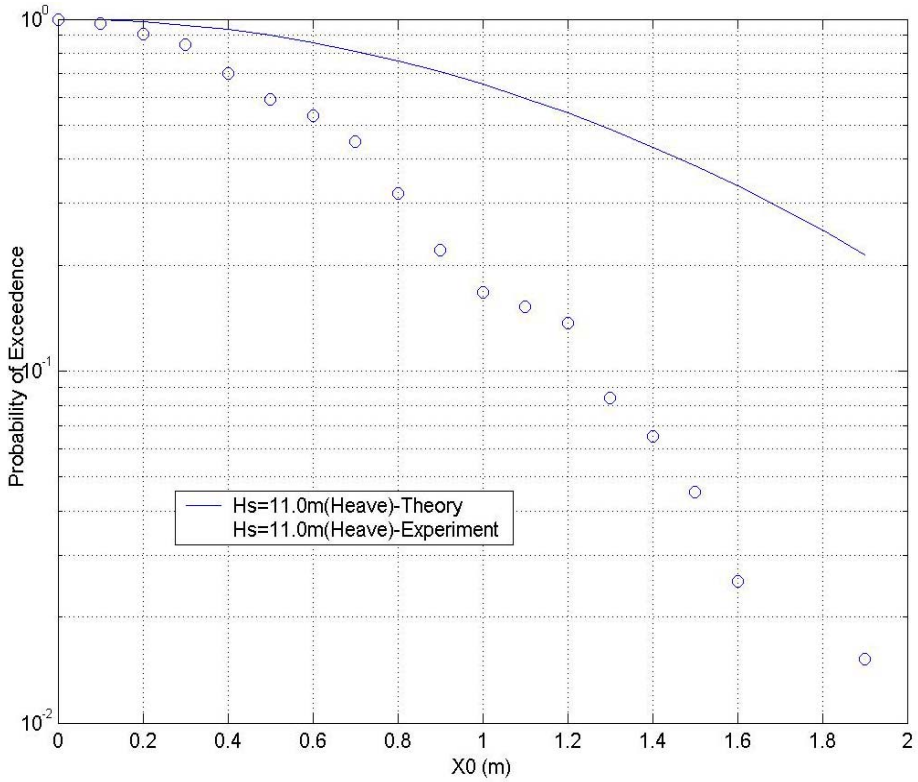

Figure 4-29: Head sea-Hs 11.0m-probability of exceedence for heave motion

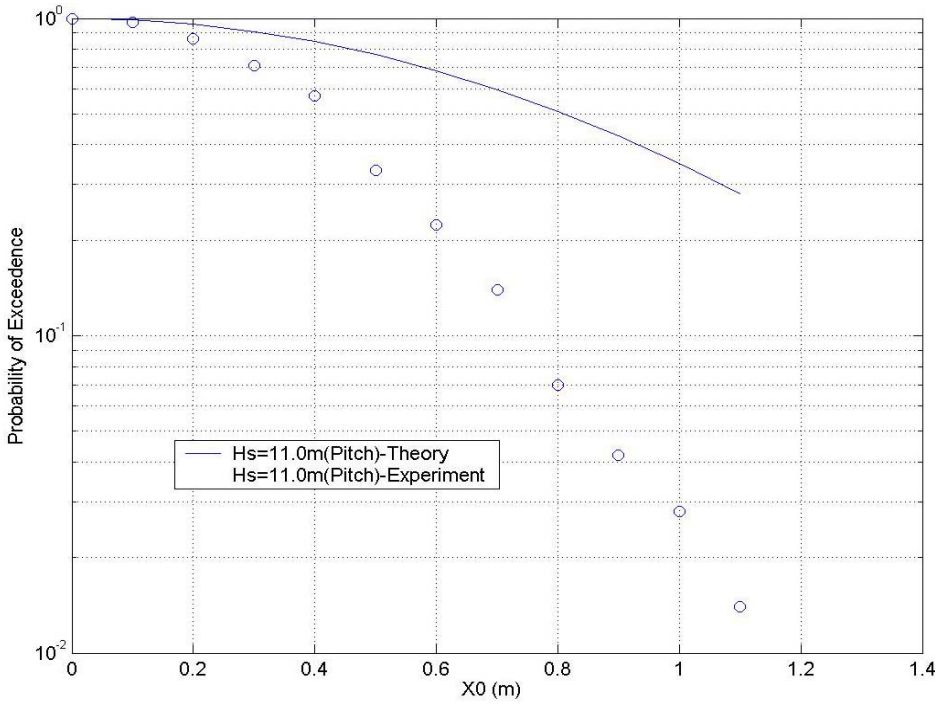

Figure 4-30: Head sea-Hs 11.0m-probability of exceedence for pitch motion

The probability of exceedence values for heave and pitch in Figure 4-30 and Figure 4-31 describe the trend which are indicative of how much the theory over estimates over the actual or experimental results. The probability values for the heave motions are ranging from X0 values of 0 to 1.95 meters, which is the maximum value of the heave response. The probability is plotted over the log scale and can be seen that trends of probability for the theoretical results see to be exceedingly large compared to actual experimental results.

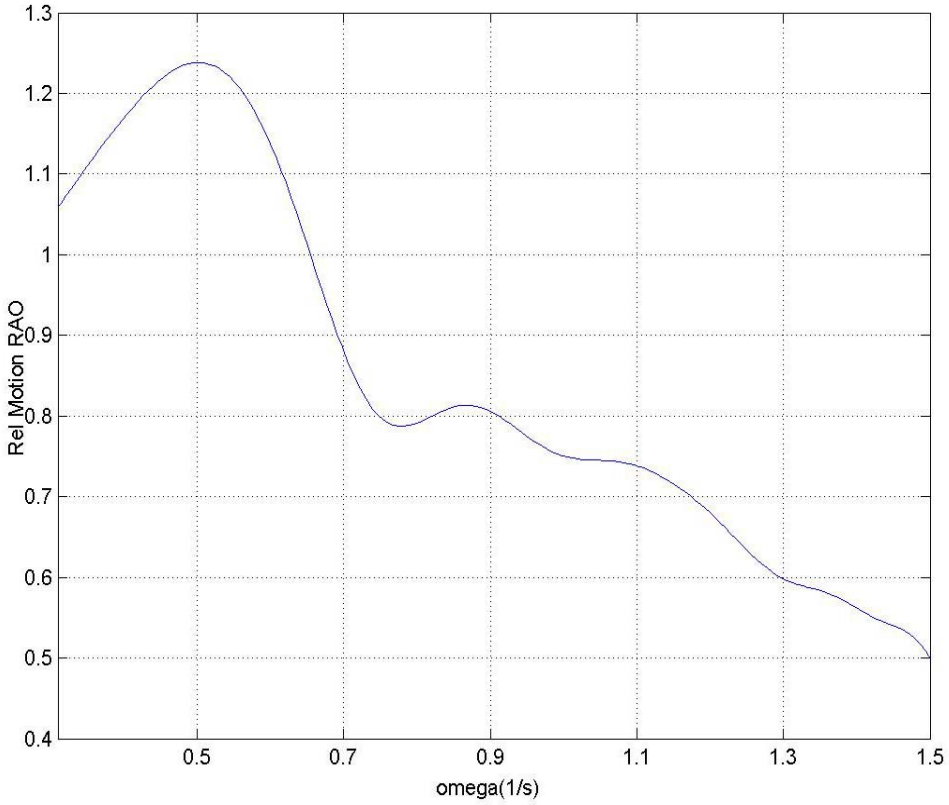

Figure 4-31: Head sea-Hs 11.0m-relative motion RAO

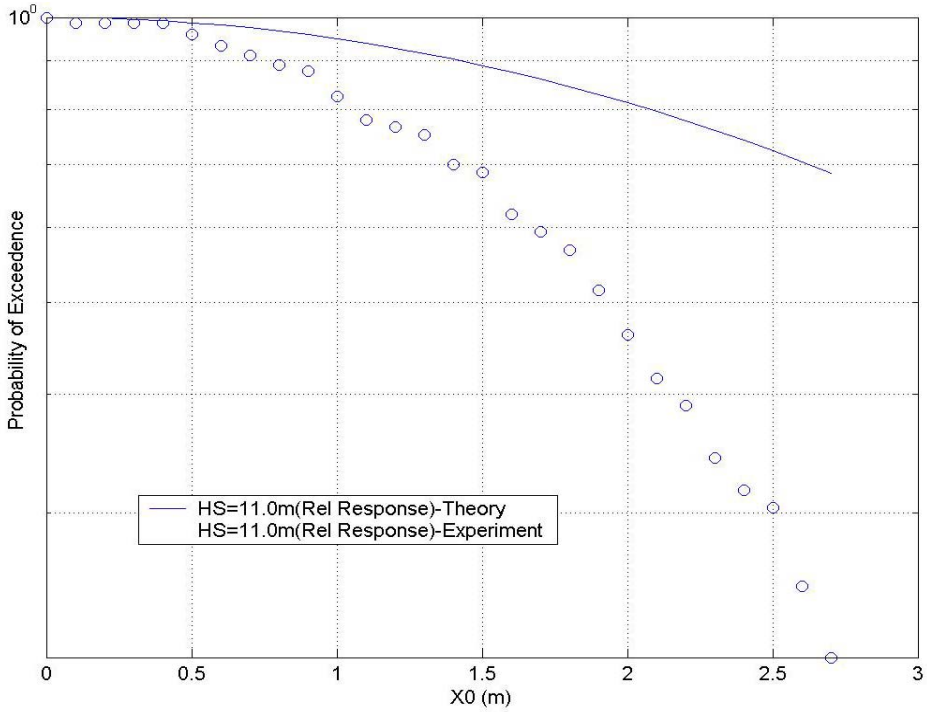

Figure 4-32: Head sea-Hs 11.0m-probability of exceedence for relative motion

The relative motion RAO shown in Figure 4-32 also follows more or less a similar trend with peak value of response occurring at a frequency of 0.5 rad/sec and then falling off abruptly over increasing frequencies. The trend indicates that the low frequency motions are more predominant and have an important impact on the relative motion response as well.

The probability of exceedence for the relative motion in Figure 4-33 shows that the theoretical estimates are definitely much above the actual results. At this sea state the deviation of the theory from that of the actual field data is seems to be quite large.

4.2 Beam sea condition

The beam sea conditions are analyzed for the ship heading in the 90 degree direction to the assumed coordinate axis. The location where the data is analyzed is the again station #1 on the SL-7 container model.

4.2.1 Case #1: Hs = 3.0 m

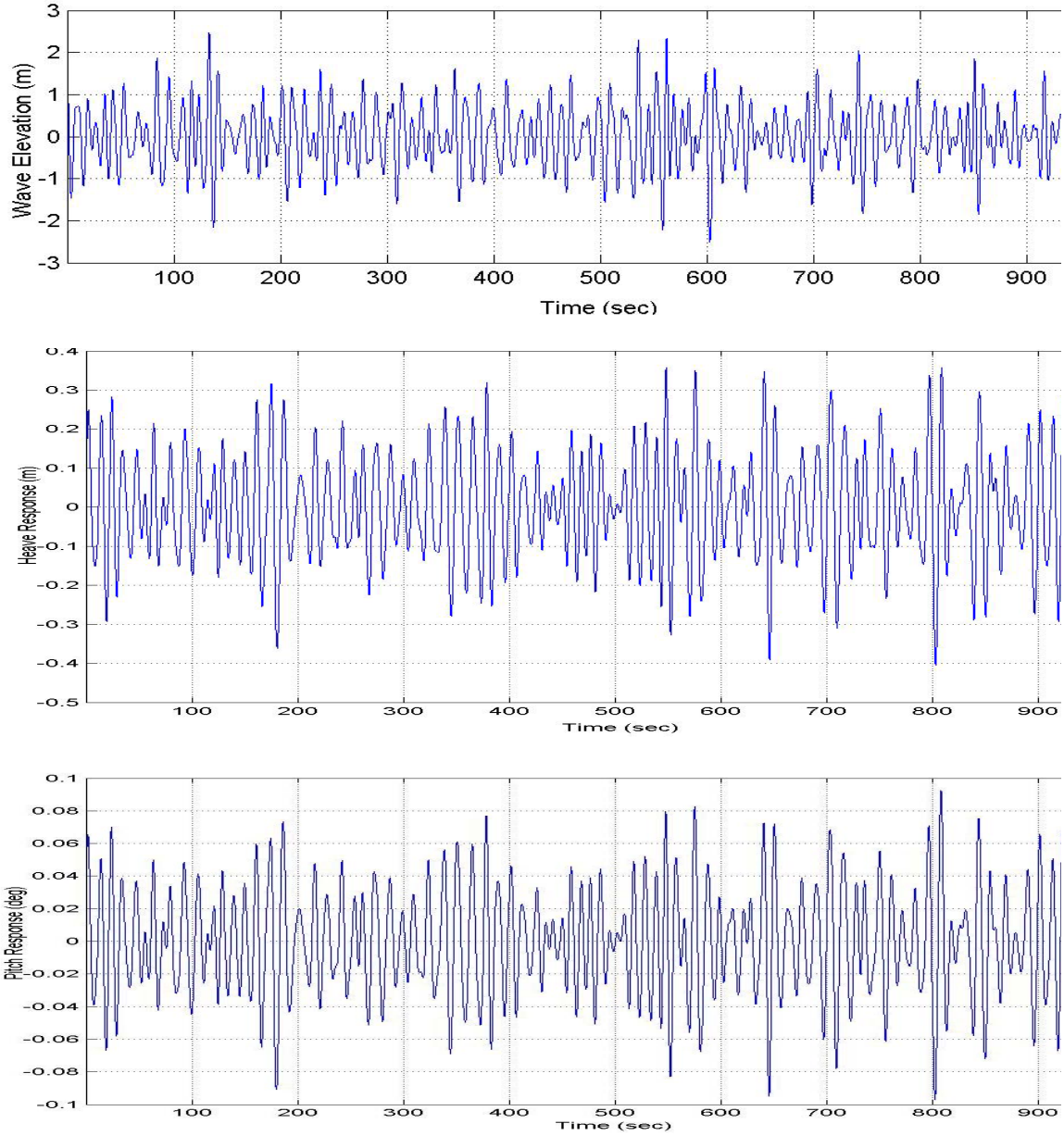

Figure 4-33: Beam sea-Hs 3.0m-input wave data, heave, and pitch response

For the beam sea conditions the heave and pitch response values as shown in Figure 4-34 will be comparatively higher than the head sea estimates. Since the same input wave is used, the data set for the input wave is seen to have the maximum wave elevation of around 0.75 meters and corresponding heave response is around 0.36 meters. The pitch response also is seen to be somewhere close to 0.095 deg. The input wave and the response can be closely observed to note that the peak response in both heave and pitch occurs at around the same time as the maximum wave elevation. Again, the response will have a lag to the response because of the inertia of the vessel as well as its hydrostatic stiffness.

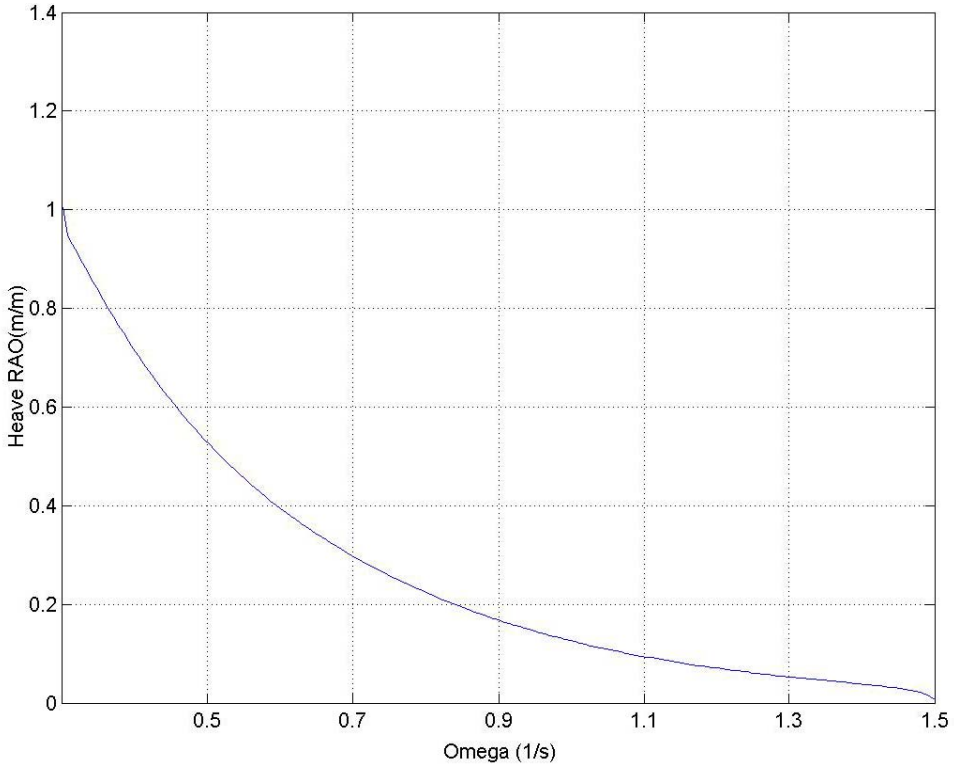

Figure 4-34: Beam sea-Hs 3.0m-heave RAO

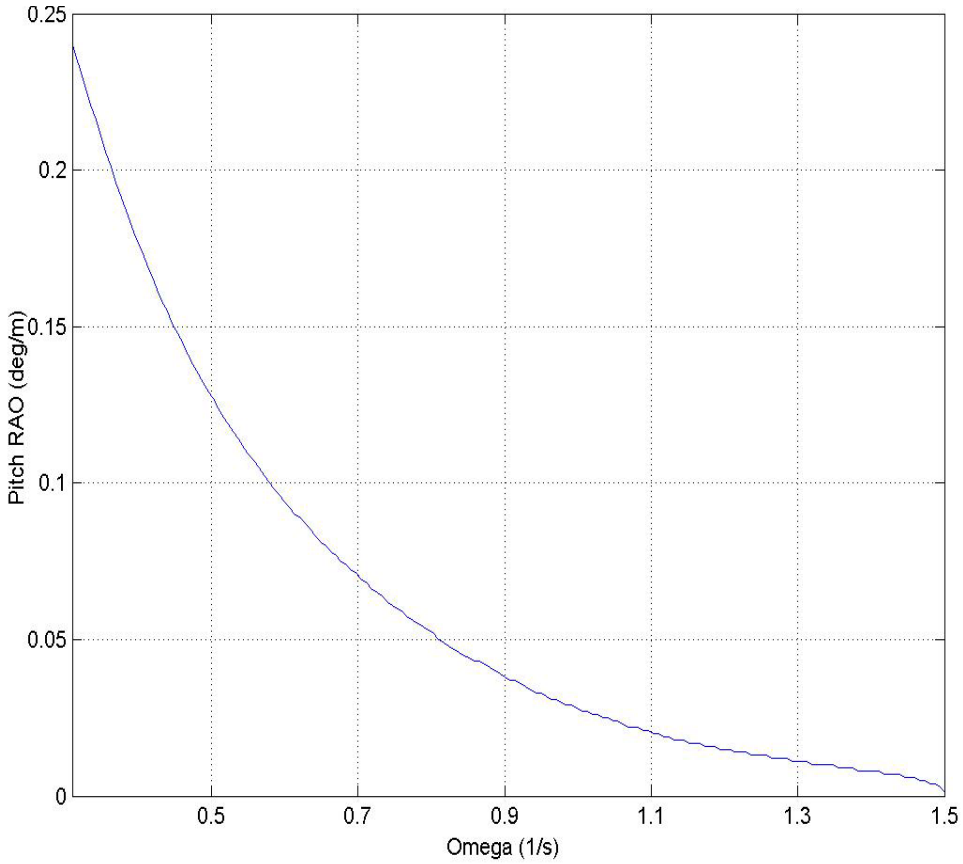

Figure 4-35: Beam sea-Hs 3.0m-pitch RAO

The heave and pitch RAO for the beam sea conditions as shown in Figure 4-35 and Figure 4-36 are fairly smooth unlike that of the head sea states. But the trends indicate that the RAO has higher influence on the structure heave and pitch response in predominantly low frequencies.

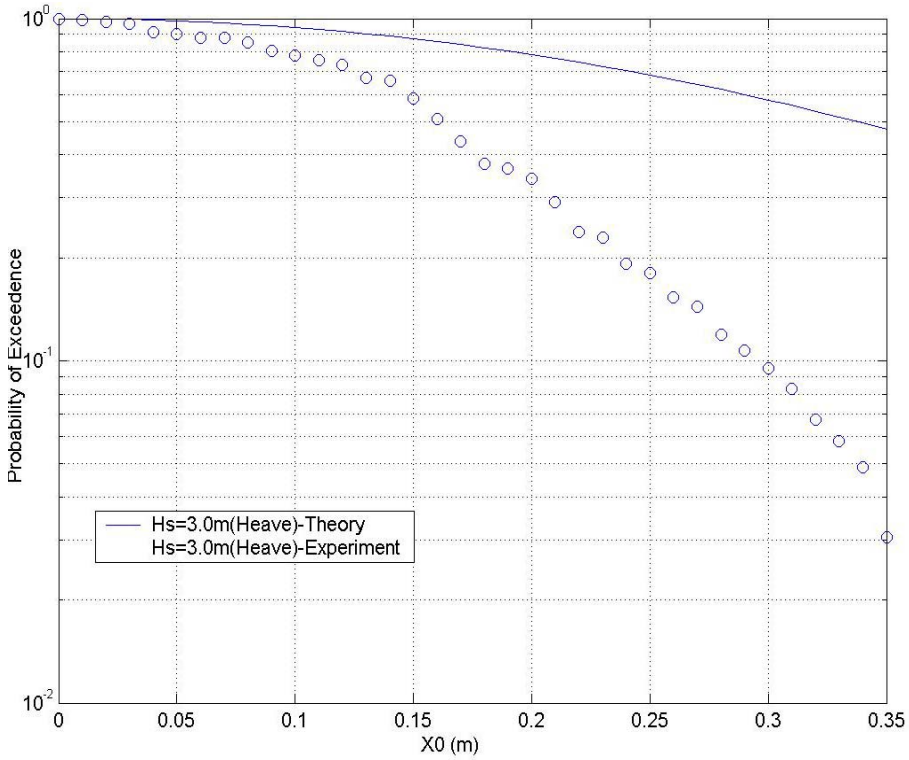

Figure 4-36: Beam sea-Hs 3.0m-probability of exceedence for heave motion

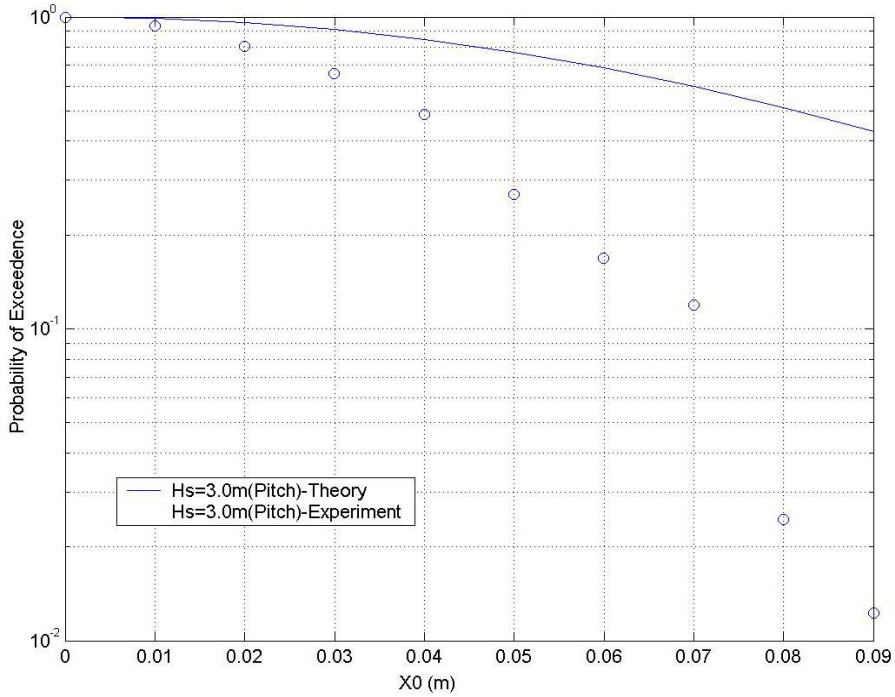

Figure 4-37: Beam sea-Hs 3.0m-probability of exceedence for pitch motion

The probability of exceedence for heave as seen in Figure 4-37 and for pitch as seen in Figure 4-38 indicates again the higher value for the experiment as compared to the theoretical results. It can also be noticed that the maximum heave values for this sea state would be 0.35m. Similarly the maximum pitch response values also would be in the around 0.09 deg/rad.

Relative motion-leeward side

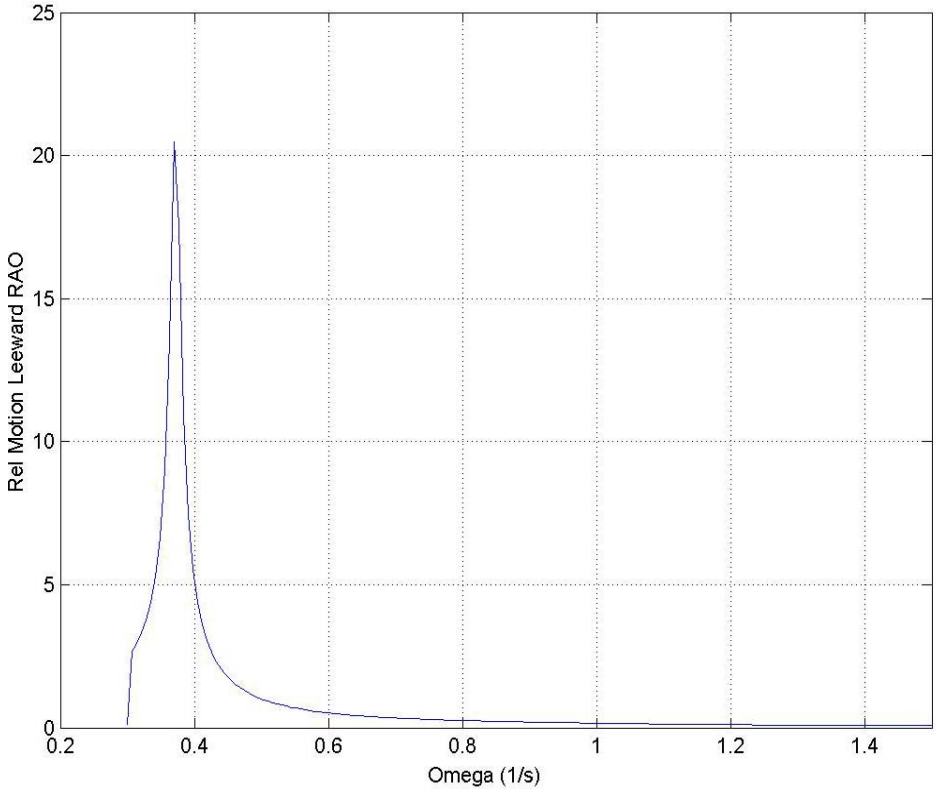

Figure 4-38: Beam sea-Hs 3.0m-relative motion RAO [leeward side]

The relative motion RAO for the leeward side as shown in Figure 4-39 indicates that an abrupt peak in the data for a low frequency range of around 0.344 rad/sec. This is analyzed and found to be the roll RAO contribution to the relative motion RAO.

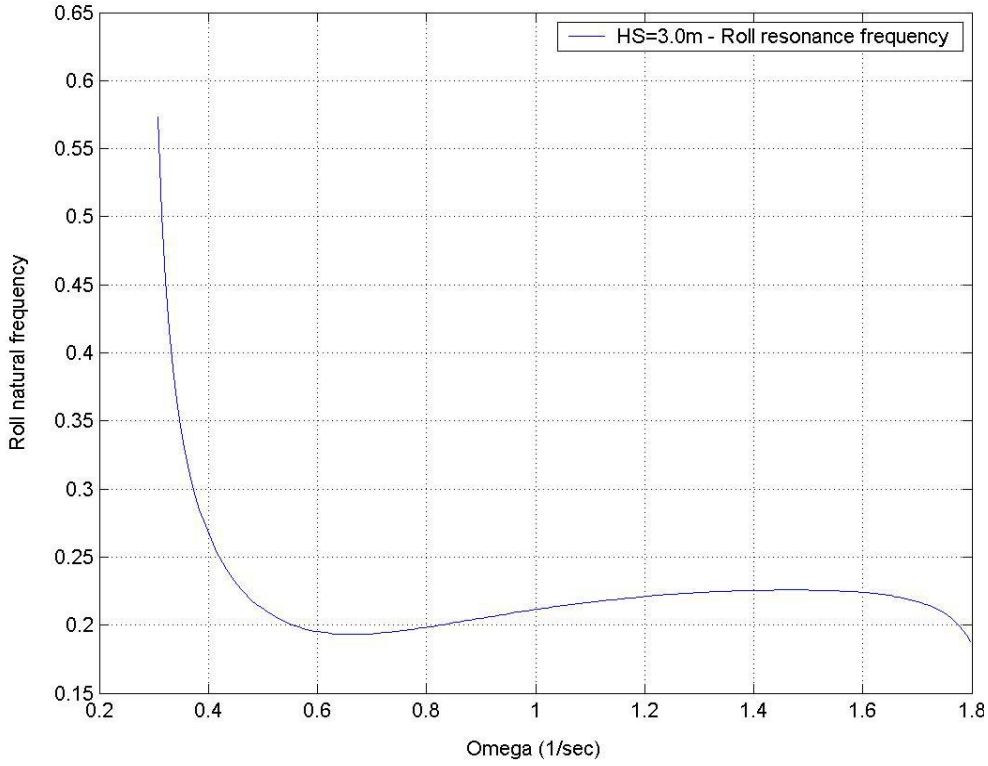

Figure 4-39: Beam sea-Hs 3.0m-roll natural frequency

Hence the relative motion response is plotted separately within the frequency range where resonance with roll motion occurs and also outside the range of this peak roll value as can been observed in Figure 4-40. The roll frequency is having a peak value for frequency value of 0.4 rad/sec and then falls abruptly to lower values. The contribution from the roll is significant especially in the low frequency regime.

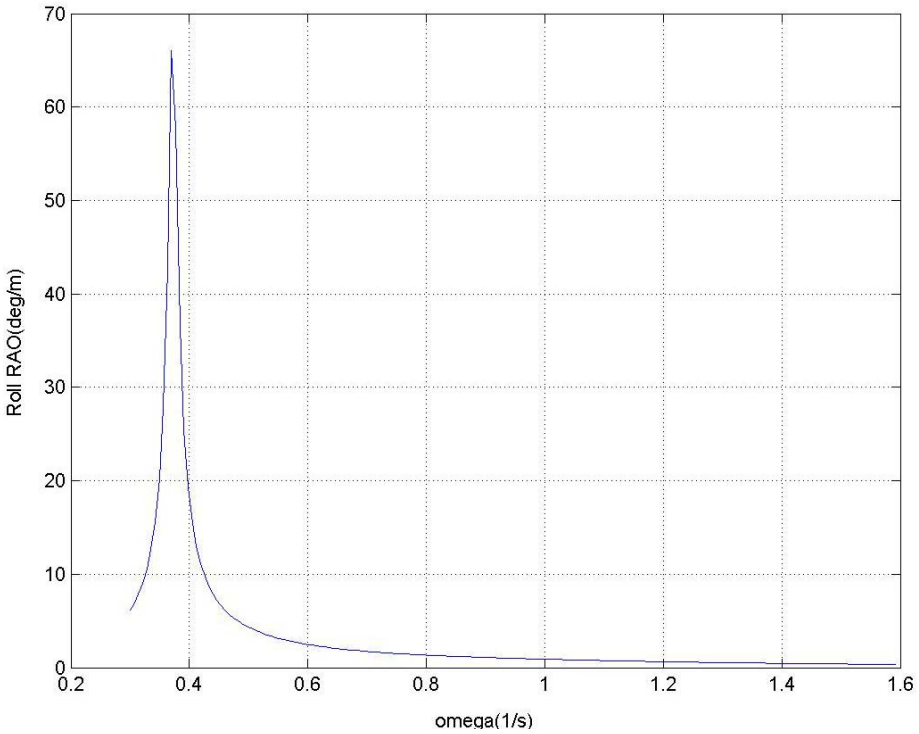

Figure 4-40: Beam sea-Hs 3.0m-roll RAO

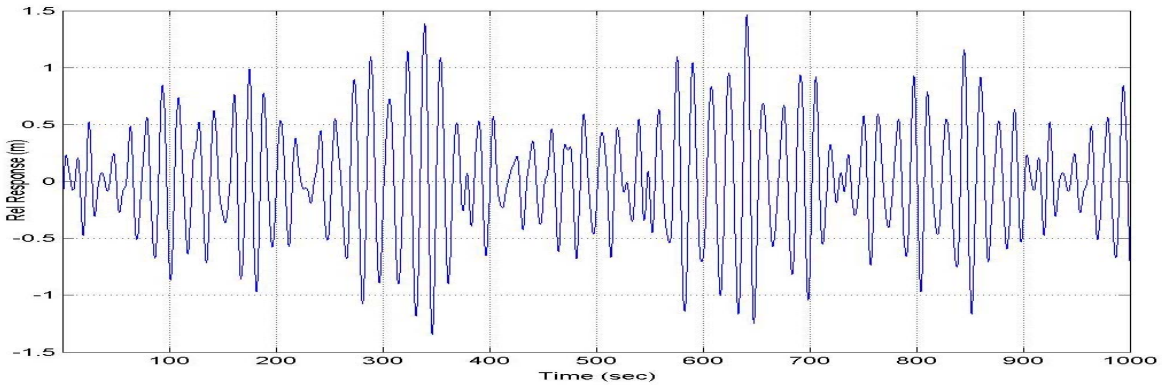

Figure 4-41: Beam sea-Hs 3.0m- relative motion with and without roll resonance [leeward side]

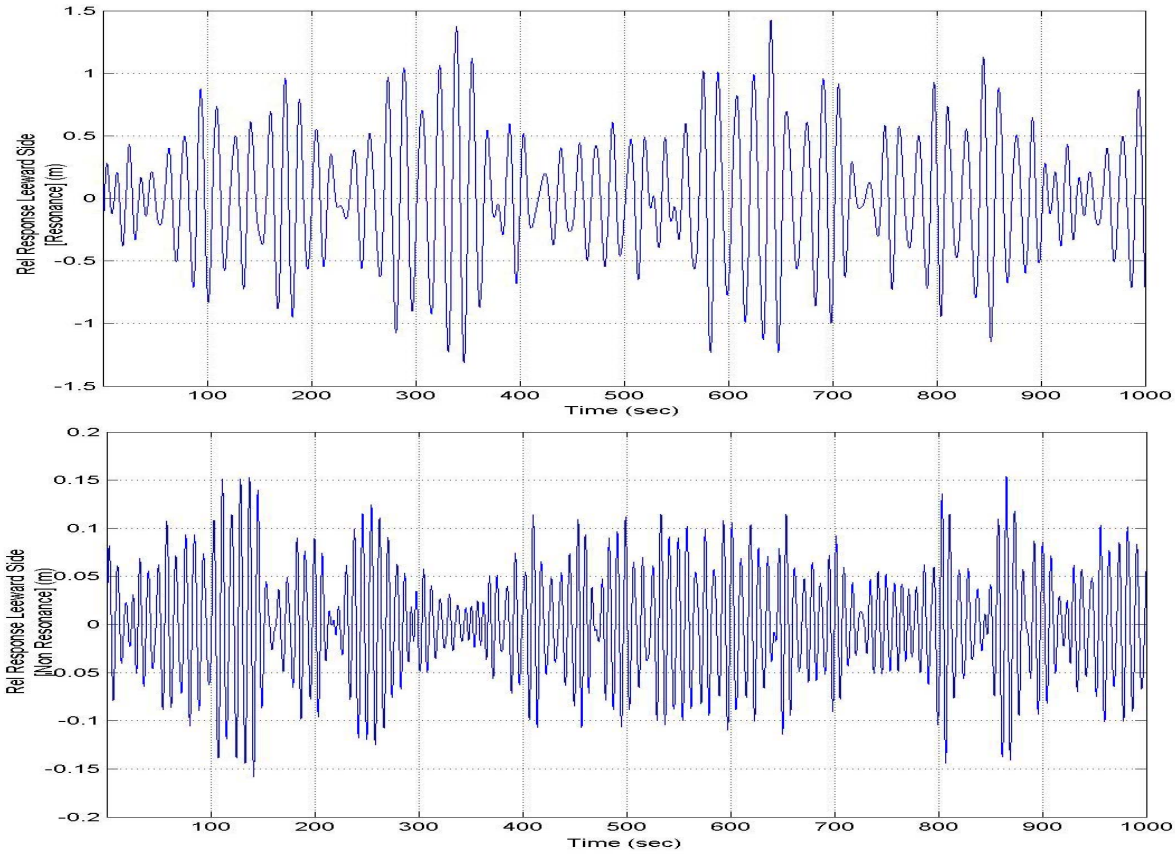

Figure 4-41: Continued

The relative motion results in Figure 4-41 indicate that the low frequency resonant response contributes significantly to the actual response. The Figure 4-42 shows that the high frequency values, which are outside the resonance, contribute a very small percentage to the actual resonance response value. So it can be observed that the roll motion is contributing significantly to the actual response in case of beam sea conditions.

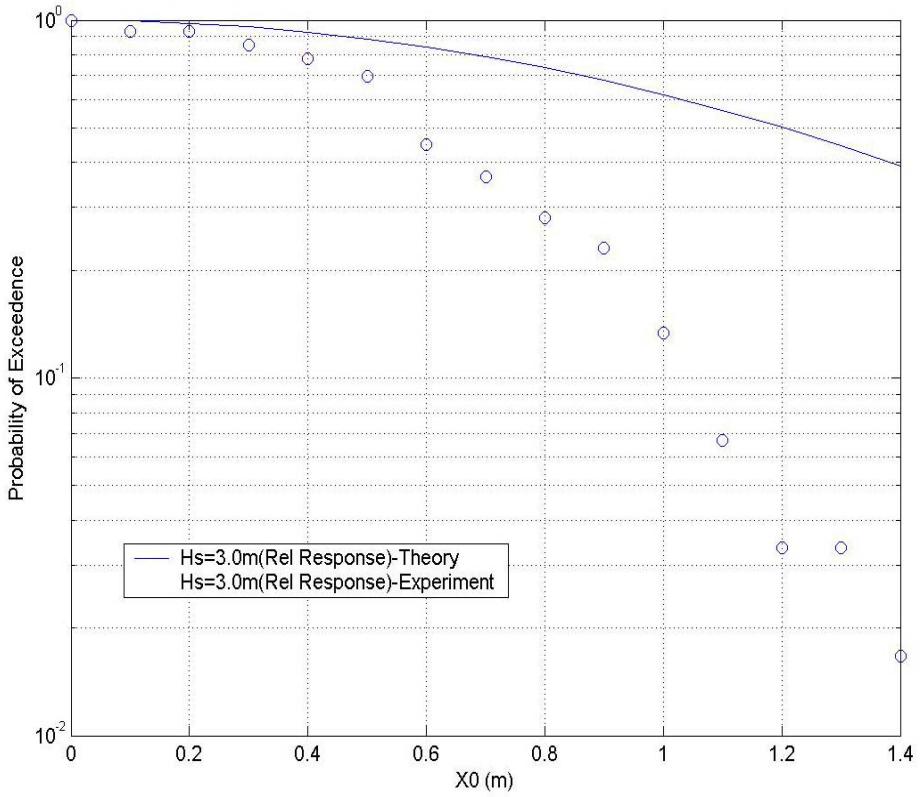

Figure 4-42: Beam sea-Hs 3.0m- relative motion probability of exceedence [leeward side]

In case of beam seas heading, the deviation from the theoretical estimates of the probability of exceedence as shown in Figure 4-43 indicate that the experimental results is seemingly large in comparison with that of the head sea condition.

The probability of exceedence for the relative motion shows that the theoretical estimates are definitely much above the actual results. At this sea state the deviation of the theory from that of the actual field data seems to be quite large.

Relative motion-weather side

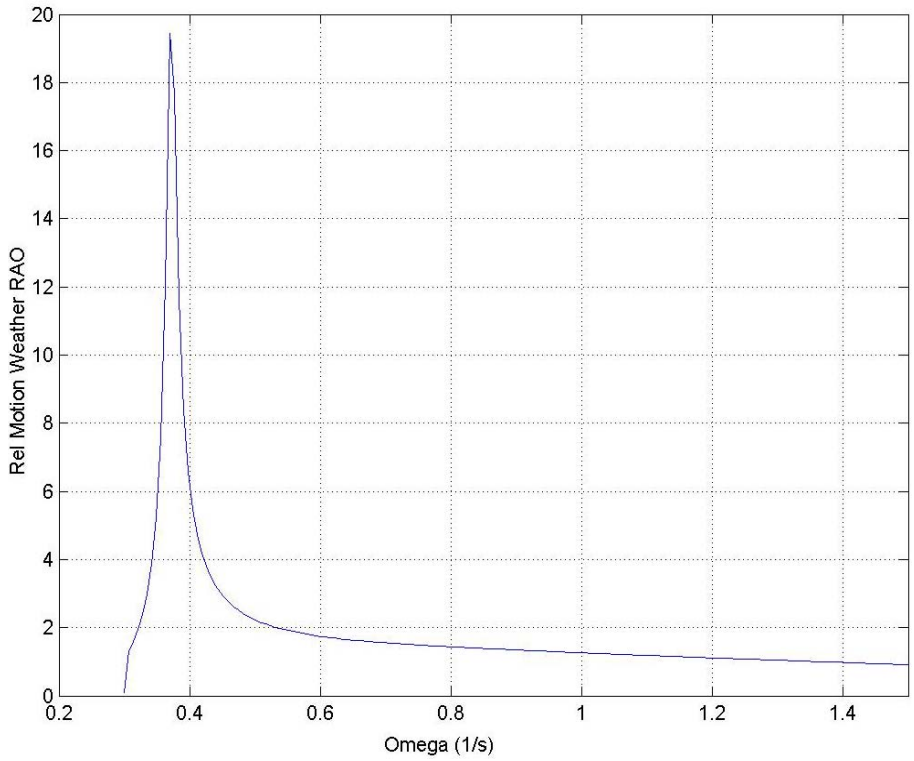

Figure 4-43: Beam sea-Hs 3.0m- relative motion RAO [weather side]

From the Figure 4-44 the relative motion RAO for the weather side also indicates an abrupt peak in the data for a low frequency range of around 0.344 rad/sec and was again found to be the roll RAO contribution to the relative motion RAO. Hence the relative motion response is plotted separately within the frequency range where resonances with roll motion occur and also outside the range of this peak roll value. Also it has been observed that the weather side response values are larger than the leeward side as shown in Figure 4-45. This is fairly justified, as the weather side will be undergoing an extensive impact due to the waves as compared to the leeward side. So

correspondingly, the weather side response would indicate response, which will also be significantly large, compared to that of the leeward side.

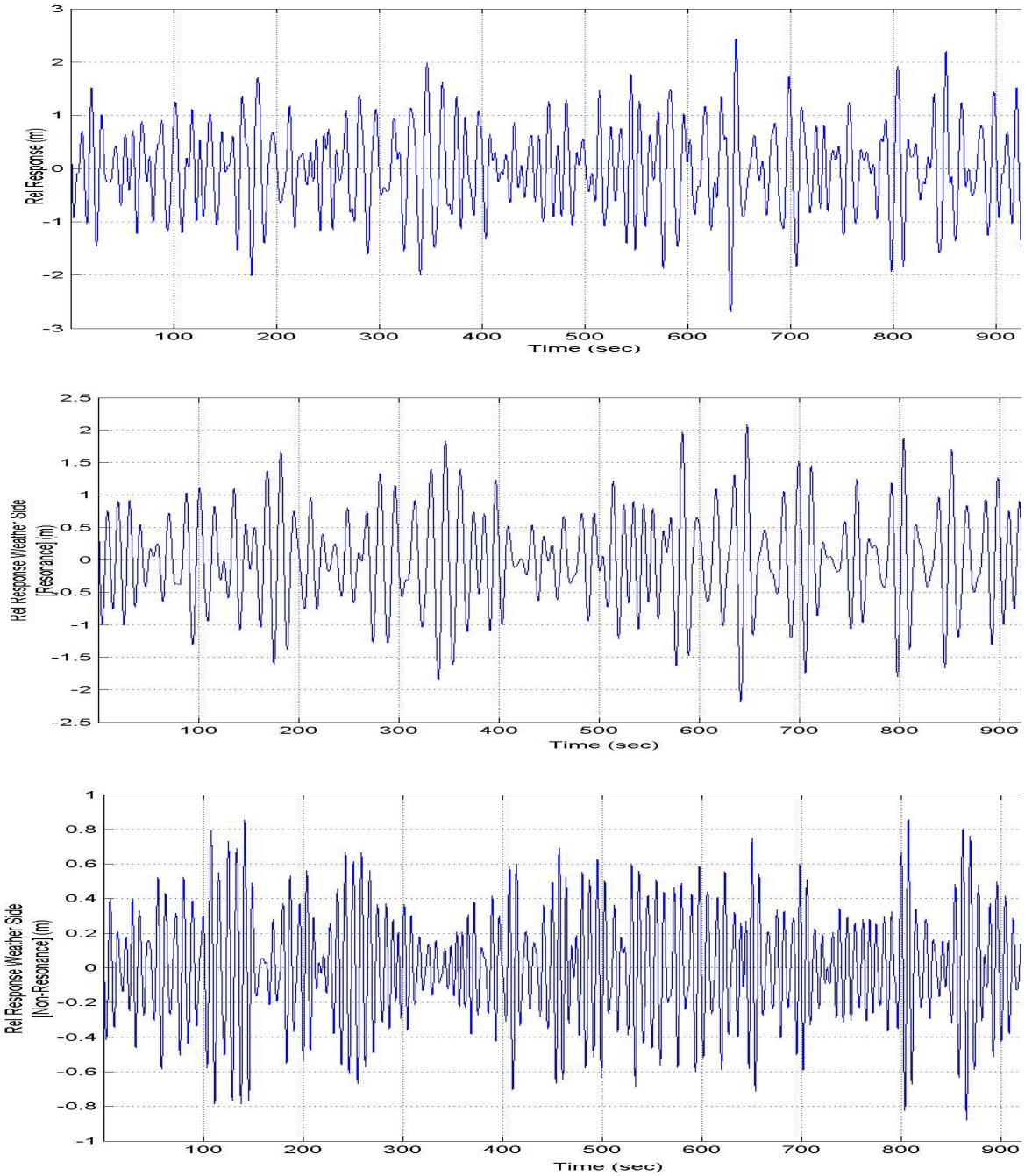

Figure 4-44: Beam sea-Hs 3.0m- relative motion with and without roll resonance [weather side]

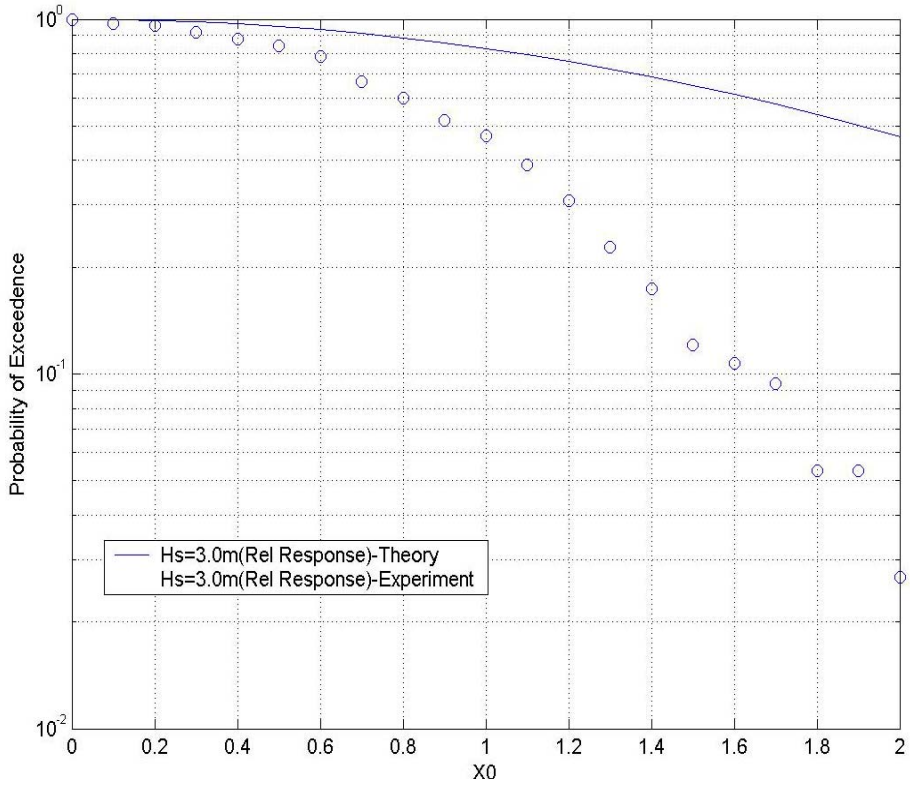

Figure 4-45: Beam sea-Hs 3.0m- probability of exceedence for relative motion

In case of beam seas heading, the deviation from the theoretical estimates of the probability of exceedence to that of the experimental results is seemingly large in comparison with that of the head sea condition. As discussed above through the Figure 4-46, the weather side probability of exceedence has a higher probability range value for X0 due to the direct impact on the structure and the consequent relative response.

4.2.2 Case #2: Hs =6.0 m

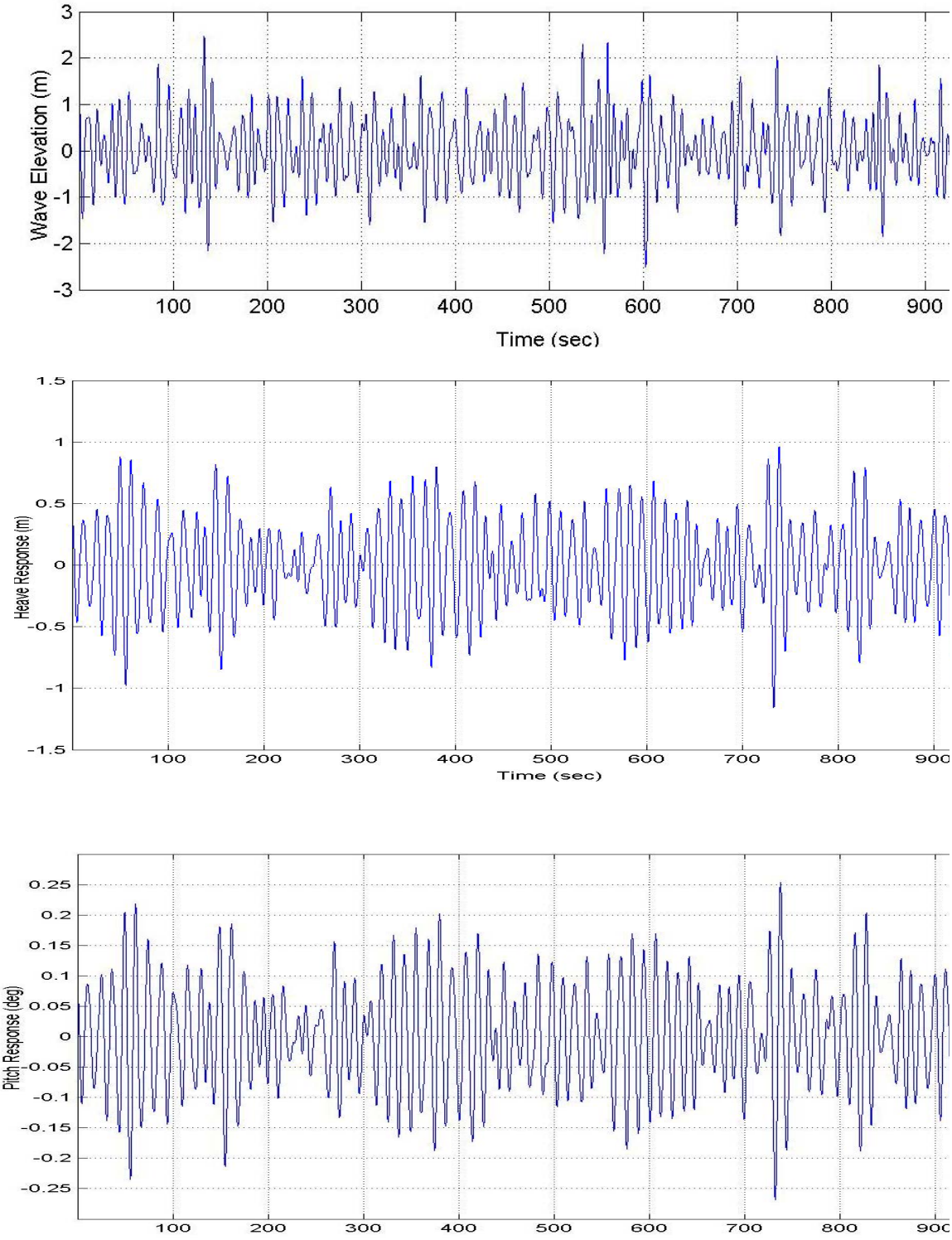

Figure 4-46: Beam sea-Hs 6.0m-input wave data, heave, and pitch response

The probability of exceedence for the relative motion shows that the theoretical estimates are definitely much above the actual results. At this sea state the deviation of the theory from that of the actual field data seems to be quite large.

For the beam sea condition the heave and pitch response values will be comparatively higher that the head sea estimates. As can be seen in Figure 4-47 since the same input wave is used, the data set for the input wave is seen to have the maximum wave elevation of around 2.5 meters and corresponding heave response is around 1.0 meter. The pitch response also is seen to be somewhere close to 0.25 deg.

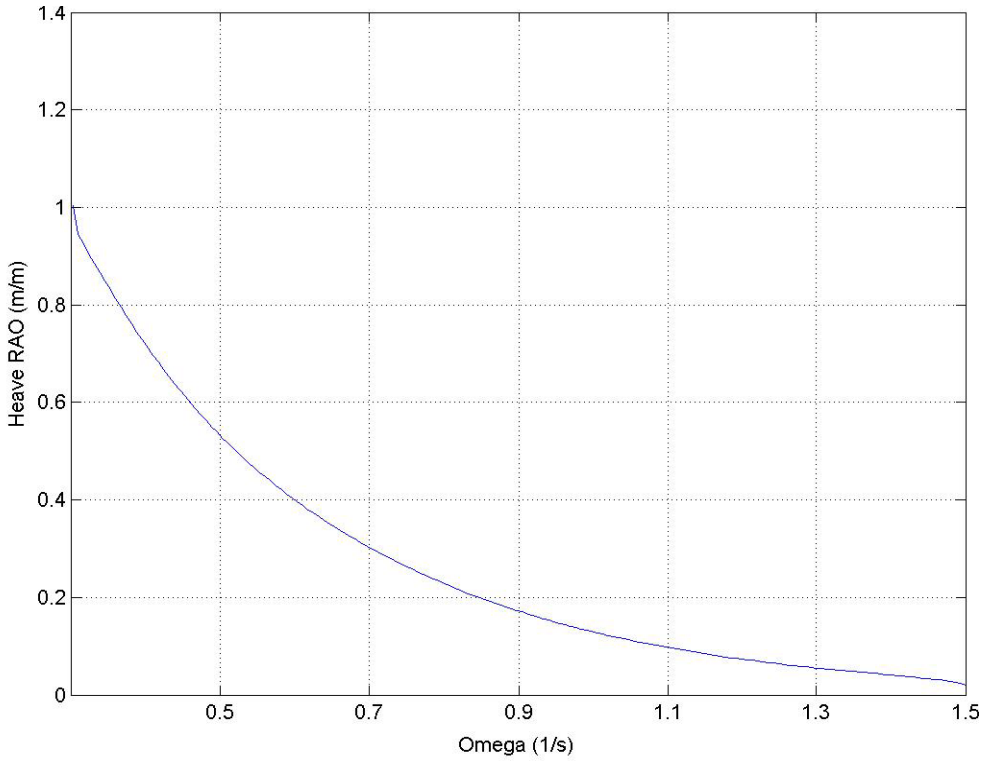

Figure 4-47: Beam sea-Hs 6.0m-heave RAO

The heave RAO trend as observed through Figure 4-48 show that the RAO range drops from the zero frequency value of 1.0 to values close to zero for high frequency range.

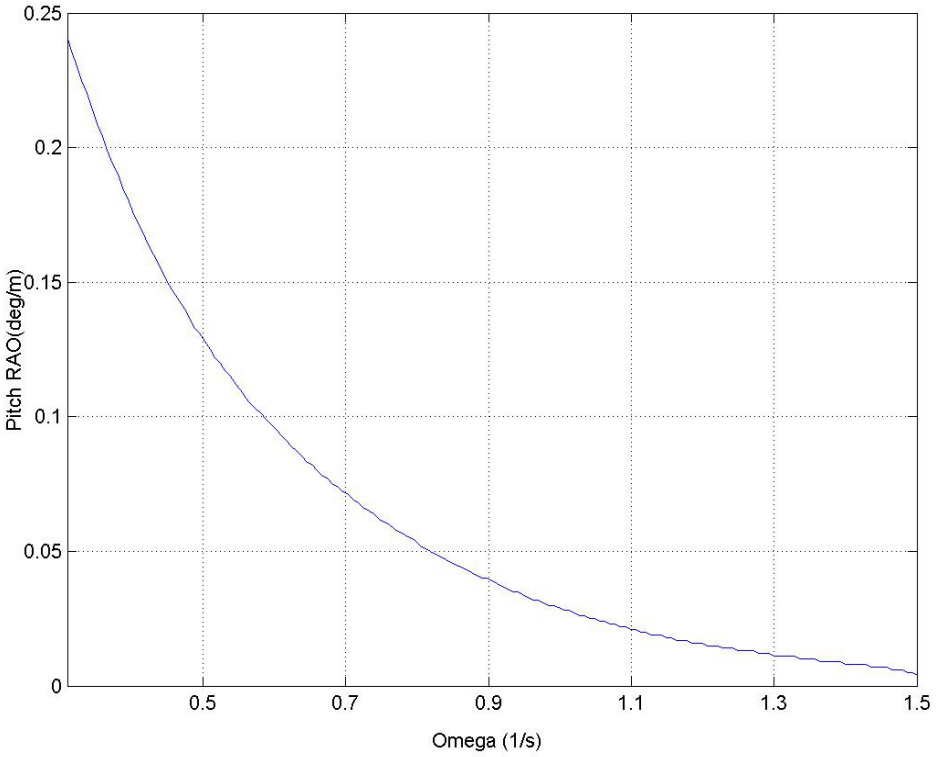

Figure 4-48: Beam sea-Hs 6.0m-pitch RAO

The pitch RAO trend as shown in Figure 4-49 show that the RAO range drops from the zero frequency value of 0.25 to values close to zero for high frequency range values. Unlike heave RAO, the pitch RAO values do not range from 1 to 0 but instead have a range which is dependent on factors specific to the form of the vessel.

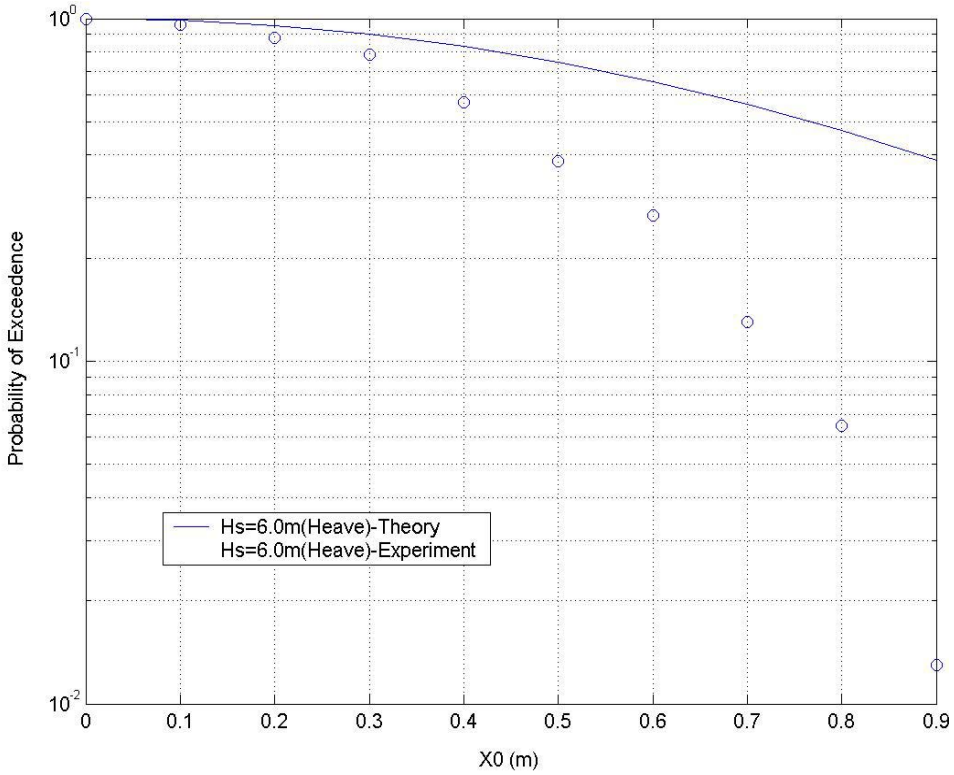

Figure 4-49: Beam sea-Hs 6.0m- probability of exceedence for heave motion

The probability of exceedence is again higher for the experiment as compared to the theoretical results. It can also be noticed in Figure 4-50 that the maximum heave values for this sea state would be 0.9m. The experimental value of heave probability of exceedence deviates from theoretical estimates for higher and higher sea states and hence showing the extent to which theory over estimates the response results.

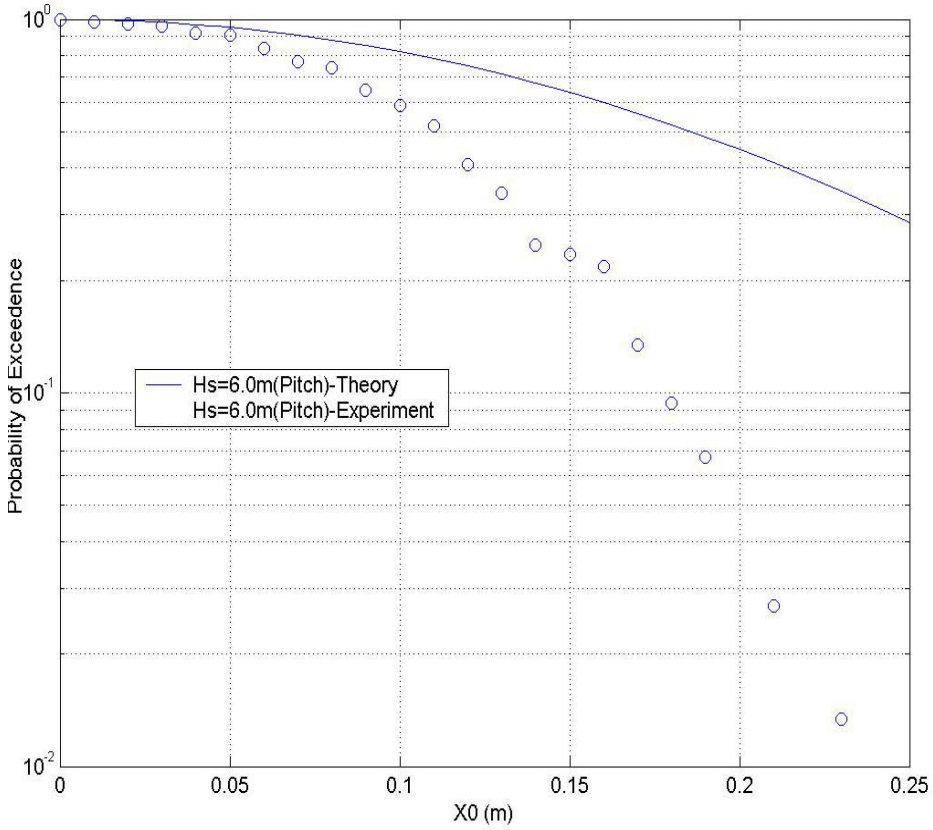

Figure 4-50: Beam sea-Hs 6.0m- probability of exceedence for pitch motion

The probability of exceedence of pitch is higher for the experiment as compared to the theoretical results. It can also be noticed in Figure 4-51 that the maximum pitch values for this sea state would be 0.25m. The experimental value of heave probability of exceedence deviates from theoretical estimates for higher and higher sea states and hence showing the extent to which theory over estimates the response results.

Relative motion-leeward side

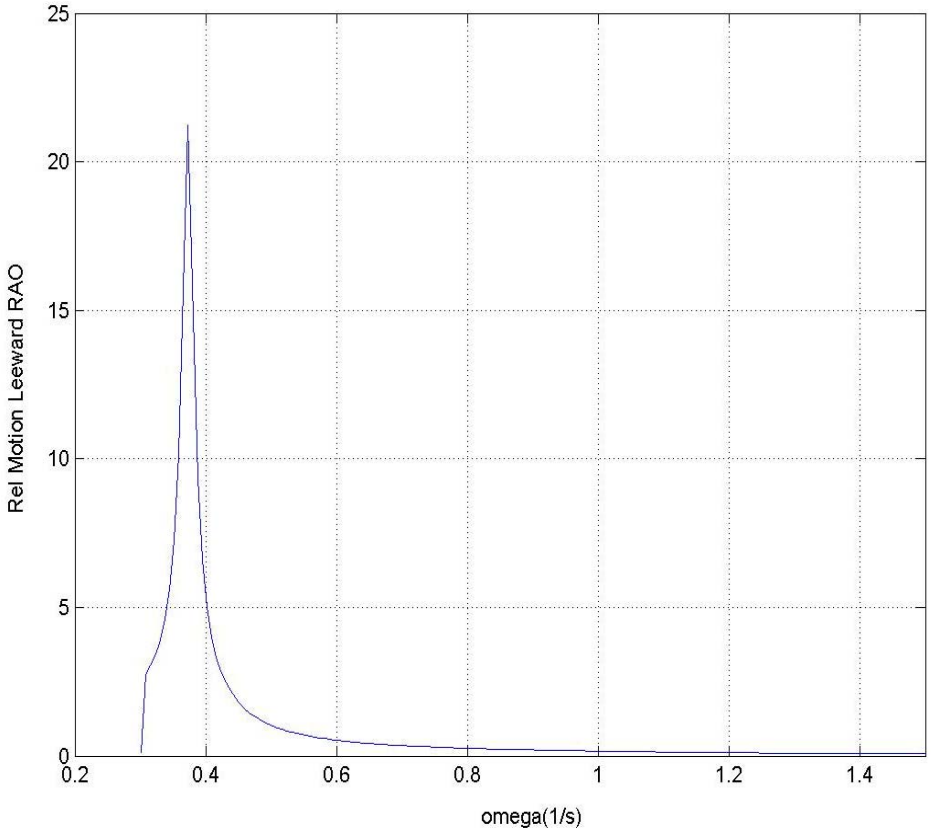

Figure 4-51: Relative motion RAO [leeward side]

The relative motion RAO for the leeward side for higher sea states also has an abrupt peak due to the roll response as seen in Figure 4-52. Hence here again the relative motion response is plotted separately within the frequency range where resonances with roll motion occurs as well as outside the range of this peak roll value.

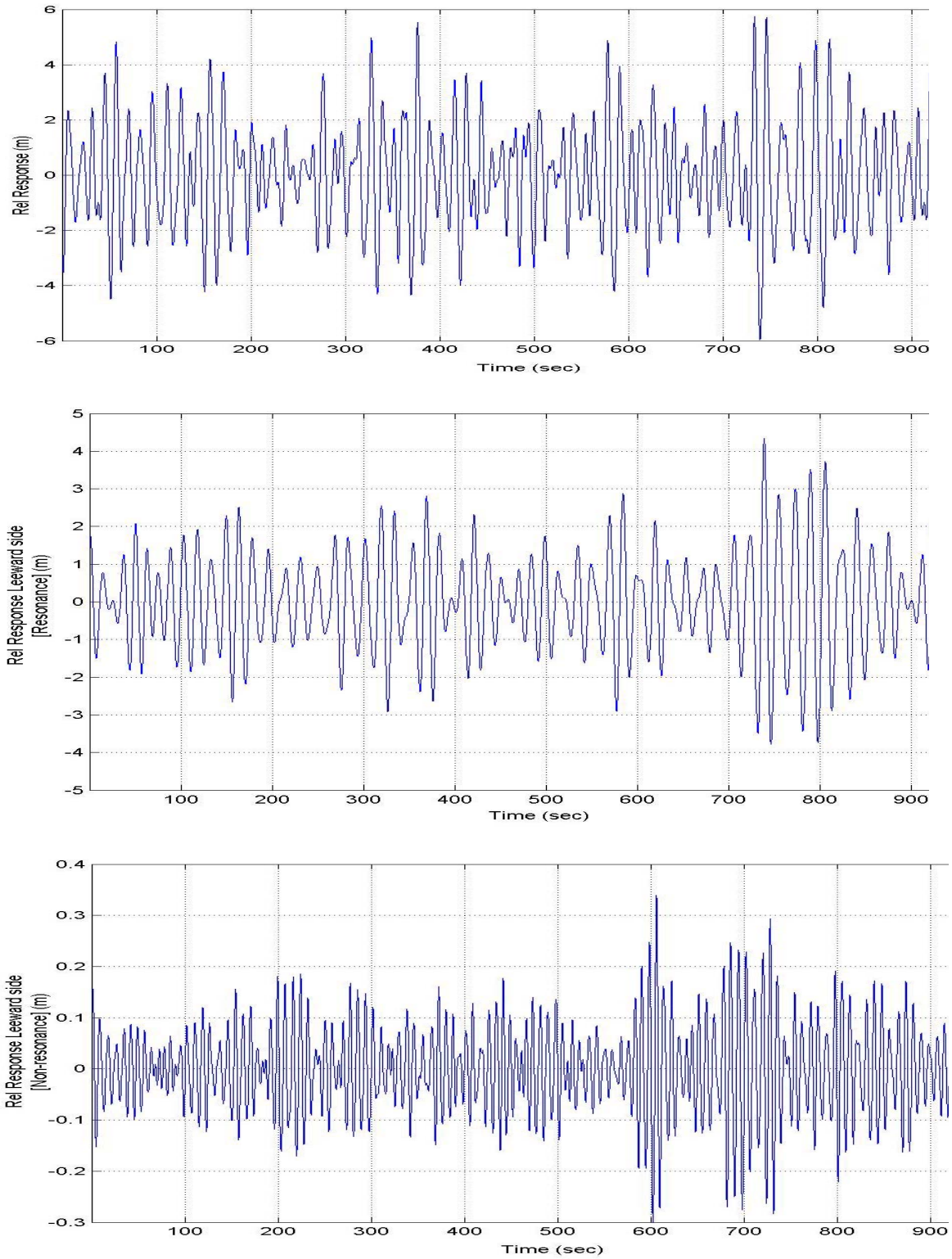

Figure 4-52: Beam sea-Hs 3.0m- relative motion with and without roll resonance [leeward side]

The relative motion response with and without response as shown in Figure 4-53 above indicate that the peak values in response is predominantly due to the roll resonance values. The probability of exceedence values for the Hs value of 6.0 meters is shown in Figure 4-54.

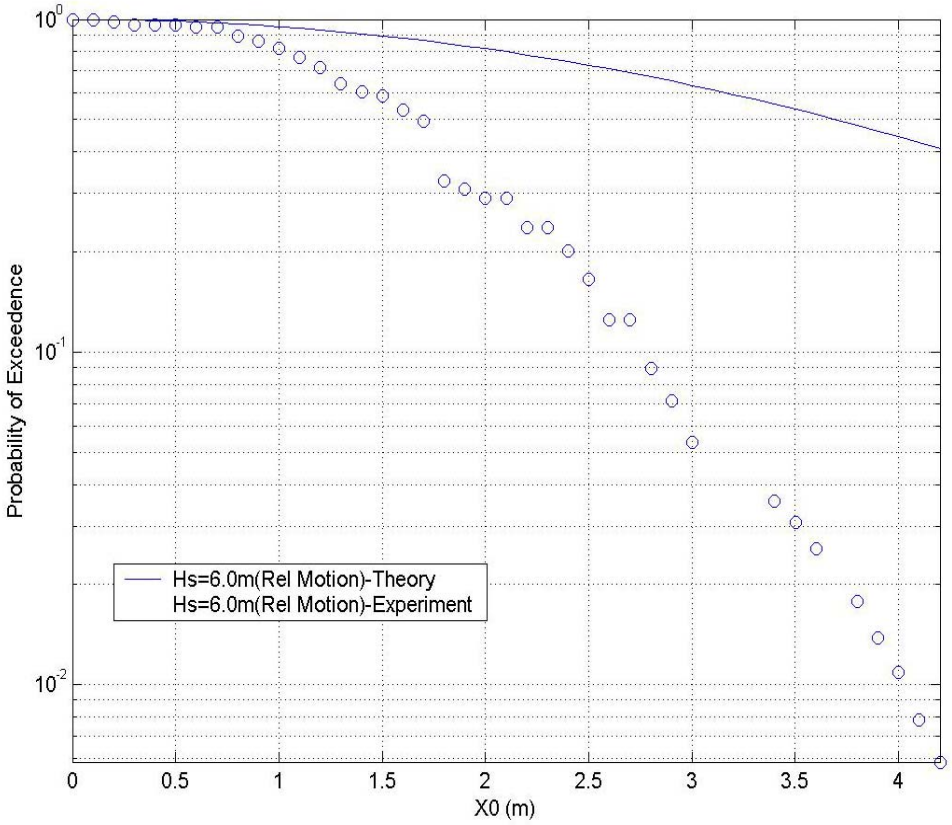

Figure 4-53: Beam sea-Hs 6.0m- probability of exceedence for relative motion [leeward side]

The weather side relative motion is also having a contribution from the roll natural frequency as seen in Figure 4-55. The roll resonance value will add to the actual relative response and the relative response value will consequently be of a very high value as can be seen in Figure 4-56.

Relative motion- weather side

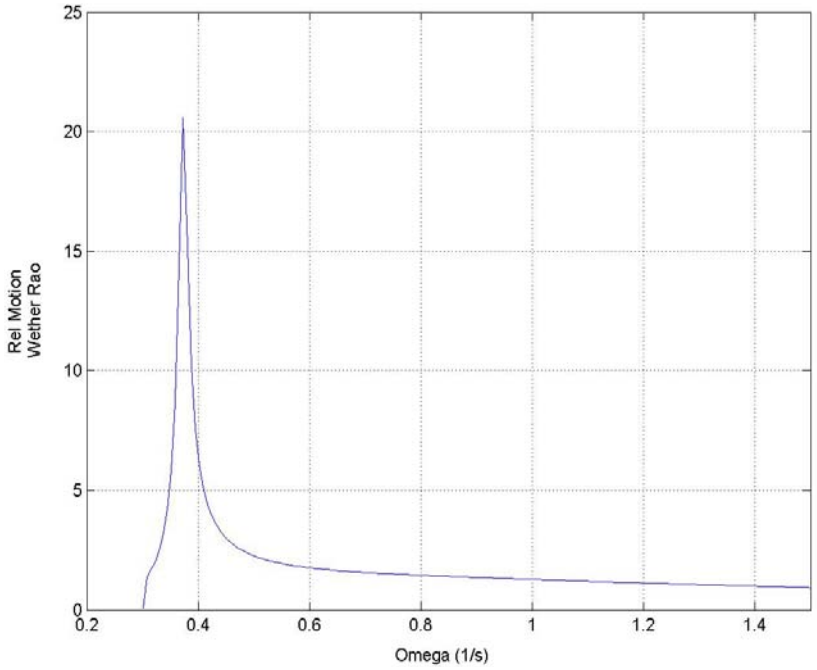

Figure 4-54: Relative motion RAO [weather side]

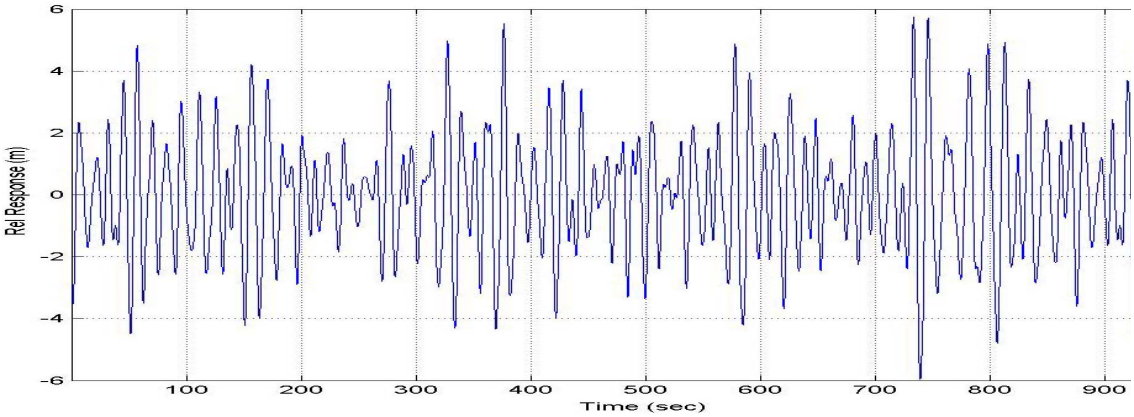

Figure 4-55: Beam sea-Hs 6.0m- relative motion with and without roll resonance [weather side]

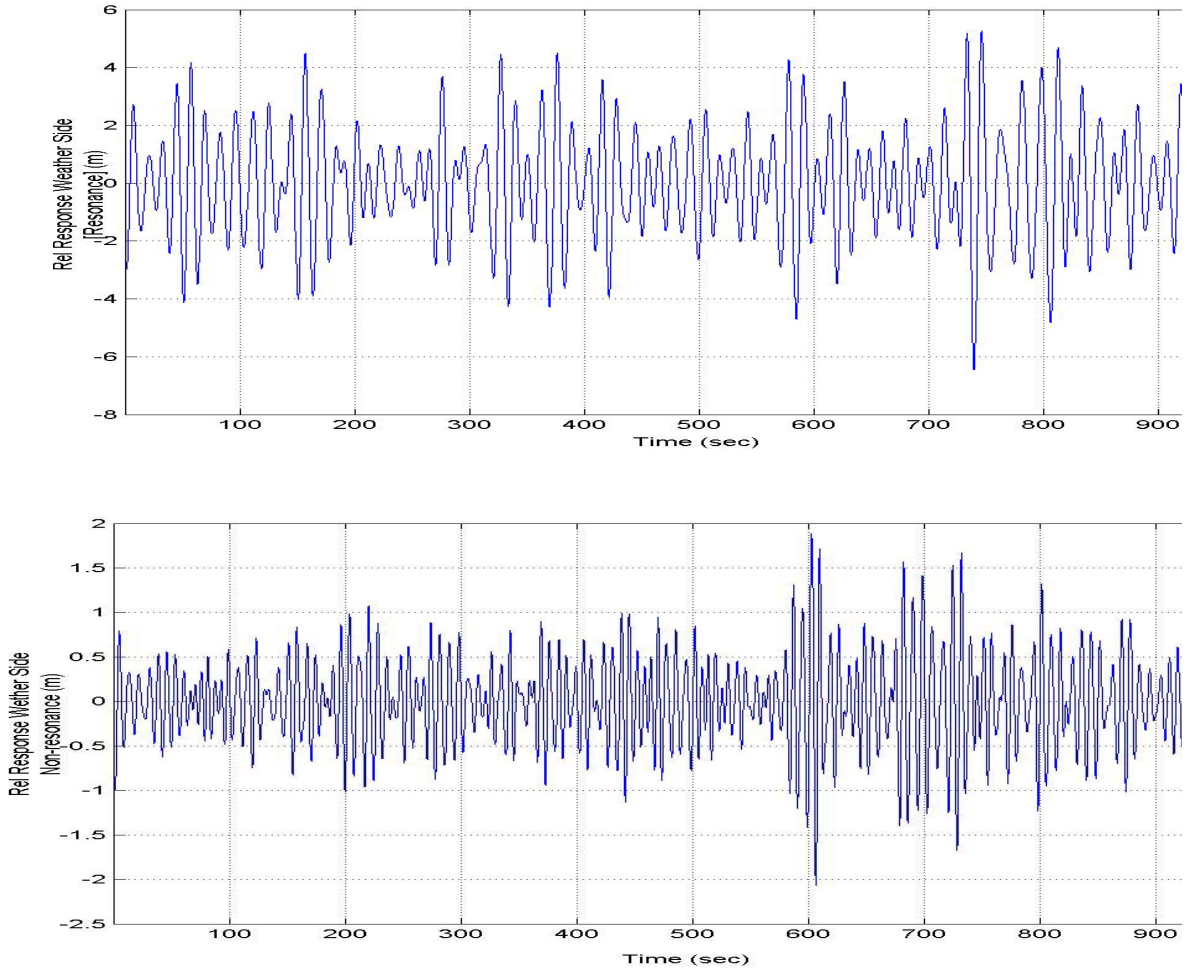

Figure 4-55: Continued

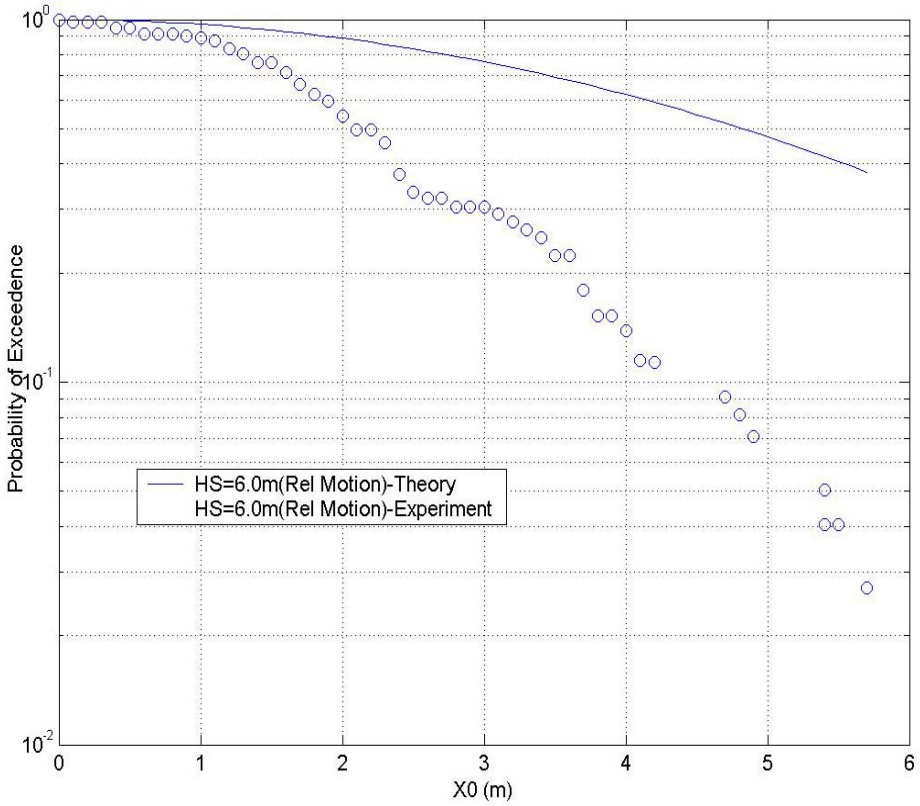

Figure 4-56: Beam sea-Hs 6.0m- probability of exceedence for relative motion [weather side]

The probability of exceedence of relative motion is higher for the experiment as compared to the theoretical results. It can also be noticed in Figure 4-57 that the maximum relative motion values for this sea state would be 6.0 m. The experimental value of relative probability of exceedence deviates from theoretical estimates for higher and higher sea states and hence showing the extent to which theory over estimates the response results.

4.2.3 Case #3: Hs =9.0 m

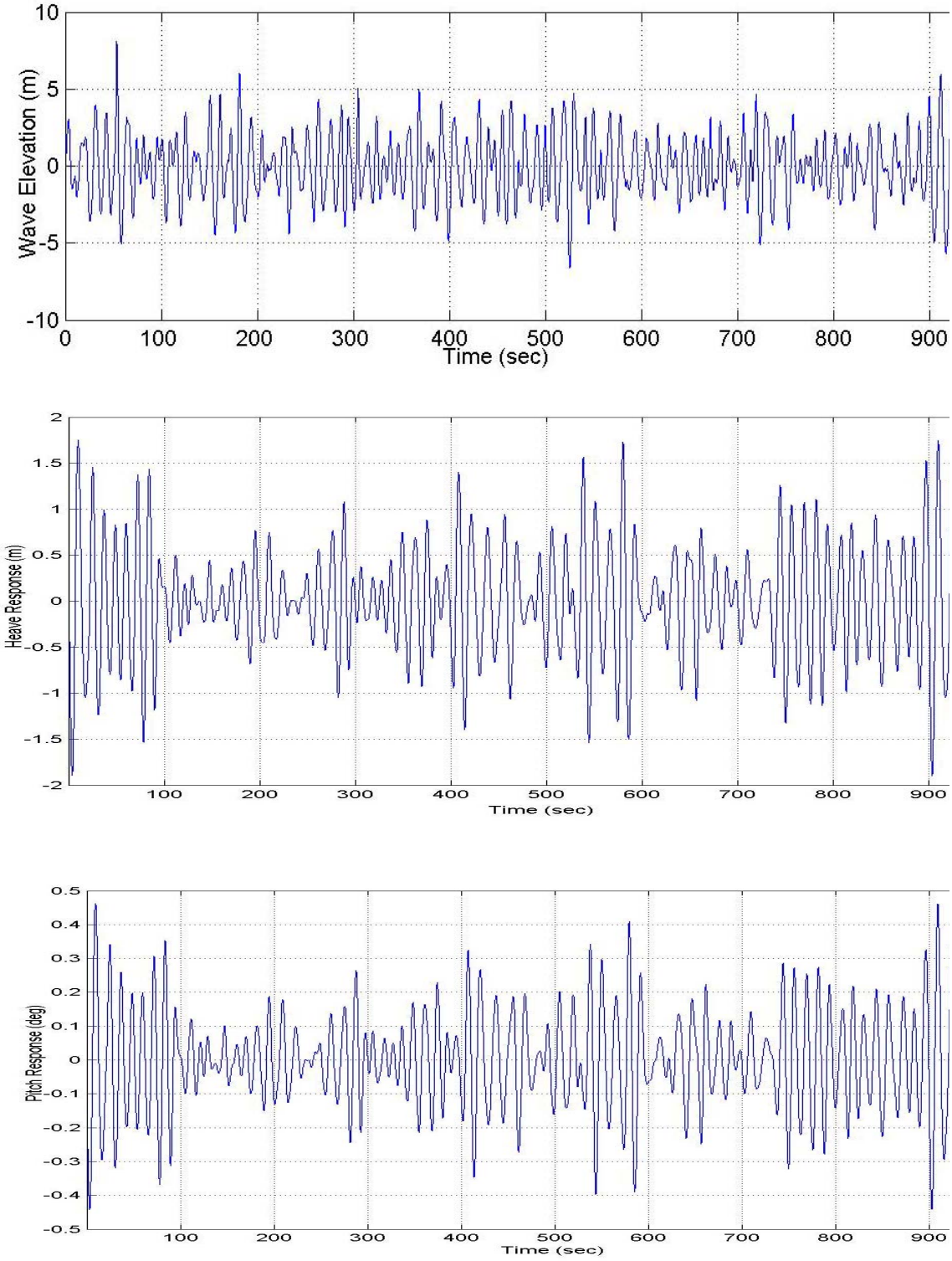

Figure 4-57: Beam sea-Hs 9.0m-input wave data, heave, pitch response

Here again it can be observed from Figure 4-58 that the beam sea condition has a higher heave and pitch response value compared to head sea estimates. Since the same input wave is used, the data set for the input wave is seen to have the maximum wave elevation of around 7.4 meters and corresponding heave response is around 1.7 meters.

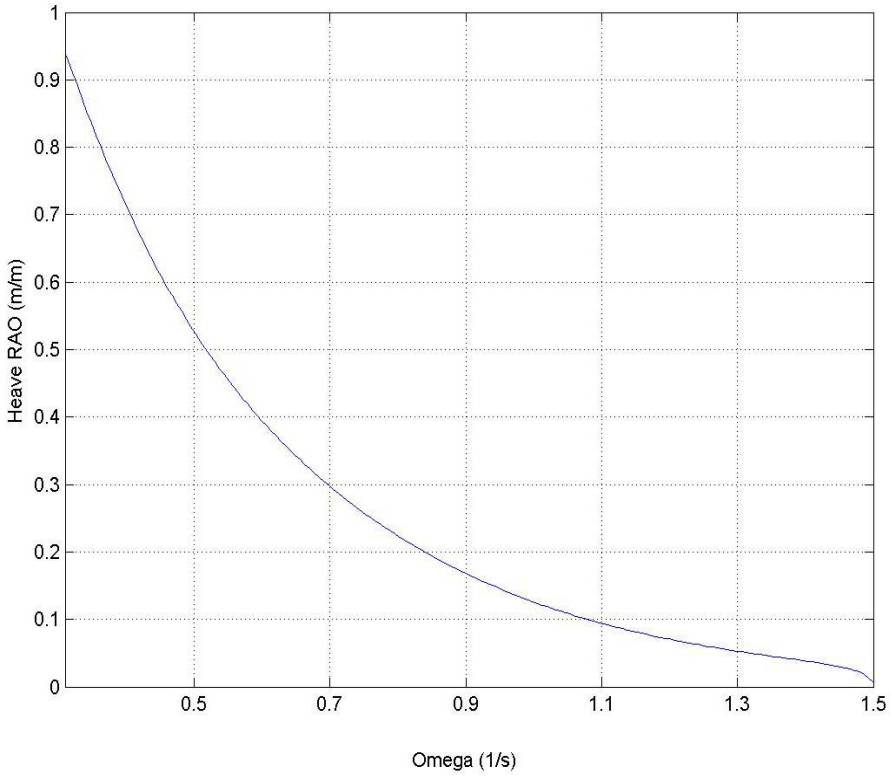

Figure 4-58: Beam sea-Hs 9.0m-heave RAO

The heave and pitch RAO values also falls over the increasing frequency range values as shown in Figure 4-59 and Figure 4-60 starting at 1.0 and dropping to zero at a frequency range of 1.5 rad/sec.

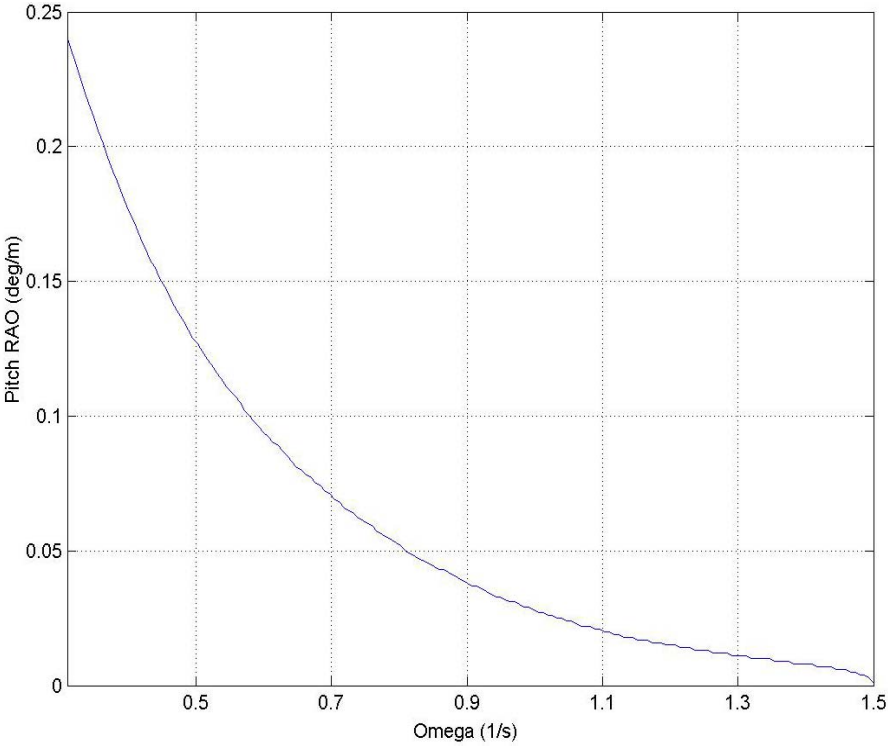

Figure 4-59: Beam sea-Hs 6.0m-pitch RAO

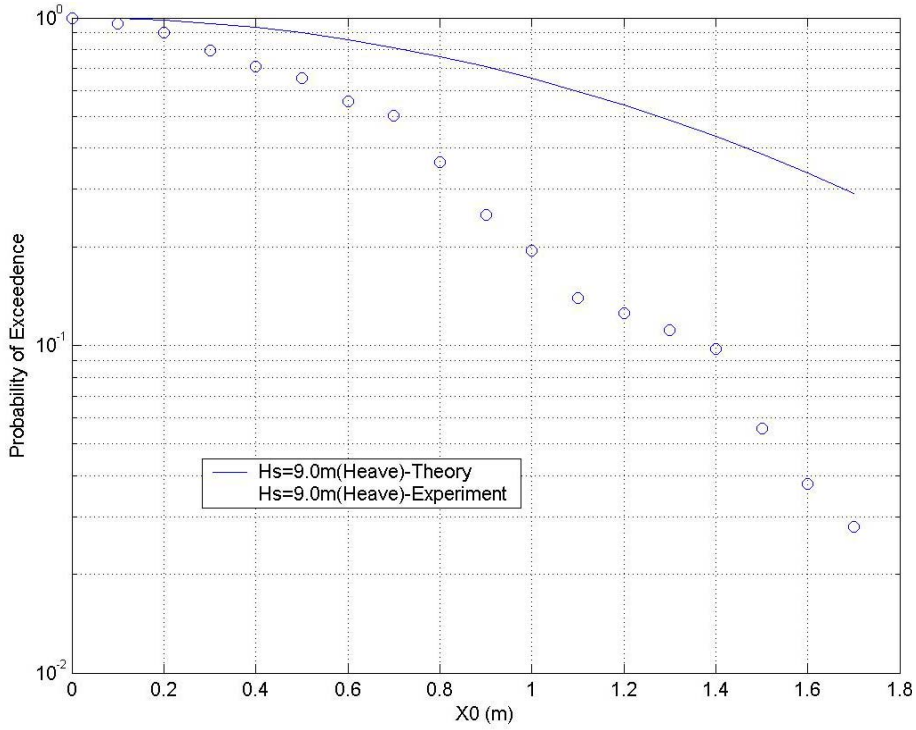

Figure 4-60: Beam sea-Hs 9.0m- probability of exceedence for heave motion

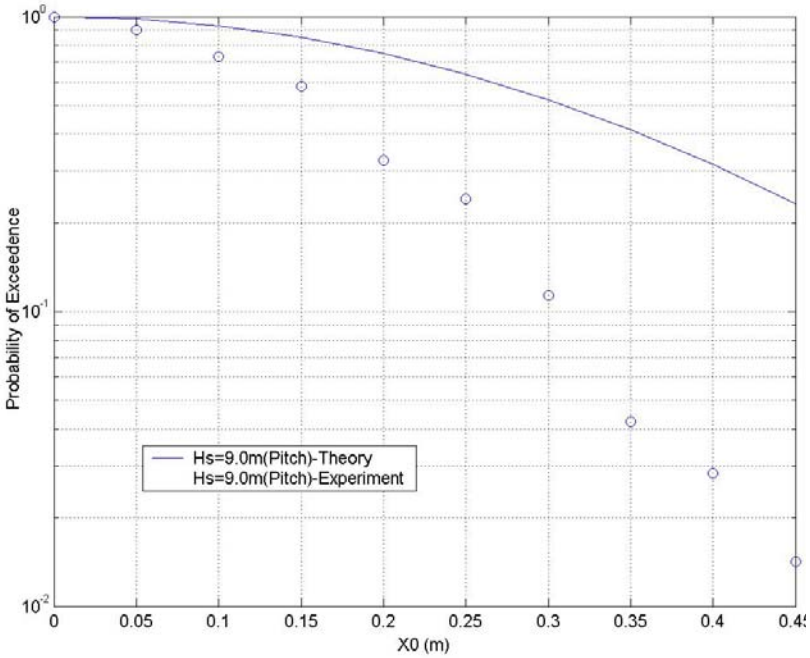

Figure 4-61: Beam sea-Hs 9.0m- probability of exceedence for pitch motion

Here again we can see in Figure 4-61 and Figure 4-62 that the theory over estimates in comparison to the experimental results in the values of the probability of exceedence for heave and pitch. It can also be noticed that the maximum heave values for this sea state would be 1.8 m in comparison to that of the linear case of Hs = 3.0 meters.

The higher frequency range values will not contribute to the heave response. This is mainly due to the tiny ripples of high frequency values that will be too small to cause and significant impact on the response.

Relative motion-leeward side

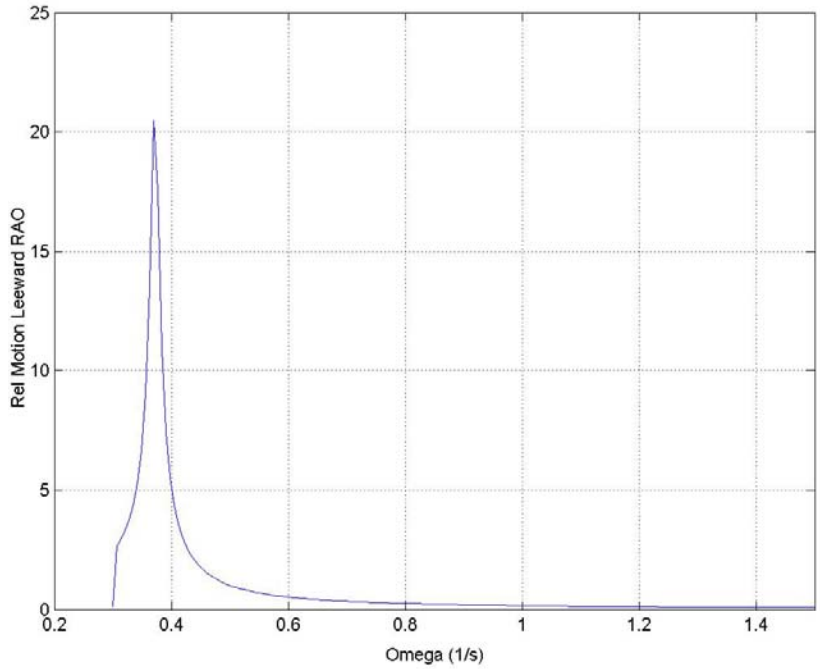

Figure 4-62: Relative motion RAO [leeward side]

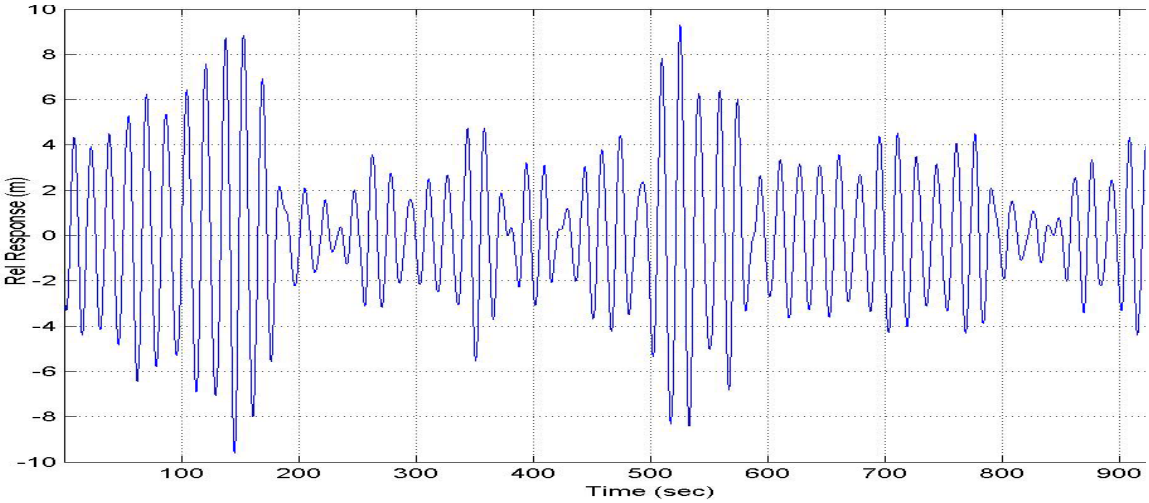

Figure 4-63: Beam sea-Hs 9.0m-relative motion with and without roll resonance [leeward side]

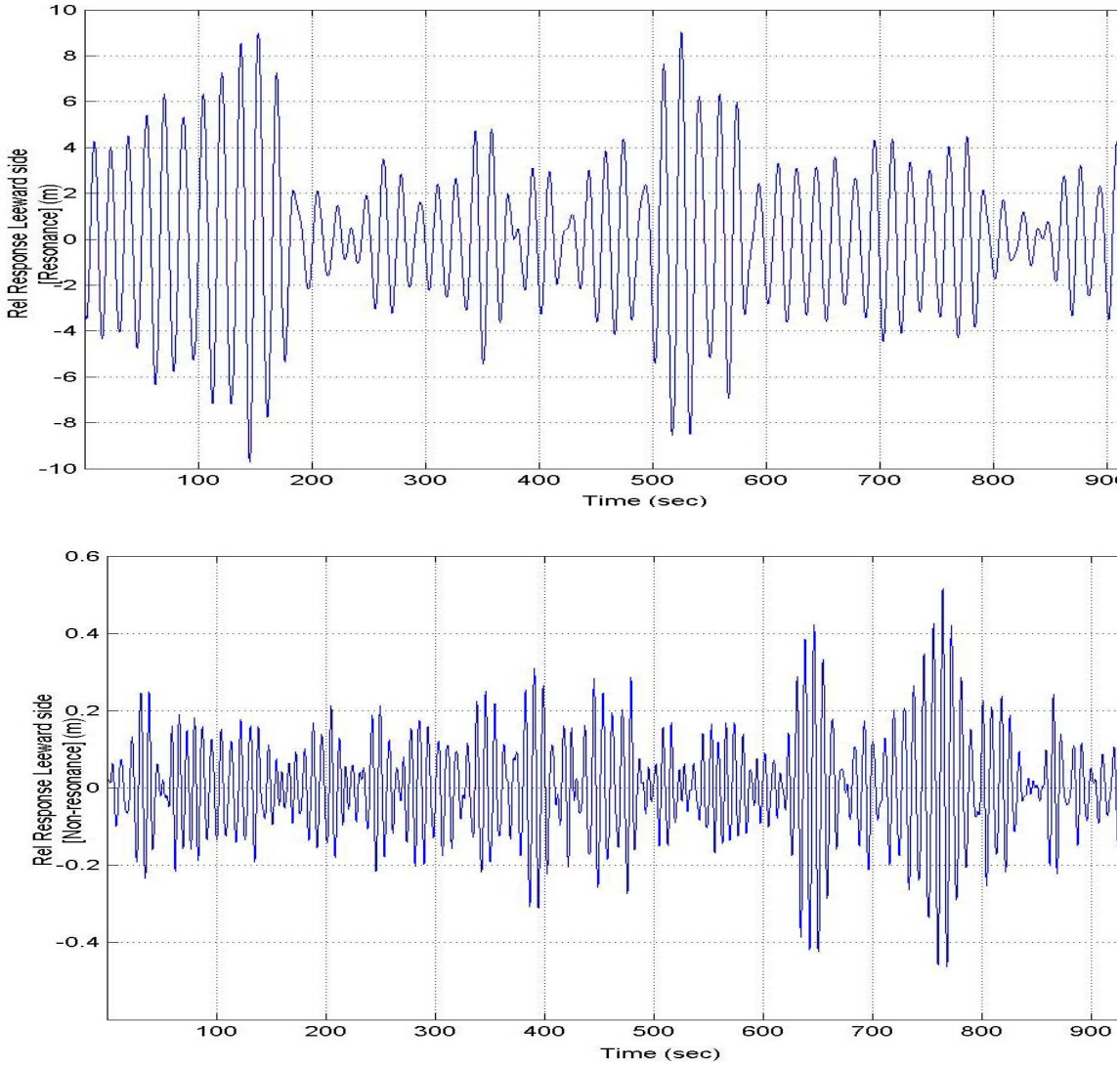

Figure 4-63: Continued

The relative motion RAO for the leeward side for this sea state also has an abrupt peak due to the roll response as shown in Figure 4-63. Here again the relative motion response is plotted separately within the resonance frequency range, which is due to the roll motion and the outside the range of this peak roll value.

From the Figure 4-64 it can be observed that the relative response in the leeward side for this sea state is also predominantly contributed by the roll natural frequency

response. The roll values, which occur at the low frequency range, contribute significantly towards the overall response in the beam sea state.

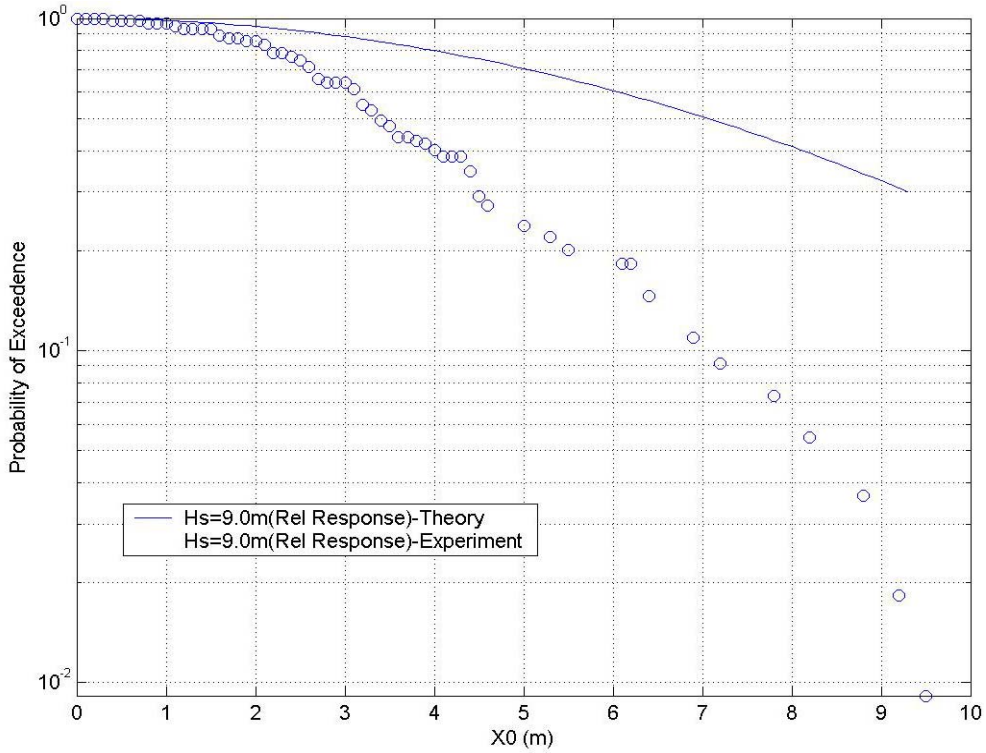

Figure 4-64: Beam sea-Hs 9.0m- probability of exceedence for relative motion [leeward side]

Here it can be observed that the leeward side response components are comparatively lesser in magnitude than the weather side components. The probability of exceedence values go up to 9.5 meters for the sea state =9.0 meters showing their deviation from the experimental estimates as shown in Figure 4-65.

Relative motion- weather side

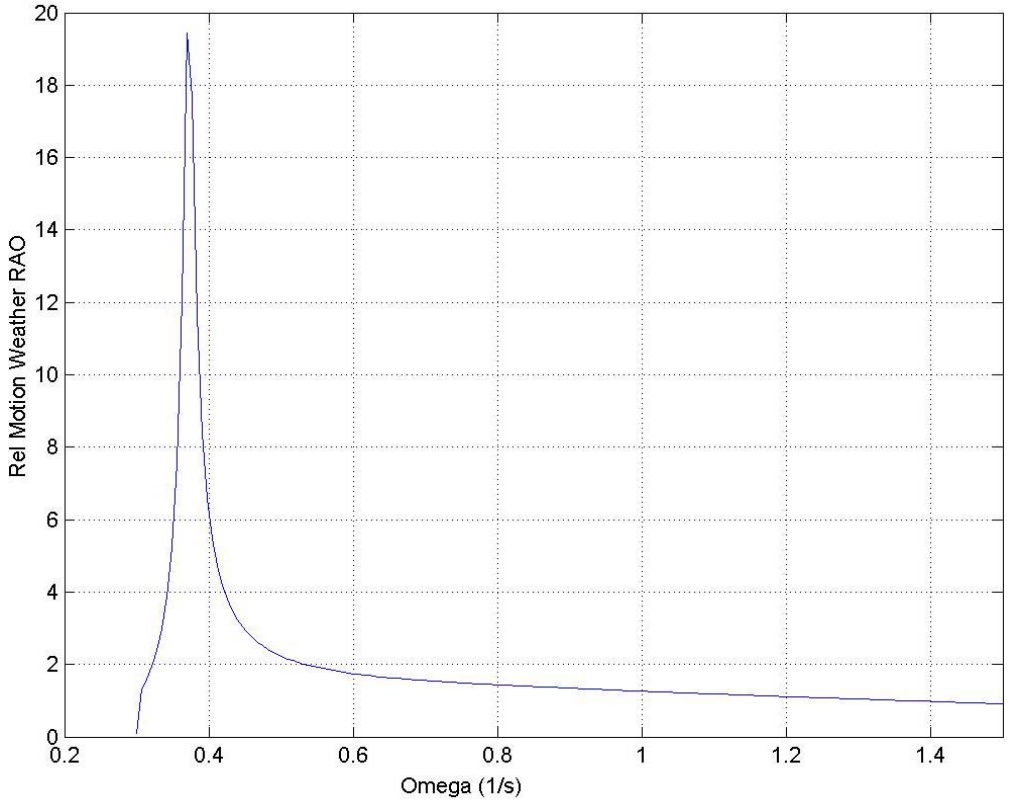

Figure 4-65: Relative motion RAO [weather side]

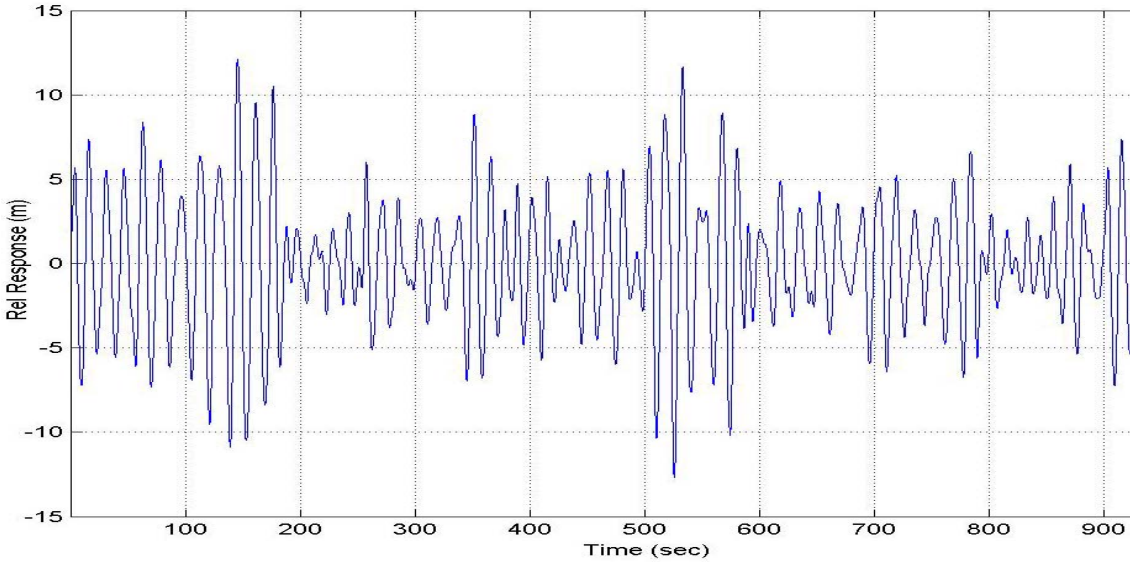

Figure 4-66: Beam sea-Hs 9.0m- relative motion with and without roll resonance [weather side]

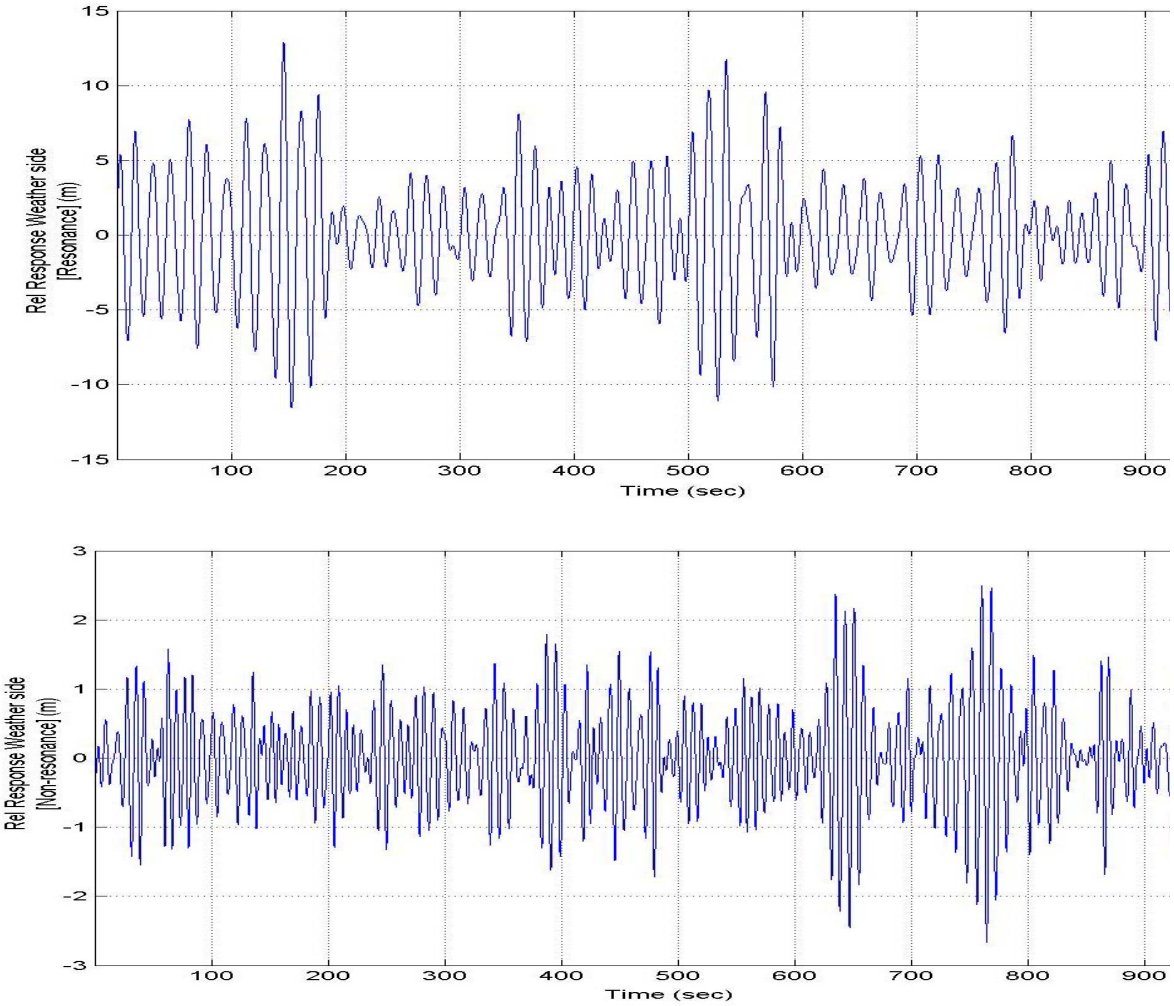

Figure 4-66: Continued

The roll values, as shown in Figure 4-66, which occur at the low frequency range, contribute significantly towards the overall response in the beam sea state. From the Figure 4-67 it can be observed that the relative response in the weather side is also significantly contributed by the roll natural frequency response.

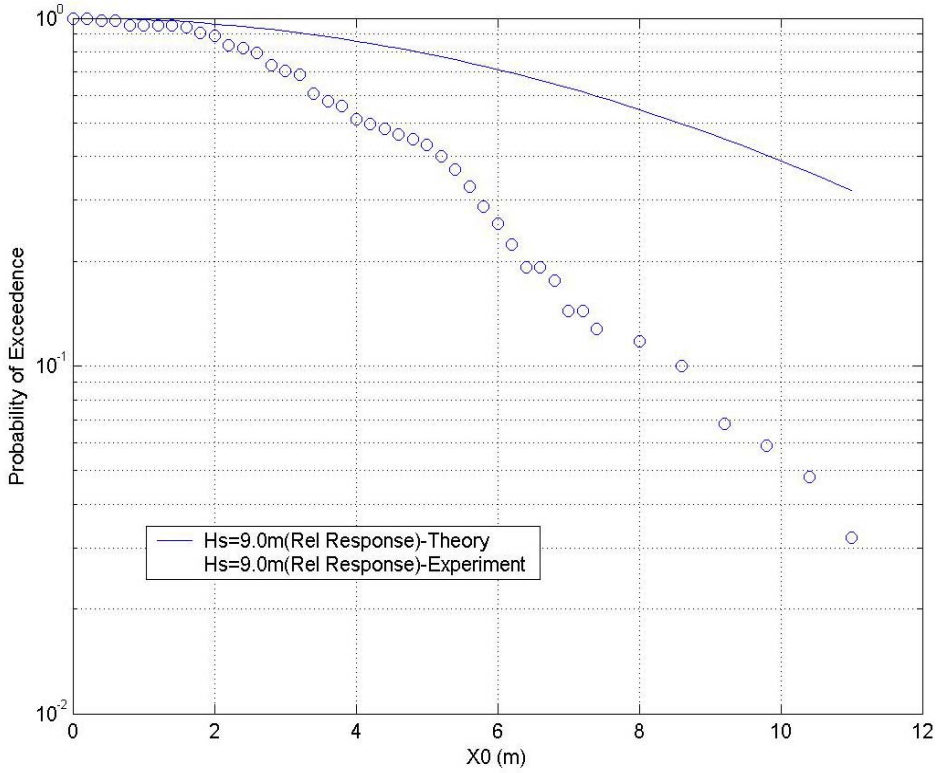

Figure 4-67: Beam sea-Hs 9.0m- probability of exceedence for relative motion [weather side]

As discussed above, the weather side probability of exceedence has a higher range of value for X0 due to the direct impact on the structure and the consequent relative response arising out of it. It can be seen from Figure 4-68 that the weather side relative response value goes up to 11.5 meters in comparison to the leeward side.

The probability of exceedence for the relative motion shows that the theoretical estimates are definitely much above the actual results. At this sea state the deviation of the theory from that of the actual field data seems to be quite large.

4.2.4 Case #4: Hs =11.0 m

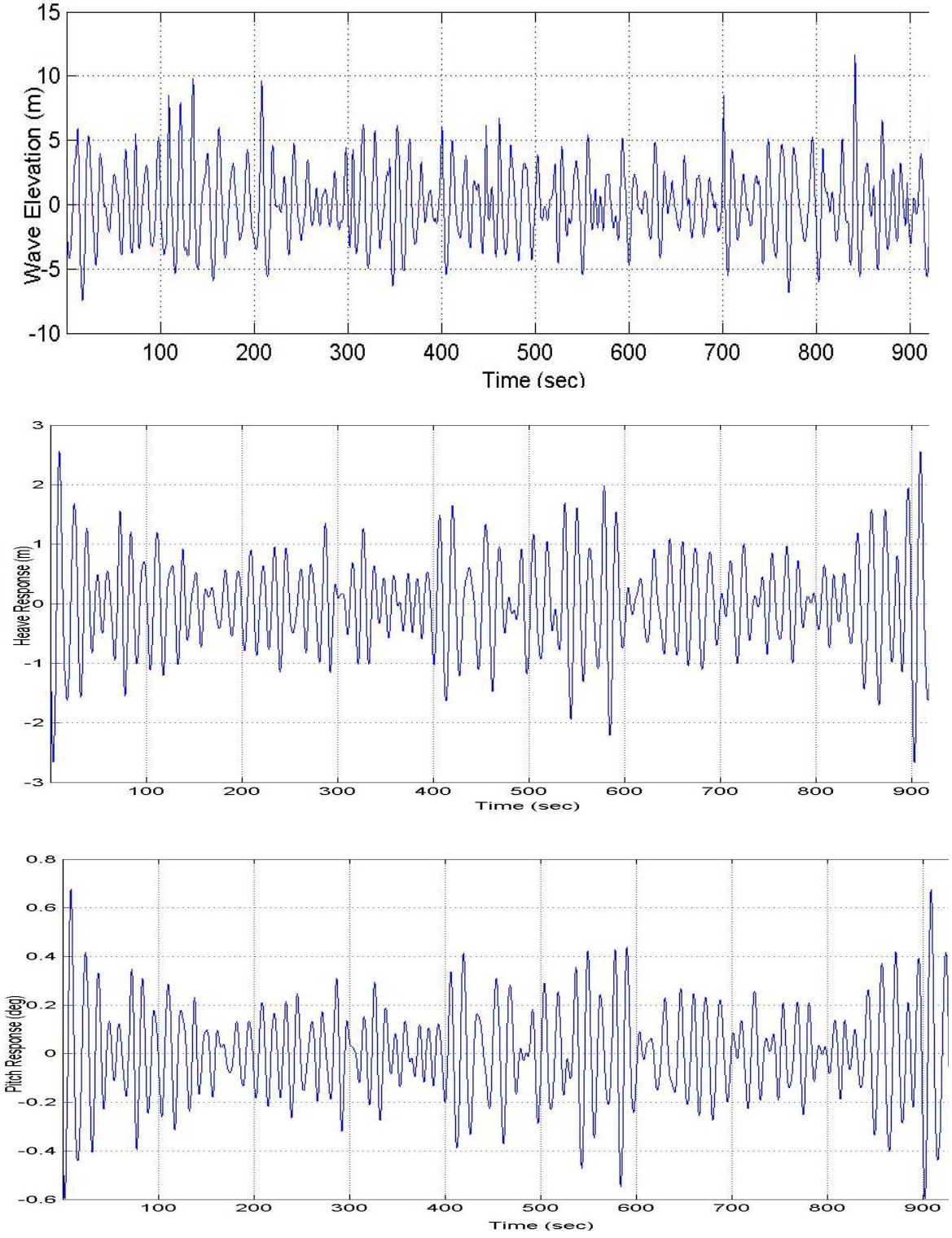

Figure 4-68: Beam sea-Hs 11.0m-input wave data, heave, pitch response

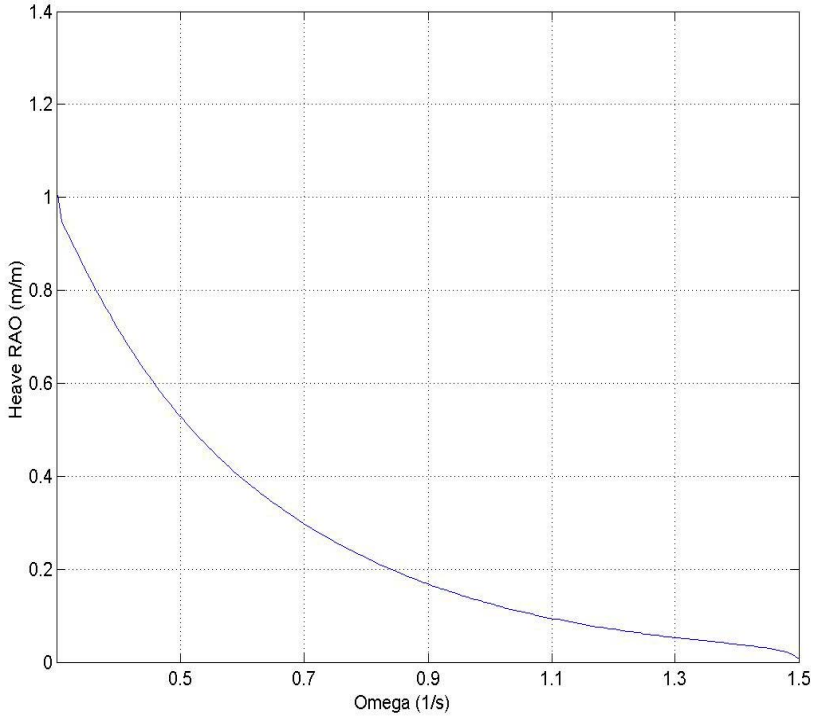

Figure 4-69: Beam sea-Hs 11.0m-heave RAO

As can be seen in Figure 4-69 in the beam sea condition the heave and pitch response values will be comparatively higher than the head sea estimates. Since the same input wave is used, the data set for the input wave is seen to have the maximum wave elevation of around 11.5 meters and corresponding heave response is around 2.45 meters.

The heave and pitch RAO for the beam sea condition are fairly smooth unlike that of the head sea states. The trends can of can be observed in Figure 4-70 and Figure 4-71. The figure indicates that the RAOs show a higher influence on the structure heave and pitch response in predominantly low frequencies.

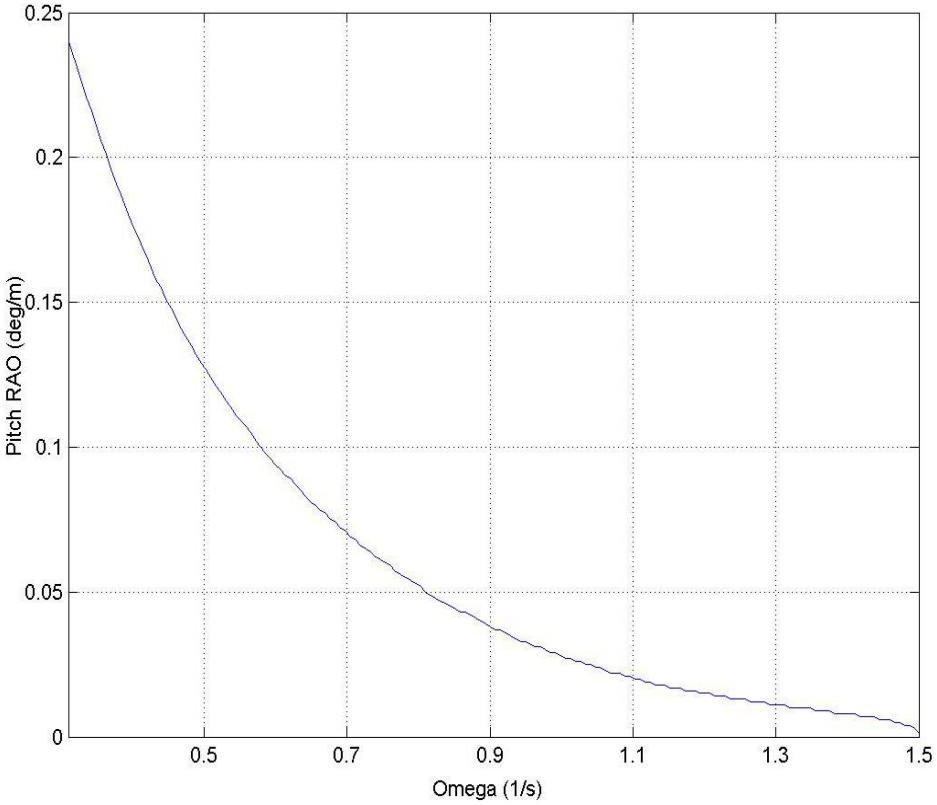

Figure 4-70: Beam sea-Hs 11.0m-pitch RAO

The pitch response also is seen to be somewhere close to 0.75 deg. The input wave and the response can be closely observed to note that the peak response in both heave and pitch occurs at around the same time as the maximum wave elevation. Again, the response will have a lag to the response because of the inertia of the vessel as well as its hydrostatic stiffness.

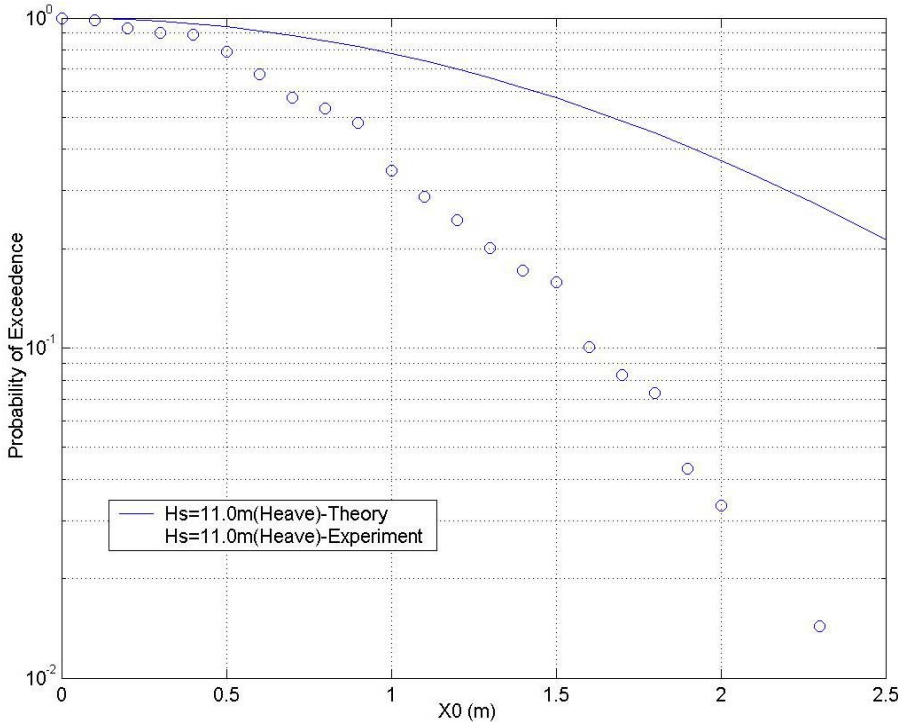

Figure 4-71: Beam sea-Hs 11.0m-probability of exceedence for heave motion

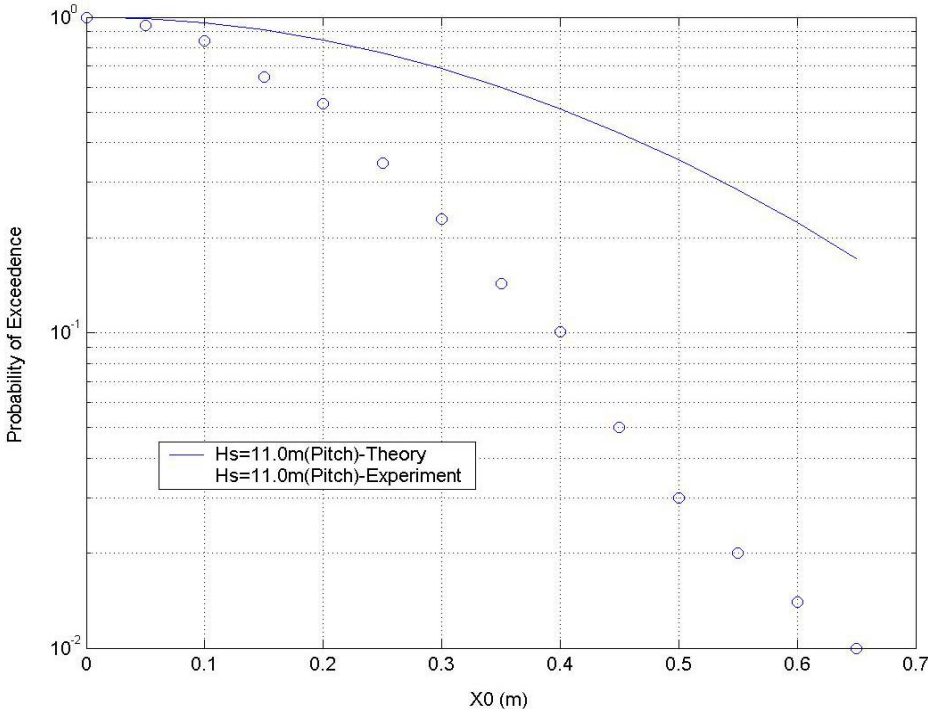

Figure 4-72: Beam sea-Hs 11.0m- probability of exceedence for pitch motion.

The probability of exceedence is again higher for the experiment as compared to the theoretical results. It can also be noticed in Figure 4-72 that the maximum heave values for this sea state would be 2.5 m. Similarly the maximum pitch response values also would be in the around 0.79 deg which is shown in Figure 4-73.

Relative motion-leeward side

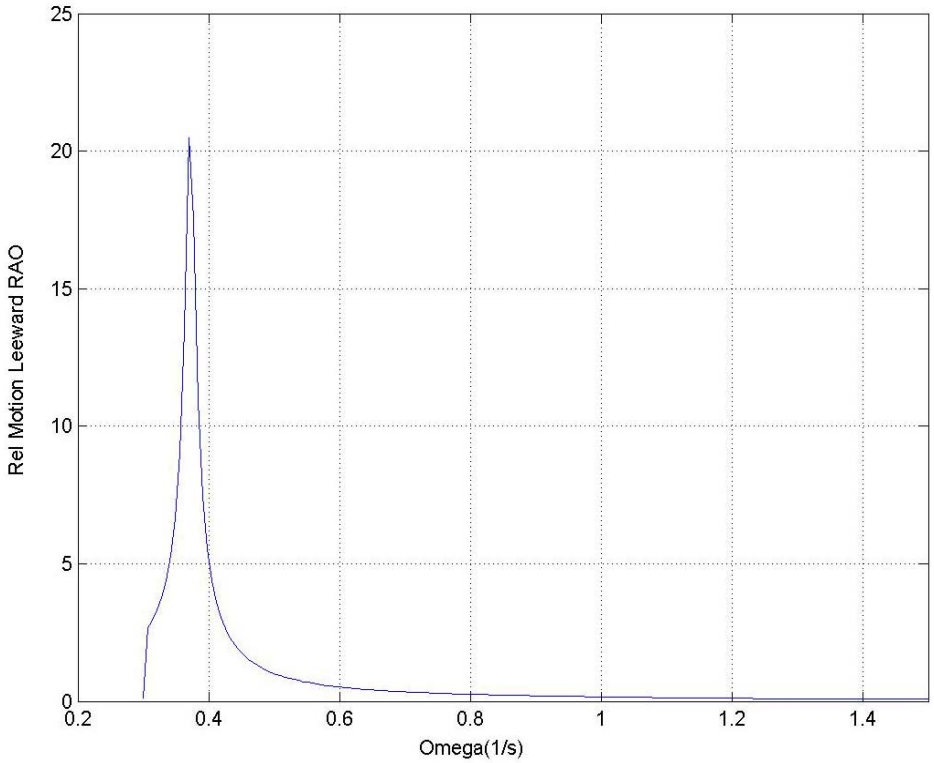

Figure 4-73: Beam sea-Hs 11.0m -relative motion RAO [leeward side]

The relative motion RAO for the leeward side indicates an abrupt peak in the data for a low frequency range of around 0.34 rad/sec as can be seen in Figure 4-74. The trend of the roll resonance frequency for this high sea state is shown in Figure 4-75.

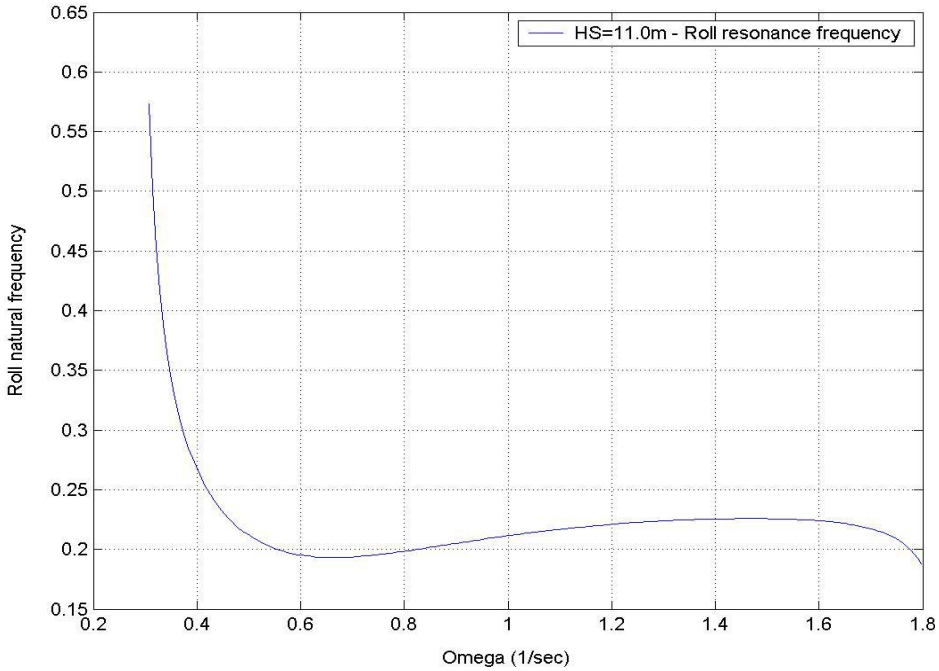

Figure 4-74: Beam sea-Hs 11.0m –roll resonance frequency

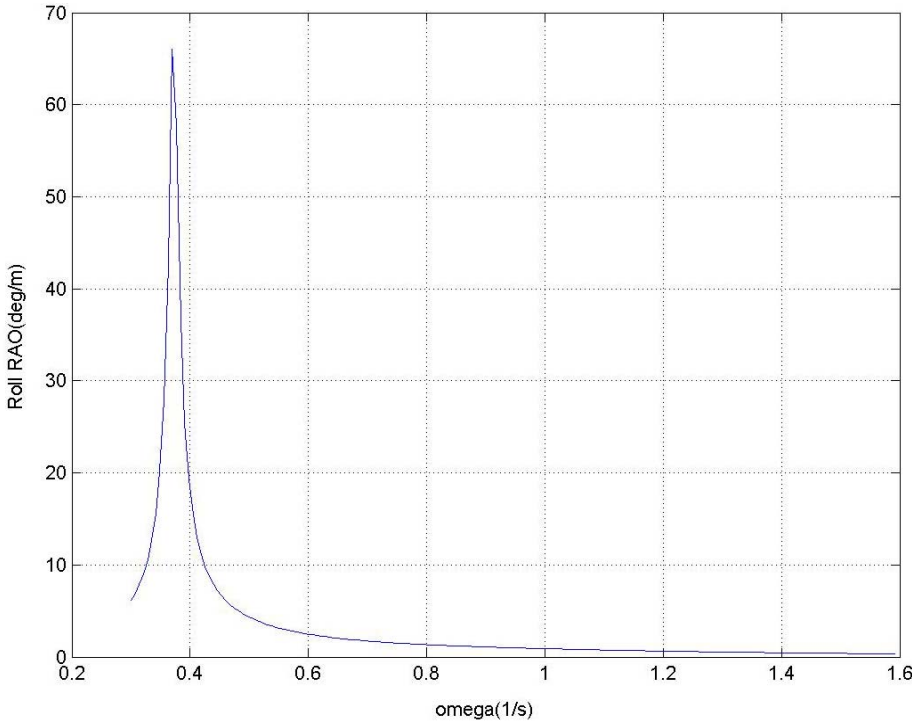

Figure 4-75: Beam sea-Hs 11.0m –roll RAO

The high frequency resonance that is shown in Figure 4-76 is analyzed and found to be the roll RAO contribution to the relative motion. Hence the relative motion response is plotted separately within the resonance frequency range and the range outside this peak roll value as can be seen in Figure 4-77 below.

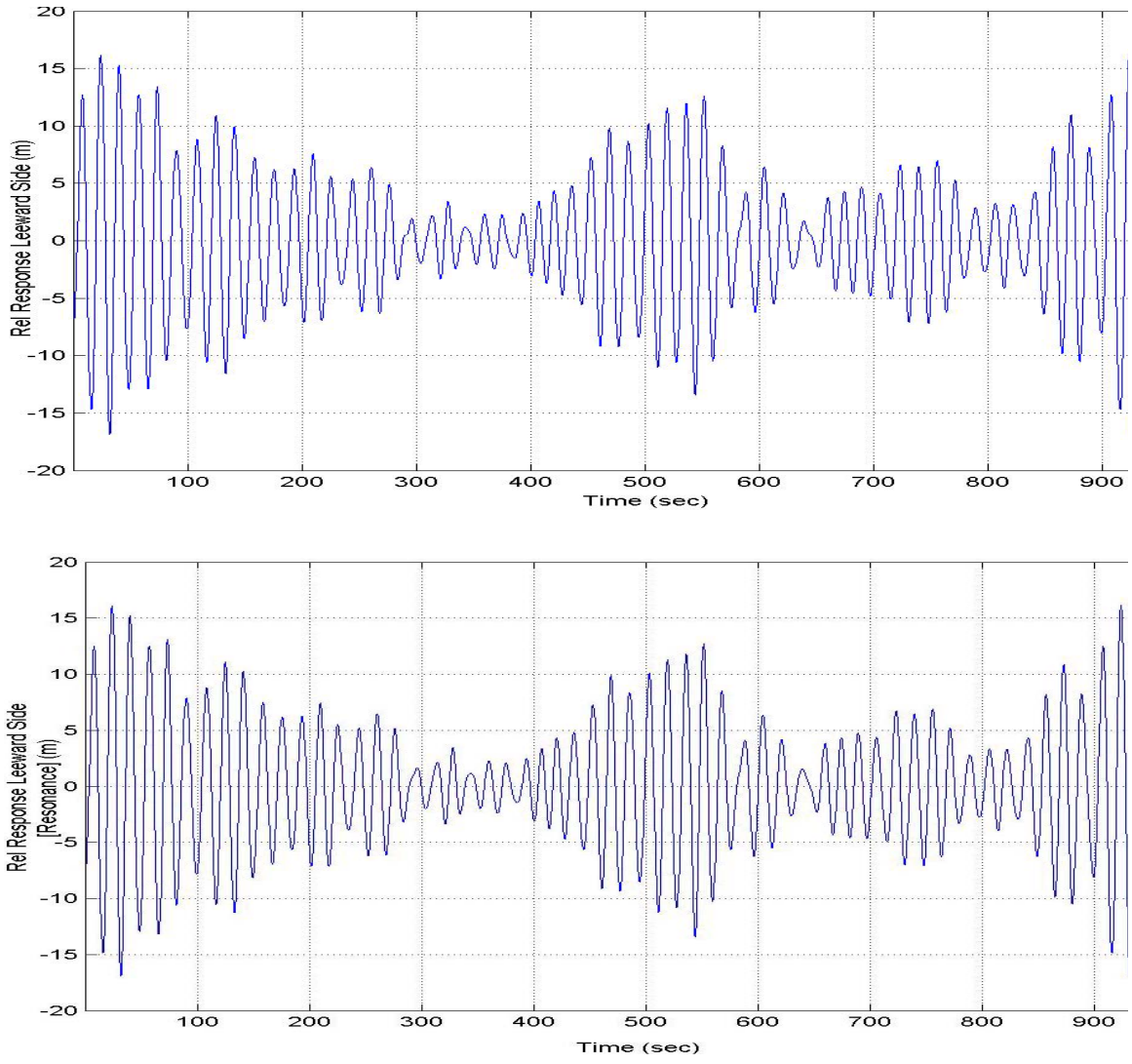

Figure 4-76: Beam sea-Hs 11.0m- relative motion with and without roll resonance [leeward side]

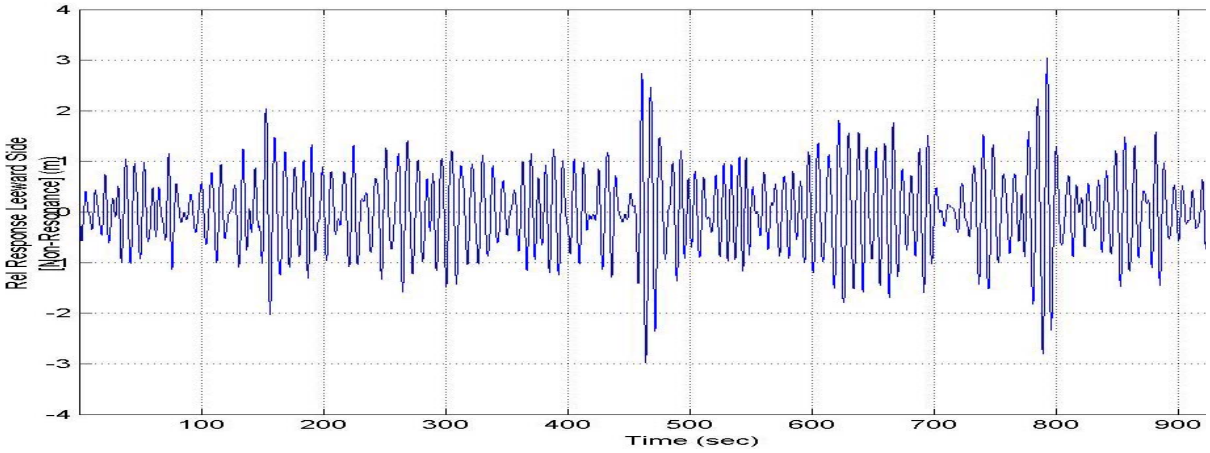

Figure 4-76: Continued

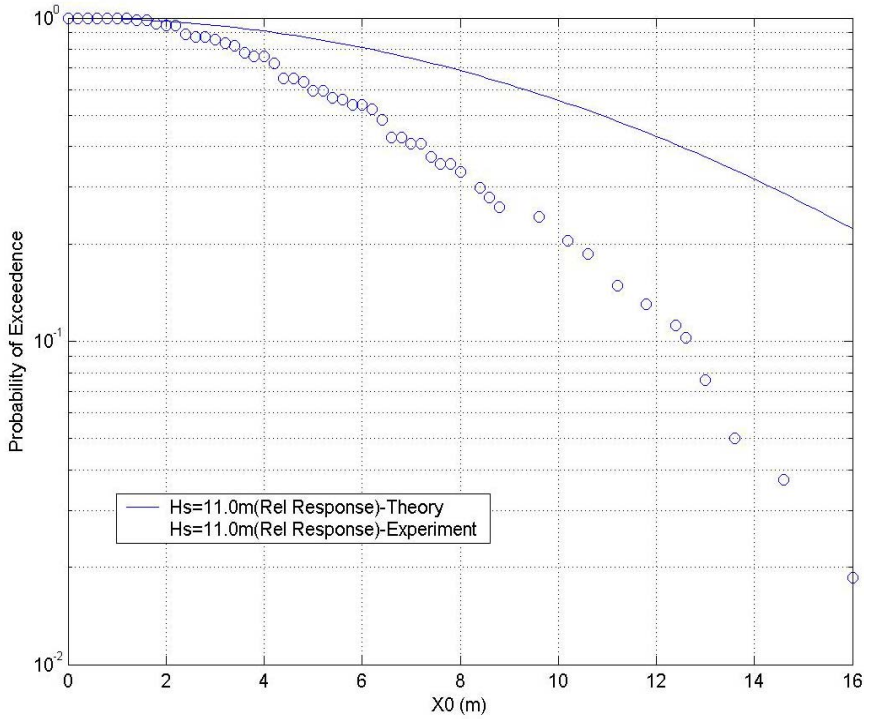

Figure 4-77: Beam sea-Hs 11.0m- probability of exceedence for relative motion

The probability of exceedence for the relative motion shows that the theoretical estimates are definitely much above the actual results. From the Figure 4-78 it can be noted that deviation of the theory from that of the actual field data seems to be quite large.

Relative motion-weather side

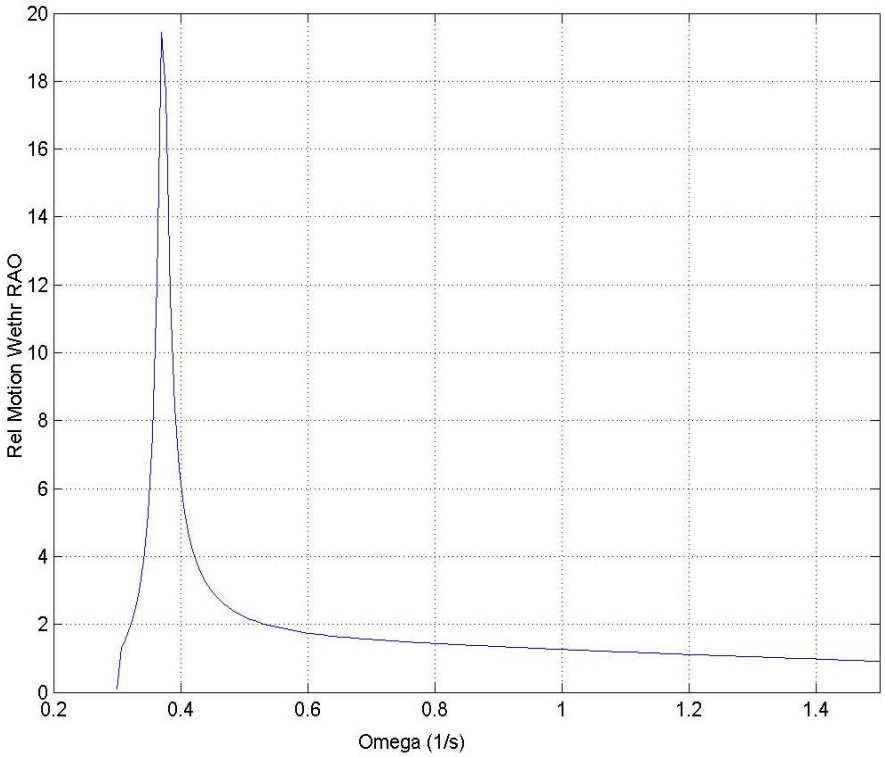

Figure 4-78: Beam sea-Hs 11.0m- relative motion RAO [weather side]

The relative motion RAO for the weather side also indicates an abrupt peak in the data for a low frequency range of around 0.344 rad/sec, which was again found to be the roll RAO contribution to the relative motion. This can be observed in Figure 4-79. Hence we plot the relative motion time series for the resonance as well as non-resonance frequency range. Also it has been observed in Figure 4-80 that the weather side response values are larger than the leeward side. This is fairly justified, as the weather side will be undergoing an extensive impact due to the waves as compared to the leeward side. So correspondingly, the weather side response would be significantly large compared to that of the leeward side.

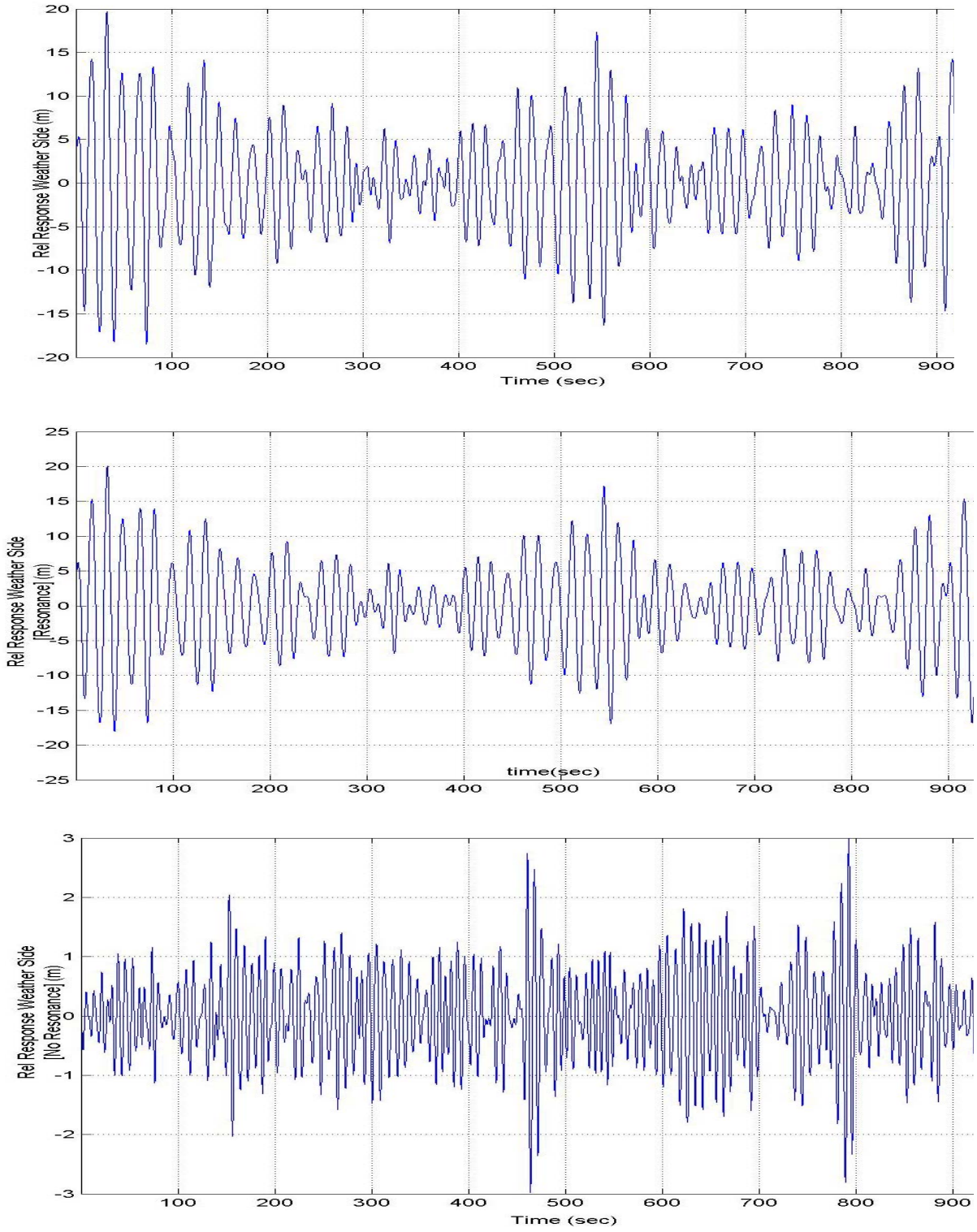

Figure 4-79: Beam sea-Hs 11.0m- relative motion with and without roll resonance [weather side]

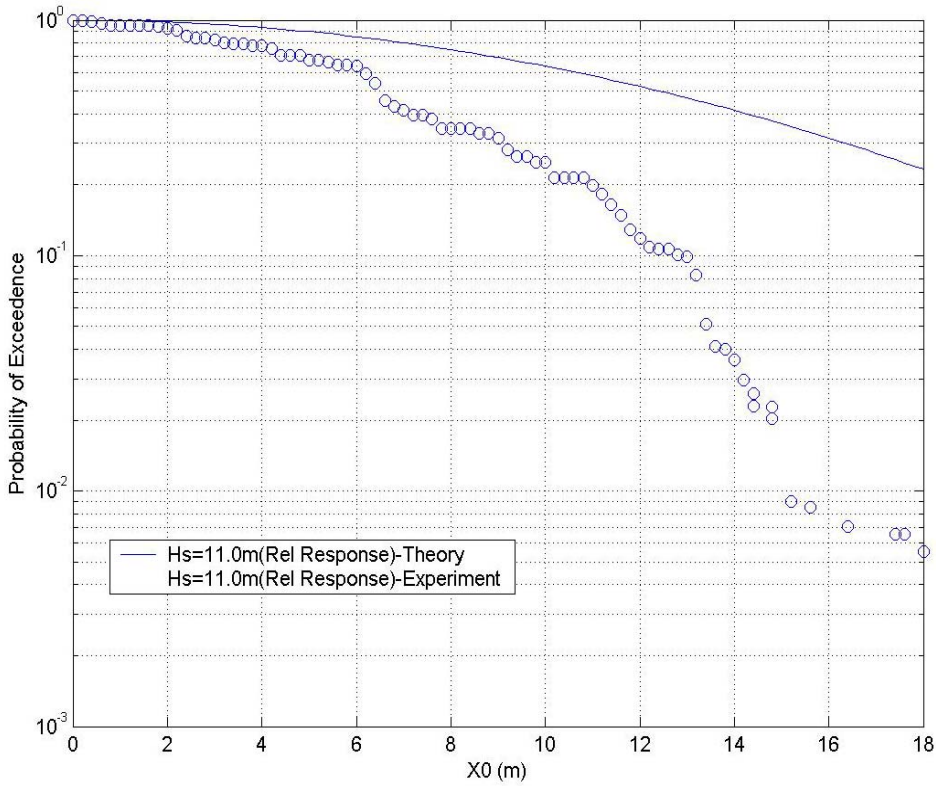

Figure 4-80: Beam sea-Hs 11.0m- probability of exceedence for relative motion

The probability of exceedence for the relative motion shows that the theoretical estimates are definitely much above the actual results. From the Figure 4-81 it can be noted that deviation of the theory from that of the actual field data seems to be quite large.

4.3 Deck wetness analysis

The deck wetness analysis is carried out from the response motion occurring at the forecastle of the ship. This deck wetting is determined by the freeboard of the vessel and the response motions predominantly at the bow of the vessel. Here the various response data obtained from the theoretical as well as experimental simulation is used for predicting the possible sea states and the response amplitudes that would cause deck wetting to occur.

From the total observations for the beam sea condition the most probable peaks are estimated and compared with the theoretical estimates. The most probable peak values are then plotted against the various significant wave heights.

The SL7 containership considered for this study has a freeboard of 5.9 m (Gu et al 2003) and a design draft of 9.5m. Hence in the head sea (180 degree) condition we can predict from the experimental results that any wave of up to significant wave height of 11.0 m would not cause overtopping and consecutive deck loading. It can be observed in Figure 4-81 that the theoretical estimates for the same would be in the range significant wave heights of 6 m or less. Hence the predictions by the conventional estimates through the linear theory are highly conservative and over estimating.

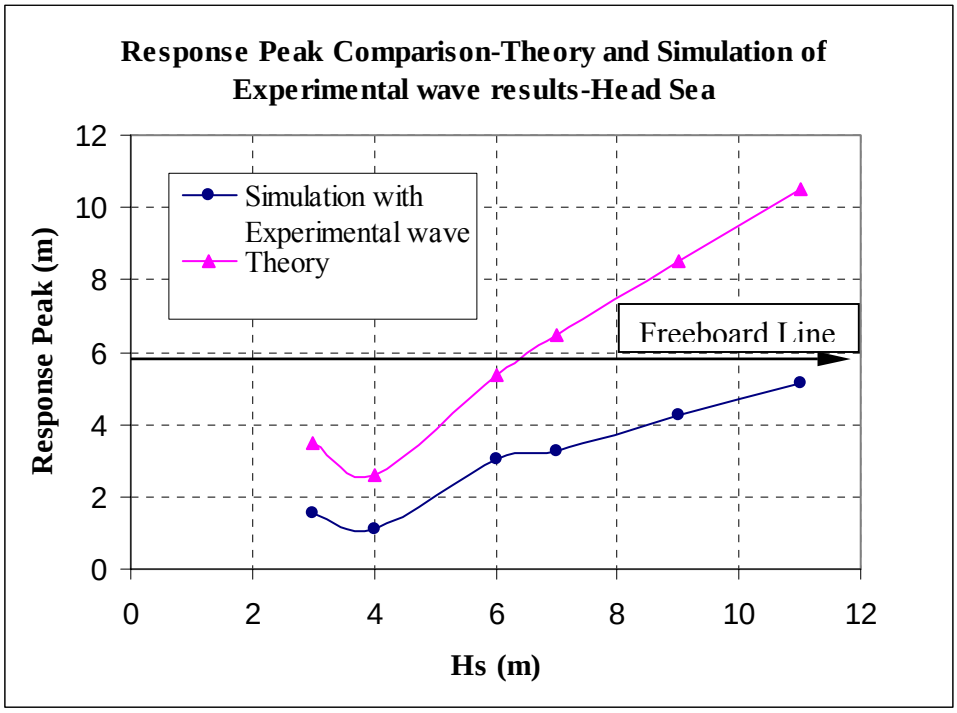

Figure 4-81: Beam sea-most probable peak response

Hence the UNIOM approach helps in predicting with a better accuracy the estimates of deck wetness in various different sea states for a given direction and amplitude of wave.

Here again it can be observed that peak response values obtained from the theory are 1.5 times more than that from of the actual experiment. It is to be noted that the theory and experiment are comparable in the lower sea states. But as the sea state increases the results tend to diverge with the theory over estimating the actual values.

The theoretical estimates are carried out as discussed in the analysis methodology section. The real data values are also compared and the most probable peak values for

the beam sea (90 degree) heading are derived which are as shown below. In the beam sea condition the weather side and the leeward side relative response peaks are separately considered.

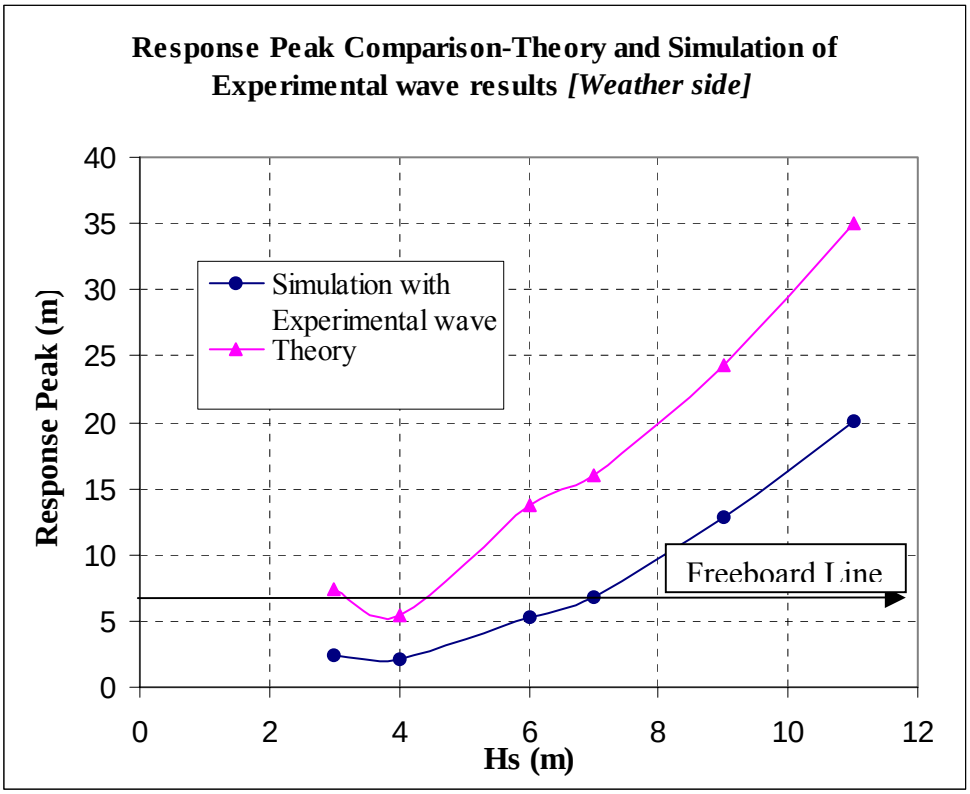

Figure 4-82: Beam sea-most probable peak response [weather side]

Here again it can be observed in Figure 4-82 that the experimental values are much higher in terms of the sea states compared to the theory. The deck wetness shipping of green water is expected to occur at sea states above 7m or above. In contrast the theoretical estimates show an over topping for sea states above 4 m.

The weather side estimates show that the theory is over estimating the peak response around 1.5 times that of the actual results. Here it can be seen that the response

peak for the head seas in both weather as well as leeward side has values much higher than the head sea conditions. This is expected as the extreme responses are noticed mostly in the beam sea environment, which is due to impact of the waves.

The response peak for the leeward side is as given in Figure 4-83 below. It is seen that the deck-wetting event will occur for significant wave heights above 7.0 m in the experimental results in contrast to the linear estimates of 5.0 m.

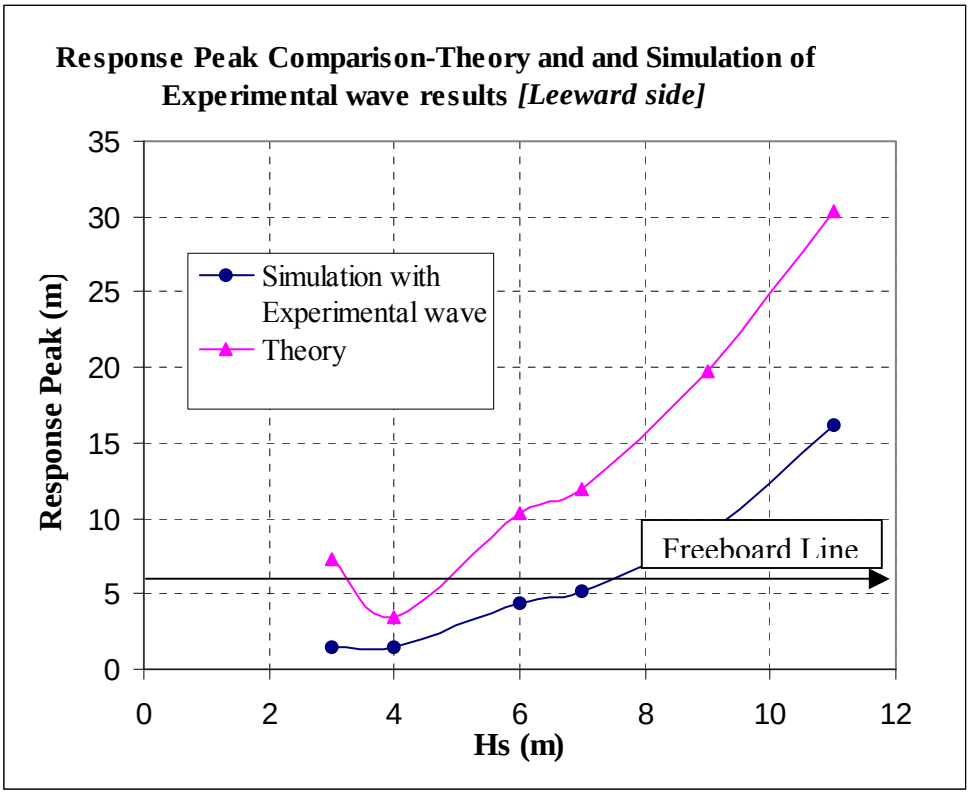

Figure 4-83: Beam sea-most probable peak response [leeward side].

5 CONCLUSION

The focus of this work was to provide a statistical prediction on the deck wetting and wave overtopping in very high seas as well as the associated relative motions and wave structure interactions towards the bow.

The results of the above analysis are used to arrive at the accuracy of the approach of UNIOM in predicting the motion response characteristics.

The above analysis with its own limitations of not having the actual response data was able to predict with a fair accuracy the relative motion characteristics of a freely floating body in the head and beam sea conditions.

The probability of exceedence results indicated the over estimation of theory over the experimental results. For any particular wave height or sea state the linear theory seemed to over estimate and thereby proving the conservative nature of the theory. The study also helped in the understanding of the various aspects of relative motions and the influence of one motion on the overall relative motion of the structure. The resonance aspects and its significance in the overall response are also analyzed.

Lastly the practical use and feasibility of this approach is also discussed with the model used for study as an example in predicting the deck wetness and prediction of the same. The deck wetting range for the various sea states is identified which would help the practical design in assessing the freeboard requirements for a given environment. The theoretical estimates using the conventional linear wave theory is shown to over estimate the possible overtopping for the various sea conditions. Hence the UNIOM approach aims at fairly more accurate estimate of the deck wetting as we have a wider range of data and experimental results.

The discussions regarding the estimations using the ship motions program SHMB5 are detailed in the appendix. They helped in validating the program as well as in reinvestigating the peak response amplitude. Also the discussions on the deck wetness studied by others are mentioned and cross-checked to ascertain the feasibility of the study.

The approach was a first step towards the understanding of the impact of non-linearity and the effectiveness of using the linear techniques to understand and analyze the non-linear wave input. The approach was fairly effective as the estimations showed consistency over the range of sea states that were tested. The approach was also consistent with other results, which were published and discussed on the estimations of the linear theory against experiments as discussed in the appendix.

The approach can be extended to the estimation of relative motion and deck wetting in case of the vessel in motion. The ship motion program developed has the capability of implementing the speed effect into analysis and would be an important approach that can be further elaborated and studied. Also due to the limited scope of this work the analysis for all the sweeps (0 to 360 degree heading) were not carried out in the study that could also be carried out as extension of the present work to give a more accurate prediction about the response behavior of structure specific to the various degrees of freedom.

The UNIOM approach was aimed at finding the accuracy of the estimates provided by the linear strip theory when used with a highly non-linear and random field data. The results indicated that the linear theory over estimates the probabilistic numbers as well as is very conservative. The conventional estimates using the widely tested linear theories would still hold good for practical design considerations.

REFERENCES

Bales N K., 1979 Minimum freeboard requirements for dry foredecks, *Proceedings of Society of Naval Architects and Marine Engineers,* Houston.

Cummins, W.E., 1973 *Pathologies of Transfer Functions*, Naval Ship Research and Development Center, Bethesda, Maryland.

Gu, X., Shen, J. and Moan, T., 2003 Efficient and simplified time domain simulation of nonlinear responses of ships in waves, *Journal of Ship Research*, **47**,262-273.

Hasselmann, J, 1975 A parametric wave prediction model: The JONSWAP spectrum *J Physical Oceanography*, **8**, 202-215.

Journee, J.M.J., 1992 Quick strip theory calculations in ship design, *PRADS'92, Conference on Practical Design of Ships and Mobile Structures*, Newcastle upon Tyne, UK.

Kim, C. H., Chou, F.S. and Tein, D. 1980 Motions and hydrodynamic loads of a ship advancing in oblique waves, *Transactions of the Society of Naval Architects and Marine Engineers*, **88**, 155-176.

Korvin-Kroukovsky, B.V., 1955 Investigation of ship motions in regular waves *Transactions of the Society of Naval Architects and Marine Engineers*, **3**,145-164.

Lee, W.T. and Bales, S.L., 1980 *A Modified JONSWAP Spectrum Only on Wave Height and Period*, David W. Taylor Naval Ship Research and Development Center, Bethesda, Maryland.

Lewis, F.M, 1929 The inertia of water surrouding a vibrating ship, *Transactions of the Society of Naval Architects and Marine Engineers*, **27**,1-20.

Newman, J.N., 1962 The exciting forces on fixed bodies in waves, *Journal of Ship Research*, **6**,222-245.

Salvesen, N., Tuck,E.O. and Falstien, O., 1970 Ship motions and sea loads, *Transactions of the Society of Naval Architects and Marine Engineers*, **78**,168-189.

Tupper, E., 1996 *Introduction to Naval Architecture,* Butterworth-Heinemann, San Diego, CA.

APPENDIX A

CORRELATION AND REINVESTIGATION OF RELATIVE MOTION OF SL7 CONTAINERSHIP

The experimental correlation that was carried out by (Kim, et al, 1980) is reinvestigated to check for the comments made at that time (Bales, 1979).

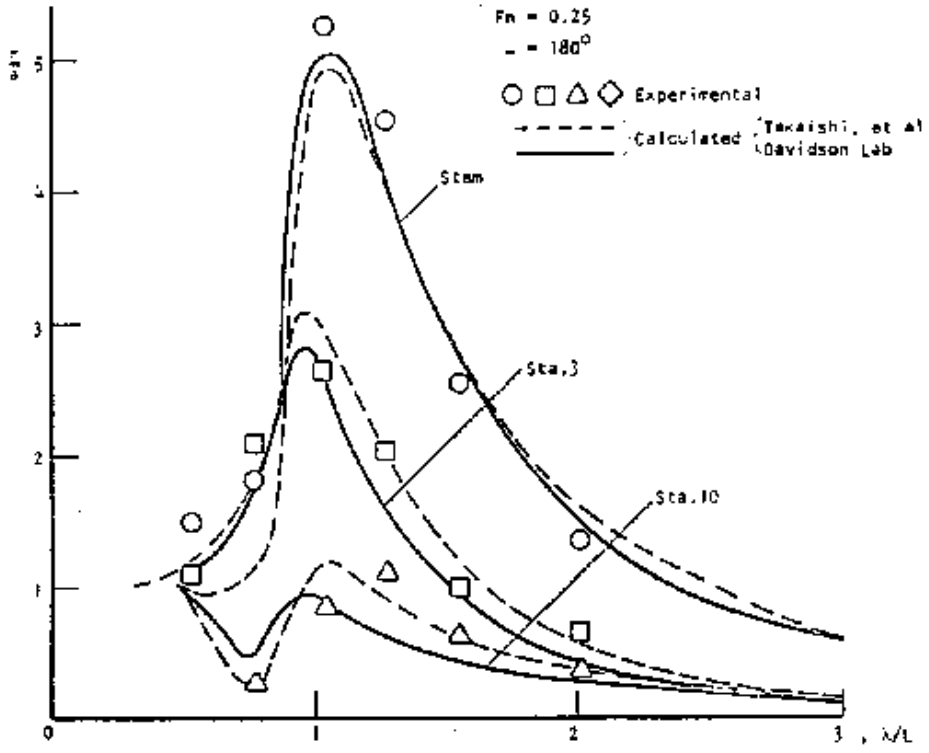

Figure A-1: Relative motion RAO for SL7 containership

It is observed that the relative motion at the forward perpendicular would not be having a higher peak as it was observed in their initial work. Here the trend suggested by Mr. Bales on the relative motion at the forward perpendicular seems to be fairly accurate.

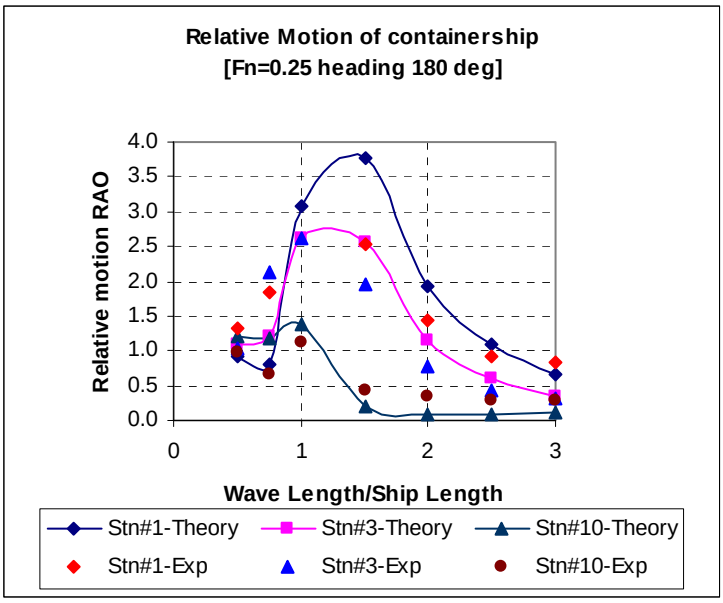

Figure A-2: Correlation of the SL7 containership results

This study and correlation helped in the better understanding of the program and its verification. It is observed that the values of the peak response at the forward perpendicular in this kind of vessel are seen to be much smaller that the experimental results. The trends are indicative of Mr. bales comments discussed above.

APPENDIX B

DECK WETNESS PREDICTION VERIFICATION

The discussion on the predicted frequency of deck wetness as shown below (Cummins, W, E, 1973) is indicative of the extent to which the linear theory over estimates the experimental results.

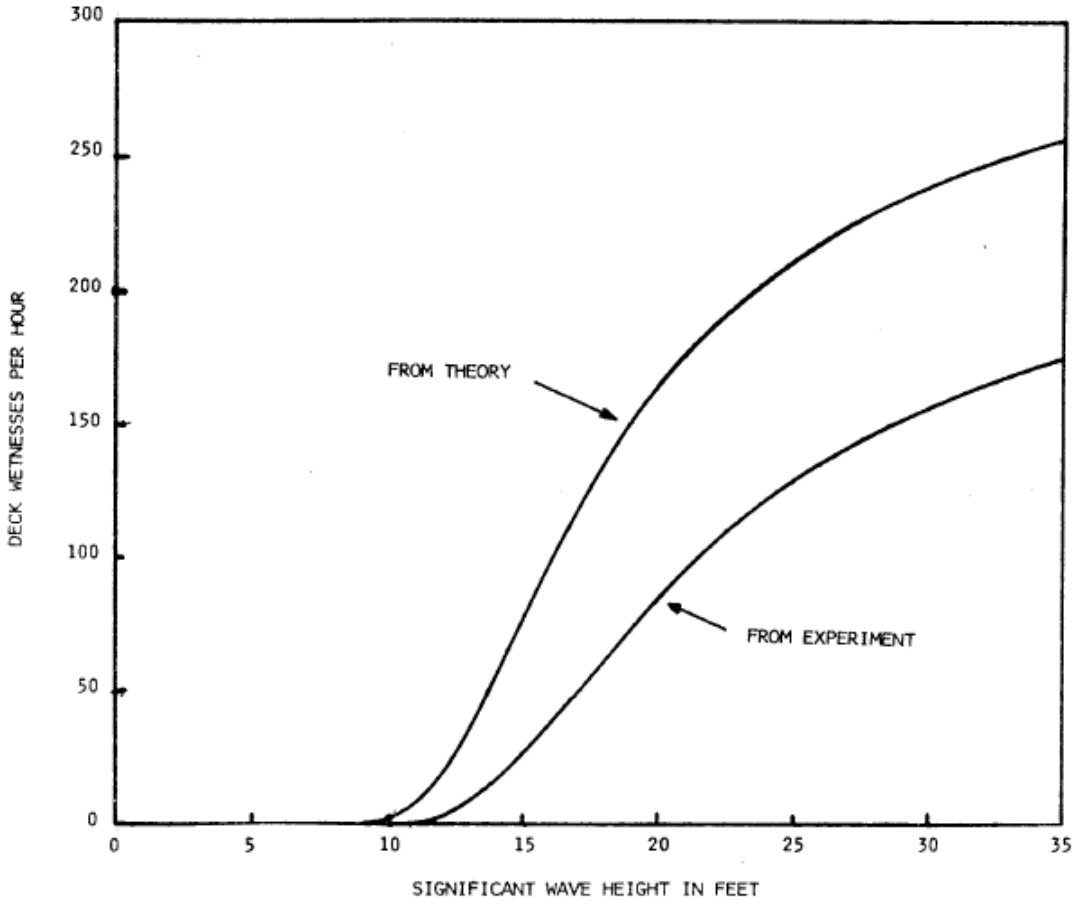

Figure B-1: Predicted frequency of deck wetness

This verifies the authenticity of the results and also we can correlate to the results obtained from our estimates, as the simulation time used is also 1 hour. Here the rate of wetness per hour is picked up for each of the significant wave heights and is observed that in the lower wave heights the trends were close to each other. As the sea state increased the deviation of theory from experiment is humongous.

APPENDIX C

INPUT WAVE TIME DOMAIN RESPONSE ANALYSIS PROGRAM

```
clc;clear;close all
loadZ:\ThesisWriteup\thesis_data_folder\Proto-scale-data\P010-
data\180deg\Proto010_trunc_new.txt

t=Proto010_trunc_new(:,1) ;
x=Proto010_trunc_new(:,2) ;
wc =3.8
dt = t(2) - t(1)                        ;  % time step
fs = 1/dt                               ;  % sampling frequency
N  = length(t)                          ;  % the number of data
%---------------------- Fourier Coefficents ----------------------
FCoeff = fft(x)                                     ;
a0     =  FCoeff(1)/N                               ;
an     =  2*real(FCoeff(2:N/2))/N                   ;
bn     = -2*imag(FCoeff(2:N/2))/N                   ;
phase  =  atan2( imag(FCoeff(2:N/2)),real(FCoeff(2:N/2)) )  ;
%---------------- Frequency axis(except w=0 or f=0) --------------
f = 1/(N*dt)*[1:1:N/2-1]'   ;
w = 2*pi*f                  ;  dw = w(2) - w(1)            ;
%---------------------  Amplitude Spectrum ----------------------
A = sqrt(an.^2 + bn.^2)         ;
%------------------------- Filter ---------------------------------
index   = max(find(w<wc))   ;
A(index:end)      = [ ]     ;    phase(index:end)  = [ ]    ; w(index:end)      = [ ]     ;
% ---------------- Reconstruction of time series ------------------------
for i= 1:length(t)
   xrc(i) =   a0 + sum(   A .* cos(w.*t(i) + phase )   )  ;         % matlab phase = -pi<paHs
e<pi
end

figure;
bar(w,phase,0.1),xlim([0 2.5]),ylim([-4 4])
xlabel('\omega(rad/s)')
ylabel('unit')
saveas(gcf,'Z:\ThesisWriteup\thesis_data_folder\Proto-scale-data\P010-
data\180deg\Response\RelResponse\fft-P010-Phase','fig');

figure;
bar(w,A,0.1),xlim([0 2.5]),ylim([0 0.7])
xlabel('\omega(rad/s)')
ylabel('unit')
saveas(gcf,'Z:\ThesisWriteup\thesis_data_folder\Proto-scale-data\P010-
data\180deg\Response\RelResponse\fft-P010-Amp','fig');
```

```
figure;
SUBPLOT(2,1,1),plot(t,x),grid
xlabel('t (s)'),ylabel('Eta(input)')
SUBPLOT(2,1,2),plot(t,xrc),grid
xlabel('t (s)'),ylabel('Eta(FFT-data)');
saveas(gcf,'Z:\ThesisWriteup\thesis_data_folder\Proto-scale-data\P010-
data\180deg\Response\RelResponse\fft-Input-comp','fig');

wstart=0.4;
wend=1.6;
index1 = min(find(w>wstart));
index2 = max(find(w<wend));
index2_f = index2 %+ 30

index_count = (index2-index1)/200;
indexcount_f=round(index_count);
in_loop = index1:indexcount_f:index2_f;
   w_new= w(in_loop)
   A_new= A(in_loop)
   phase_new=phase(in_loop)

figure;
bar(w_new,A_new,0.05),xlim([0.2 1.6]),ylim([0 0.7])
xlabel('omega (s)'),ylabel('Amplitude(m)')
saveas(gcf,'Z:\ThesisWriteup\thesis_data_folder\Proto-scale-data\P010-
data\180deg\Response\RelResponse\Wnew-Anew','fig');

figure;
bar(w_new,phase_new,0.05),xlim([.2 1.6]),ylim([-3.5 3.5])
xlabel('omega (s)'),ylabel('Phase(rad)')
saveas(gcf,'Z:\ThesisWriteup\thesis_data_folder\Proto-scale-data\P010-
data\180deg\Response\RelResponse\Wnew-Phase','fig');

for i= 1:length(t)
   xrc_new(i) =   sum(   A_new .* cos(w_new.*t(i) + phase_new )   )   ;          % matlab
phase = -pi<paHs e<pi
end

figure;
subplot(2,1,1),plot(t,xrc),grid
xlabel('t (s)'),ylabel('Eta(input)')
subplot(2,1,2),plot(t,xrc_new),grid
xlabel('t (s)'),ylabel('Eta(truncated)')
```

```
saveas(gcf,'Z:\ThesisWriteup\thesis_data_folder\Proto-scale-data\P010-
data\180deg\Response\RelResponse\Oldwave-Newwave','fig');

figure;
plot(t,xrc_new),grid
xlabel('t (s)'),ylabel('Eta(truncated)')
saveas(gcf,'Z:\ThesisWriteup\thesis_data_folder\Proto-scale-data\P010-
data\180deg\Response\RelResponse\Newwave','fig');

data3 = [w_new A_new phase_new];
save                              Z:\ThesisWriteup\thesis_data_folder\Proto-scale-data\P010-
data\180deg\P010_trunc_data.xls data3 -ascii -tabs;

t=0.3710:0.3710:3600;
Rel_temp=0;
i=1;
%-----------------------Response Time Series--------------------------------
for hrdr= 28:42:9240
   Mystring     ='Y:\SHMB5\SHMB5_new\Relative-motion\Relative\Case1-Head180\No
speed-200 records\P010-Data\180 deg\REL_MOT_RES'
   [Stn,Wethr,Leewrd,WethrPh,LeewrdPh]=resptext(Mystring,hrdr)

      PltWethrRao(i)=Wethr(1);
      PltWethrPh(i)=WethrPh(1);
      PltLeewrdRao(i)=Leewrd(1);
      PltLeewrdPh(i)=LeewrdPh(1);
         Relat=abs(A_new(i))*abs(Wethr(1))*cos(w_new(i)*t-phase_new(i)-WethrPh(1))
         Rel_temp=Rel_temp+Relat
      i=i+1
end

w_plot=w_new(1:(i-1));
lambda = ((2*pi*9.81)./w_plot.^2);
shiplen = 175;
lam_plot = lambda/shiplen;

figure;
plot(lam_plot,PltWethrRao);
grid on;
xlabel('Wave len/ship len'),ylabel('Rel Motion Rao');
saveas(gcf,'Z:\ThesisWriteup\thesis_data_folder\Proto-scale-data\P010-
data\180deg\Response\RelResponse\Wethr-rao-shiplen','fig');

figure;
plot(w_plot,PltWethrPh);
```

```
grid on;
xlabel('omega(1/s)'),ylabel('Rel Motion Phase');
saveas(gcf,'Z:\ThesisWriteup\thesis_data_folder\Proto-scale-data\P010-
data\180deg\Response\RelResponse\Wethr-phase','fig');

figure;
plot(w_plot,PltWethrRao);
grid on;
xlabel('omega(1/s)'),ylabel('Rel Motion Rao');
saveas(gcf,'Z:\ThesisWriteup\thesis_data_folder\Proto-scale-data\P010-
data\180deg\Response\RelResponse\Leewrd-rao-shiplen','fig');

figure;
plot(w_plot,PltLeewrdPh);
grid on;
xlabel('omega(1/s)'),ylabel('Rel Motion Phase');
saveas(gcf,'Z:\ThesisWriteup\thesis_data_folder\Proto-scale-data\P010-
data\180deg\Response\RelResponse\Leewrd-phase','fig');

data4 = [t' Rel_temp'];
save  Z:\ThesisWriteup\thesis_data_folder\Proto-scale-data\P010-
data\180deg\Response\RelResponse\P010-Rel_Resp_data.xls data4 -ascii -tabs;
figure;
plot(t,Rel_temp),grid
xlabel('time(sec)')
ylabel('Rel Response(m)')
saveas(gcf,'Z:\ThesisWriteup\thesis_data_folder\Proto-scale-data\P010-
data\180deg\Response\RelResponse\Rel-resp-data','fig');
```

APPENDIX D

CALCULATION OF EXPERIMENTAL PROBABILITY AND ZERO CROSSING ANALYSIS PROGRAM

```
clear all;close all;

W = [0.4002:0.0054:1.5830];
length(W);
dW= 0.0054;
Tm = 12.09;
Wm = 2*3.14/Tm;
gamma = 1.5;
Hs  = 6.0;
%*********************************************************************
*
%                Calculation of theoretical Spectrum
%*********************************************************************
*
index = max(find(W<Wm));
   for i=1:1:index
      sigma = 0.07;
         Somega(i)=(5/16)*Hs          ^2*Wm^4*W(i)^(-5)*exp(-1.25*(Wm/W(i))^4)*(1-
         0.287*log(gamma))*gamma^(exp(-(W(i)-Wm)^2/(2*sigma^2*Wm^2)));
   end
for i=index + 1:1:length(W)
      sigma = 0.09;
         Somega(i)=(5/16)*Hs          ^2*Wm^4*W(i)^(-5)*exp(-1.25*(Wm/W(i))^4)*(1-
         0.287*log(gamma))*gamma^(exp(-(W(i)-Wm)^2/(2*sigma^2*Wm^2)));
end
Somega(1)=0;
Mypath = 'junk';
[Wsxx,Sxx] = Spectral_Density(Mypath);
figure;
plot(W,Somega),grid
xlabel('omega'), ylabel('somega')
hold on;
bar(Wsxx,Sxx,0.1),grid on;
saveas(gcf,'Z:\ThesisWriteup\thesis_data_folder\Proto-scale-data\P010-
data\180deg\Response\NewResponse\PitchResponse\P010-Spctr-comp','fig');
%*********************************************************************
*
%                Calculation of Response Spectrum
%*********************************************************************
*
i=1;
Mean_temp = 0;
NumM0 = trapz(Wsxx,Sxx);
AnaM0 = trapz(W,Somega);
for hrdr= 14:42:9240
```

```
   Mystring     ='Y:\SHMB5\SHMB5_new\Relative-motion\Relative\Case1-Head180\No
speed-200 records\P010-Data\180 deg\REL_MOT_RES'
[Heave,Heaverao,HeavepHs                                    ,Pitch,Pitchrao,PitchpHs
]=heavepitchraotext(Mystring,hrdr);
   PltHeave(i)=Heaverao;
   PltHeavepHs (i)=HeavepHs ;
   PltPitch(i)=Pitchrao;
   PltPitchpHs (i)=PitchpHs ;
         Syy(i)=abs(Somega(i))*abs(Pitchrao^2);
      i=i+1
   end

M0= trapz(W,Syy);
data11 = [NumM0 AnaM0 M0];
save Z:\ThesisWriteup\thesis_data_folder\Proto-scale-data\P010- data\180deg
\Response\NewResponse\PitchResponse\M0_comparison.txt data11 -ascii -tabs;
%*********************************************************************
*
%          Calculation of Theoretical Probability of Exceedence
%*********************************************************************
*
X0 = [0:0.1:1.5];
Prob = exp(-(X0.^2/(2*M0)));
LgProb = log(Prob);
Log10Prob = log10(Prob);
hrdr = 27;
%*********************************************************************
*
%                Calculation of Experimental Probability
%*********************************************************************
*
Newstring='Z:\ThesisWriteup\thesis_data_folder\Proto-scale-data\P010-
data\180deg\Response\NewResponse\PitchResponse\ZC_WAVES.OUT'
[Indx,Height,Period,Crstht,Trdepth]=zcrostext(Newstring,hrdr);
r=1
for LpX0= 0:0.1:1.5
   count =0;
   for j=1:1:max(Indx)
      if Crstht(j) > LpX0
         count =count+1;
      end;
   end;
   if count ==0
      break;
   else
```

```
        Nprob(r) = count/max(Indx);
        r=r+1;
    end;
end
plotX0 = X0(1:(r-1));
plotProb =Prob(1:(r-1));
figure;
semilogy(plotX0,plotProb),grid on
xlabel('X0 (m)')
ylabel('Probability of Exceedence')
legend('HS =6.0m(Pitch)-Theory','HS =6.0m(Pitch)-Wave data')
hold on;
semilogy(plotX0,Nprob,'o'),grid on
saveas(gcf,'Z:\ThesisWriteup\thesis_data_folder\Proto-scale-data\P010-
data\180deg\Response\NewResponse\PitchResponse\Log-Prob-of-exe-010','fig');
hold off;

figure;
plot(plotX0,plotProb),grid on
xlabel('X0 (m)')
ylabel('Probability of Exceedence')
legend('HS =6.0m(Pitch)-Theory','HS =6.0m(Pitch)-Wave data')
hold on;
plot(plotX0,Nprob,'o'),grid on
saveas(gcf,'Z:\ThesisWriteup\thesis_data_folder\Proto-scale-data\P010-
data\180deg\Response\NewResponse\PitchResponse\Prob-of-exe-010','fig');
hold off;
figure;

subplot(1,2,1),plot(plotX0,plotProb),grid on
xlabel('X0 (m)')
ylabel('Probability of Exceedence(%)')
legend('HS =6.0m(Pitch)-Theory','HS =6.0m(Pitch)-Wave data')
hold on;
plot(plotX0,Nprob,'o')

subplot(1,2,2),semilogy(plotX0,plotProb),grid on
xlabel('X0 (m)')
ylabel('Probability of Exceedence(log)')
legend('HS =6.0m(Pitch)-Theory','HS =6.0m(Pitch)-Wave data')
hold on;
semilogy(plotX0,Nprob,'o')
saveas(gcf,'Z:\ThesisWriteup\thesis_data_folder\Proto-scale-data\P010-
data\180deg\Response\NewResponse\PitchResponse\Prob-exe-percent-log-010','fig');
hold off;
```

```
data1 = [plotX0' plotProb' Nprob'];
saveZ :\ThesisWriteup\thesis_data_folder\Proto-scale-data\P010-
data\180deg\Response\NewResponse\PitchResponse\Prob-data-010.xls  data1  -ascii  -
tabs;

%*********************************************************************
*%                Zero Crossing Routine
%*********************************************************************
*function [Indx,Height,Period,Crstht,Trdepth]=zcrostext(pathname,hrdr)
[Zindx,Zheight,Zperiod,Zcrstht,Ztrdepth]=textread(pathname,'%s%s%s%s%s','headerlin
es',hrdr) ;
counter= max(str2double(Zindx))
for j=1:counter
   Indx(j)=str2double(Zindx(j))
   Height(j)=str2double(Zheight(j))
   Period(j)=str2double(Zperiod(j))
   Crstht(j)=str2double(Zcrstht(j))
   Trdepth(j)=str2double(Ztrdepth(j))
End
```

VITA

Adam Adil

ADDRESS

301 Wilcrest Drive, Apt #3102,

Houston, TX 77042

Ph: 979-255-6129

EDUCATION

• Master of Science. Graduation date: December 2004

Major: Ocean Engineering

Texas A&M University

GPA: 3.44

• Bachelor of Technology. Graduation date: December 2000

Major: Naval architecture and ship building

Cochin University of Science and Technology

GPA: 3.80

EXPERIENCE

• Texas A&M University, College Station, Texas (Dec. 2002– August 2003)

Graduate teaching assistant for classes in fluid mechanics, hydromechanics, naval architecture and dynamics of offshore structures.